8-2023

Injury induced neuroplasticity and cell specific targeting of the lumbar enlargement for gene therapy.

Brandon Lee Brown
University of Louisville

INJURY INDUCED NEUROPLASTICITY AND CELL SPECIFIC TARGETING OF THE LUMBAR ENLARGEMENT FOR GENE THERAPY

By

Brandon Lee Brown
B.S., Indiana University, 2014
M.S., Indiana University, 2016

A Dissertation
Submitted to the Faculty of
the Graduate School of the University of Louisville
in Partial Fulfillment of the Requirements
For the Degree of

Doctor of Philosophy in
Interdisciplinary Studies: Specialization in Translational Neuroscience

Interdisciplinary Studies
University of Louisville
Louisville, Kentucky

August 2023

INJURY INDUCED NEUROPLASTICITY AND CELL SPECIFIC TARGETING OF THE LUMBAR ENLARGEMENT FOR GENE THERAPY

By

Brandon Lee Brown
B.S., Indiana University, 2014
M.S., Indiana University, 2016

A Dissertation Approved on

July 26, 2023

By the following Dissertation Committee:

_____
David S.K. Magnuson

_____
Scott R. Whittemore

_____
Chad L. Samuelsen

_____
Dale Ding

_____
Kathryn J. Jones

DEDICATION

This thesis dissertation is dedicated to my parents

Mr. Gary Paul Brown

and

Mrs. Helen Geneava Brown

who have given me invaluable opportunities
and supported me throughout my education

and to my fiancé

Ms. Kelsey Marie Rupert

who has been of constant support

ACKNOWLEDGMENTS

I would like to thank Dr. Scott Whittemore and David Magnuson for their guidance and input. I would also like to that the other committee members, Dr. Dale Ding, Dr. Chad Sameulsen, and Dr. Kathryn Jones for their comments and assistance during my graduate studies. Specifically, Dr. Kathryn Jones who entrusted me to run studies and explore my ideas in her laboratory prior to starting this dissertation. Her compassion and pursuit of science continues to inspire to this day. Lastly, Dr Jonathan Kopechek has assisted in many of the experiments done here, without his knowledge, expertise, and willingness to collaborate many of these studies would not have been possible.

ABSTRACT

INJURY INDUCED NEUROPLASTICITY AND CELL SPECIFIC TARGETING OF THE LUMBAR ENLARGEMENT FOR GENE THERAPY

Brandon L. Brown

July 26, 2023

This dissertation is an examination of spinal cord injury induced neuroplasticity and tests whether noninvasive gene therapy can successfully target neurons in the lumbar spinal cord. It begins with an overview of neural control of locomotion and a brief summary of therapeutics that are used and/or in development for treating spinal anatomically characterize s subset of neurons in the spinal cord, long ascending propriospinal neurons, that are involved in interlimb coordination. Characterization of these neurons allows for subsequent evaluation of their potential involvement in injury induced neuroplasticity.

This dissertation is divided into five chapters, covering spinal cord injury and therapeutics. Chapter One gives background on locomotor control, propriospinal neurons, spinal cord injury, and therapeutics. Chapter Two develops and characterizes viral tracing methods for spinal cord anatomy. Chapter Three then uses these methods to characterize long ascending propriospinal neurons and evaluate their involvement in injury induced plasticity.

Chapter Four then focuses on the development of noninvasive delivery of gene transfer to the lumbar enlargement. This involves optimizing focused ultrasound and intravenous microbubble delivery to focally and transiently permeabilize the blood spinal cord barrier of the lumbar spinal cord. This optimization then allows for successful gene transfer in neurons in the lumbar spinal cord following intravenous delivery of viral vector. Lasty, Chapter Five discusses the implications for all of these findings and how these findings have contributed to our understanding spinal cord anatomy and injury, and how the proof-of-concept in Chapter 4 provides a promising new avenue for spinal cord injury therapeutics.

TABLE OF CONTENTS

PAGE
ACKNOWLEDGMENTS……iv
ABSTRACT……v
LIST OF TABLES……ix
LIST OF FIGURES……x

CHAPTER I – Background……1

Descending motor systems for locomotion……2

Spinal circuits for locomotor execution……7

Propriospinal neurons' role in recovered function following spinal cord injury….10

Therapeutics for spinal cord injury……12

CHAPTER II – Dual-viral transduction utilizing highly efficient retrograde lenti virus improves labeling of long propriospinal neurons……21

Materials and methods……25

Results……31

Discussion……37

CHAPTER III – Long ascending propriospinal neurons are heterogenous and subject to spinal cord injury induced anatomic plasticity……43

Materials and methods……46

Results……55

Discussion……69

CHAPTER IV – Focused ultrasound and intravenous microbubbles confer focal cell specific gene transfer in the rodent lumbar spinal cord……..…………………..…22

Materials and methods…………………………………………………………….…………………..……83

Results.……………………………………………………………………………….………………………...90

Discussion…………………………………………………………………….…………………….………….102

CHAPTER V – Discussion and contributions to the field……………….……………………………….109

We know what we don't know, yet it goes unstudied: Cruxes of spinal cord injury research ………………………………………………………………………..……………………………109

Injury-induced neuroplasticity. What matters? What doesn't?.........................114

Locomotor function post-SCI. The circuitry doesn't need to be perfect, just Good enough ……………………………………………………………………………..…………………118

A potential path forward for treating spinal cord injury. Is there a silver bullet?...120

Epilogue: contribution to the field and personal development………..……………….125

REFERENCES…………………………………………………………………………………………..………………..127

CURRICULUM VITA……………………………………………………………………………..……………………185

LIST OF TABLES

TABLE PAGE

1. Functional improvements from circuit modifications……..……..……117

LIST OF FIGURES

FIGURE PAGE

1. Experimental design and overview for labeling left ipsilateral long ascending propriospinal neurons……26

2. The number of labeled neurons in the lumbar spinal cord is significantly impacted by the tracing method(s) used……33

3. Specificity of labeling is impacted by the tracing method used……34

4. The number of labeled neurons counted with the MATLAB program and manually counting are similar and correlated……36

5. Experimental design and overview for labeling and reconstruction of long ascending propriospinal neurons……49

6. LAPNs differ anatomically based on soma and neurite characteristics……57

7. 150kdyn T10 SCI produces no gross functional deficits at 5 weeks post-SCI……59

8. 5 weeks post-SCI limb coupling is impaired but other key features of locomotion are unaltered……62

9. 5 weeks post-SCI LAPNs morphologically group into 3 clusters, and post-SCI LAPNs morphologically differs from uninjured LAPNs……64

10. 5 weeks post-SCI LAPN axon collaterals densities differ by target……68

11. SCI does not alter LAPN axon collaterals in the reticular formation……70

12. Laminectomy is required for ultrasound delivery to thoracolumbar spinal foramen ……92

13. 2.5% microbubble dose allows for maximal rostrocaudal targeting of the spinal cord without disruptions in tissue morphology……95

14. 2.5% and 5% microbubble doses cause astrocyte reactivity and hemoglobin

extravasation into the lumbar spinal cord parenchyma……97

15. 7 days following FUS + 2.5% MB potential side effects in the lumbar enlargement are resolved……..99

16. **I**ntravenous AAV delivery following FUS+MB successfully targets neurons in the lumbar spinal cord with >90% accuracy……103

17. Functional deficits following FUS+MB and intravenous AAV are minimal……105

CHAPTER I
INTRODCUTION

"The brain is a world consisting of a number of unexplored continents and great stretches of unknown territory." These words from Ramon y Cajal in 1906 still hold true in 2023, which is not surprising given the 100 billion neurons in the human brain [1,2] and 250 million neurons in the spinal cord [3], each of which forms thousands of synapses[4,5]. Despite this seemingly infinite complexity, technological advances such as near infrared spectroscopy, diffusion weighted magnetic resonance imaging and resting-state functional magnetic resonance imaging have improved our understanding of macroscale connectivity and have led to the development of The Human Connectome Project [6]. Similarly, advances in biology and virology have allowed for the development of the Allen Mouse Brain Connectivity Atlas [7], which provides the most comprehensive macro- and meso-scale connectomics map of the rodent brain to date.

The primary focus of connectomics has been to elucidate pathways and connectivity throughout the brain. However, there has yet to be concerted effort to map the spinal cord with this level of fidelity. The lack of knowledge regarding spinal cord pathways and connectivity hinders the development of treatments for spinal cord diseases. pathologic spinal cord both anatomically and functionally to develop current and future therapies for spinal cord pathologies. To move forward as a field, there must be a greater understanding of the non

Descending motor systems for locomotion

The most conserved movement among species is locomotion, or the ability to move or propel oneself from one area to another. Locomotion may be expressed as a goal-directed, an exploratory, or an escape behavior. Expression of locomotion requires motor circuits throughout the neuroaxis to learn, select, initiate, execute, and modify motor output for the successful activation and coordination of muscles to navigate a given environment. In vertebrates, the spinal cord contains all the required circuitry for the execution of locomotion [8]. Briefly, the cervical and lumbar enlargements contain local circuitry for rhythmic output to each of the limbs (expanded upon in Section 2) and are interconnected by local and long interneurons for coordination of the forelimbs (arms) and hindlimbs (legs). Dorsoventrally, the spinal cord gray matter is topographically organized into lamina based on cellular architecture, neurochemical properties, and connectivity [9-11]. The most dorsal are lamina I-IV that are generally responsible for processing, modulating, and relaying sensory inputs [12-14]. The intermediate gray matter consists of lamina VI-VIII and X, which integrate and process multimodal inputs to modulate and produce motor output [15-17]. Ventrally, lamina IX primarily contains motoneurons which are the final output from the spinal cord to skeletal muscle [10,18].

While spinal circuity will be the focus of this dissertation, an overview of higher motor centers projecting to the spinal cord that play a role in locomotion will aid in interpretation of acquired data and in the overall understanding of locomotor circuitry.

Corticospinal tracts (primary sensory and motor cortices)

Beginning in the brain, the primary motor cortex (M1) descends via the corticospinal tract to innervate all levels of the spinal cord; however, in multiple species the cervical spinal cord is targeted more than the thoracic or lumbar spinal cords . M1 projections to the spinal cord are primarily found in spinal lamina III and IV and sparsely in I, II, and V [19,20]. Additionally, in Old World monkeys, great apes, and humans, M1 has direction projections to motoneurons in lamina IX suggesting greater cortical control of motor output for precise muscle activation and movement [21-24]. In these higher primates, these direct projections are mostly seen in the cervical enlargement for control of the upper limb and digits, and many of the projections to the lumbar spinal cord project to inhibitory circuits [25,26]. Interestingly, lesioning M1 or the corticospinal tract results in only transient deficits in overground stepping [27,28], suggesting that this pathway plays little role in overground locomotion. However, stimulation of M1 modulates electromyography characteristics during ongoing locomotion, insinuating that M1 may grossly increase the excitability of the locomotor network without altering the timing and coordination of muscle activation [29]. Additionally, M1 is required if/when locomotion need be modified for navigating unstable or unfamiliar environments [30,31].

The primary somatosensory cortex (S1) also contains descending corticospinal projections but unlike M1, only projects to the cervical and thoracic spinal cords [20,32]. S1 densely projects to lamina IV in multiple species, to lamina I, II and III in nonhuman primates [20], and to lamina V in mice [32]. S1 has been shown to play a direct role in locomotor speed, as S1 stimulation leads to increased speed while inhibition decreases speed, ultimately leading to cessation of locomotion [32].

Brainstem nuclei and spinal tracts

Numerous brainstem structures are involved in the direct control of spinal locomotor circuits. These nuclei are situated throughout the midbrain, pons, and medulla and have differential impacts on the speed, initiation, and termination of locomotion. The largest of these structures is the reticular formation which extends from the midbrain through the medulla and can grossly be broken into median, medial, and lateral columns. The medial and median columns in the pons and medulla give rise to the reticulospinal tract which projects to all levels of the spinal cord [33]. The medial pontine and medullary reticular formation contain numerous nuclei, two of which are known to be involved in locomotion: the gigantocellular nucleus (GCN) and the lateral paragigantocellular nucleus (LPGi). In multiple species, GCN innervates lamina VII – X in the cervical and thoracic spinal cords, and targets lamina V – VI in the lumbar spinal cord [34,35]. GCN is generally thought of as a relay for descending commands from the mesencephalic locomotor region (MLR) in the midbrain [36], but neuronal subpopulations in GCN have distinct functions related to locomotion. Glutamatergic neurons in GCN are involved in "resetting" locomotor pattern during ongoing locomotion [37], and a Chx10 expressing subset of glutamatergic neurons cause cessation of ongoing locomotion, suggesting that descending glutamatergic drive from GCN is primarily involved in pausing or stopping ongoing locomotion likely via activation of inhibitory interneurons in the spinal cord [38]. The LPGi also projects to all levels of the spinal cord, targeting lamina VI-X [39,40]. Activation of glutamatergic LPGi neurons induces high-speed locomotion and can tune input from MLR to increase locomotor speed [26].

The median column of the reticular formation contains the raphe nuclei (raphe pallidus, raphe obscuris, raphe magnus, and raphe dorsalis) which provide serotoninergic (5-hydroxytryptamine, 5-HT) innervation to all levels of the spinal cord. Raphe projections target lamina VII – X in the cervical and thoracic spinal cords and target all lamina in the lumbar spinal cord [41,42]. Classical studies show that exogenous 5-HT drives fictive locomotion in multiple species and increases locomotor burst amplitude [43-45]. However, increasing endogenous 5-HT *in vivo* inhibits and destabilizes locomotor output [46-48], and ablating 5-HT neurons does not impact open field locomotion in mice [49]. These findings indicate an unclear role for 5-HT in the generation of locomotion and suggest that 5-HT may decrease overall locomotor output rather than drive it.

In the midbrain, the red nucleus is located rostral to the reticular nuclei and can be subdivided into the parvocellular and magnocellular nuclei. Red nucleus projections descend via the rubrospinal tract to target all levels of the spinal cord and innervate laminae V-VII in multiple species [48,49]. In non-human primates and humans, the size of the magnocellular nucleus decreases, likely reflecting a smaller role in processing postural and proximal limb feedback. However, in lower Mammalia where the magnocellular nucleus plays a larger role in processing afferent feedback from the limbs, ablation and stimulation studies suggest that this tract is involved in flexor activity during locomotion and plays a role in propulsive and braking forces [50,51].

Opposing the rubrospinal system's flexor activation, the vestibulospinal system is involved in extensor activation. Grillner *et al*. [52,53] and Orlovsky *et al*.[54] show that extensor muscle activity increases with lateral vestibular nucleus stimulation and does

not interrupt the timing or coordination of locomotion. Furthermore, vestibulospinal neuron ablation produces no gross locomotor deficits but does impact precision locomotion, as indicated by deficits in balance and proprioception. These findings are supported by vestibulospinal anatomy, as 66% of vestibulospinal neurons project to the lumbar spinal cord [55] and terminate in lamina VII-IX [56,57].

The cerebellospinal tract arises from the fastigial and interposed nuclei in the cerebellum, which project to the cervical and lumbar spinal cord, respectively [58].Inactivation of fastigial cerebellospinal neurons has no impact on overground locomotion but does impair the ability to learn "skilled" locomotion [58]. Little is known about the function of the interposed nuclei, but terminals of these neuronal projections are primarily found in lamina VII [59].

Lastly, while it does not have direct projections to the spinal cord, the mesencephalic locomotor region (MLR) is responsible for the initiation of locomotion via its direct projections to the reticular formation [60]. Numerous higher brain centers including the subthalamic locomotor region, substantia nigra pars reticualta, the amygdala, and various sensory systems converge onto MLR making it an important control center for determining the initiation of locomotion based a multitude of inputs [61-63]. Additionally, MRL or its homolog(s) are seen in vertebrate species ranging from lampreys to humans, indicating that it provides an evolutionarily conserved means to initiate locomotion.

Other structures such as basal ganglia, and thalamus also take part in the selection, initiation, and modification of locomotor output. However, as these areas do

not target the spinal cord directly, their anatomy and function related to locomotion will not be expanded upon here but see Ferriera-Pintao et al. for an excellent review [64].

Spinal circuits for locomotor execution

Current model of spinal circuitry and locomotor central pattern generators.

Our current working model of the spinal circuitry that executes locomotor commands is driven by computer modeling and *in vivo* and *ex vivo* experimental data in multiple species [65]. Central pattern generators (CPGs) lie at the core of this model. Two CPGs are located in the lumbar enlargement and two in the cervical enlargement with each corresponding to one of the four limbs. CPGs are comprised of ensembles of neurons capable of producing stereotypic, rhythmic motor behaviors and flexor-extensor alternation of each limb. While the CPGs in the referenced model relate to locomotion, it is important to note that CPGs regulate other stereotypic rhythmic behaviors such as coughing, swallowing, chewing, breathing and micturition [66-68].

Thomas Graham Brown first began elucidating the presence of spinal CPGs in 1911 by showing that in the absence of afferent feedback and supraspinal drive, "the spinal efferent neurons may show some degree of independence of the afferent neurons and some of the phenomena of reciprocal innervation when functionally separated" [69,70]. Since Graham, numerous studies have confirmed the presence of locomotor CPGs. These studies frequently use *in vitro* spinal cord preparations to elicit fictive locomotion. By applying cocktails of N-methyl-D-aspartate and serotonin to the lumbar spinal cord, fictive locomotor bursts can be seen in both neonatal mouse and rat spinal *in vitro* preparations [71,72]. Likewise, this locomotor-like activity can also be provoked if the same

cocktail is applied to the cervical enlargement [73]. However, rhythm generating capabilities are most robust in the rostral portion of the lumbar enlargement: L2 in rodents and L4 in cats [71,74].

In 1903, Sir Charles Sherrington first postulated the concept of a long descending pathway in the spinal cord as he noted that cutaneous stimulation between the shoulders elicited a scratch reflex involving the hindlimb muscles, which he called a "long spinal reflex" [75]. Subsequent neuroanatomical studies have provided evidence of this pathway in multiple species, and this pathway is now broadly referred to as the long descending propriospinal neurons (LDPNs) [76-78]. Electrophysiologic studies show that LDPNs respond to cutaneous stimuli and joint motion [79], receive input from multiple supraspinal [80,81], and are involved in interlimb coordination during locomotion [82,83]. The current working model includes long propriospinal neurons to coordinate the ipsilateral and contralateral hindlimb-forelimb pairs as well as local commissural interneurons for coordination and timing of the forelimb and hindlimb pairs [65].

Long ascending propriospinal neurons and locomotion

Studies have focused primarily on LDPN pathways as they are anatomically positioned to relay commands from higher motor centers to the caudal spinal cord. Despite this, ascending reciprocal pathway(s) exist, and are generally referred to as long ascending propriospinal neurons (LAPNs). LAPNs and LDPNs can be broadly defined by three criteria: 1) they are neurons contained within the spinal cord, 2) their axons project three or more spinal segments, and 3) their axonal projections show rostrocaudal directionality. By these criteria, tract tracing using chemical tracers has

provided anatomical evidence for LAPNs in multiple species [84-87]. Early cat electrophysiology studies demonstrated that hindlimb afferents can drive forelimb motoneurons and facilitate and/or depress forelimb reflexes, suggesting a role for LAPNs in coordinating the hindlimbs and forelimbs [88,89]. Juvin *et al* [90] showed that stimulation of the lumbar enlargement could influence output of the cervical CPGs, further indicating that long ascending connections play a role in linking the hindlimb and forelimb locomotor CPGs in the spinal cord.

As mentioned above, LAPNs comprise a broadly defined sets of neurons. However, for the remainder of this dissertation, we will focus on a subset of LAPNs which have somata at lumbar levels 2/3 (L2/3) and at least one axon terminal at cervical levels 5/6 (C5/6). The majority of LAPN somata are found in the intermediate gray matter of L2/3 and have axonal projections that ascend in the outer rim of the spinal white matter through the ventrolateral funiculus (VLF) to C5/6. 46% of LAPNs project ipsilaterally, while 54% have axons that cross mid-line at or near the level of the cell body and ascend in the contralateral VLF.[91] The importance of L2, where LAPN somata reside, was elucidated by injecting kainic acid into the intermediate gray matter of rats. Independent of motoneuron loss, L2 injections resulted in severe locomotor impairments, compared to those at more rostral lumbar levels, indicating that somata in the intermediate gray matter of L2 are important to locomotor function [92,93]. Thus far, only one study has attempted to describe LAPN morphology. English *et al* [84] demonstrated that LAPN soma and dendrite morphology correlate with soma position in the intermediate gray matter in cats.

Despite the lack of anatomical knowledge, there have been attempts to classify the functional significance of LAPNs. Using a conditional and reversible dual-viral silencing system, LAPN function *in vivo* was characterized by Pocratsky *et al.*[94] and reproduced by Shepard *et al* [95]. This system allowed for LAPNs to be "silenced" for weeks to months and permitted evaluation of locomotion in awake, freely moving animals. LAPN silencing led to disruptions in the coordination of the contralateral forelimb-hindlimb pairs and in the left-right forelimb and hindlimb pairs but did not impact intralimb coordination. Interestingly, the disruptions in coordination were only apparent during non-exploratory overground locomotion on a high friction surface, and were not seen on low friction surfaces, during treadmill locomotion, or during swimming. These results indicate that LAPNs are a flexible, task-specific network of neurons involved in securing interlimb coordination. As little is known about LAPN morphology, further characterization of LAPN anatomy is necessary to understand the functional implications suggested in these studies.

Propriospinal neurons' role in recovered function following spinal cord injury

Clinically, most SCIs are anatomically incomplete with a rim of white matter remaining intact. This indicates that axons from LAPNs and other propriospinal systems are potentially intact and may provide pathways to relay information across the injury site [96,97]. Magnetic resonance images from clinical studies and histopathology from pre-clinical studies show that the superficial white matter within the ventrolateral funiculus, the location of propriospinal axons, is often spared. In these cases, the amount of tissue sparing correlates with functional outcomes, such as locomotion and lower limb

function [98,99]. Bareyre et al [100] first showed that following thoracic SCI, descending cervical propriospinal neurons with projections caudal to the injury were increasingly contacted by the CST and were maintained chronically. These new connections may represent an attempt to relay top-down signals caudal to the injury. Similarly, reticulospinal axons also sprout and form new contacts with descending propriospinals post-SCI [101,102]. Courtine et al [103] performed a staggered and delayed hemisection injury, leading to disruptions in all direct descending input from higher motor centers to the lumbar enlargement. Their findings suggested that subsets of descending propriospinal neurons are involved in detour circuit formation, which aid in the recovery of locomotor function. However, in a more clinically relevant model of SCI, silencing descending propriospinal neurons with somata at C6 and axon terminals at L2 in awake and freely moving rats led to improved locomotor function, indicating that this subset of LDPNs may be involved in injury-induced maladaptive plasticity [83]. These differences in findings are likely due to different injury models and the subsets of descending propriospinal neurons that were evaluated in each study. Nonetheless, the overall function of descending propriospinal pathways remains up for debate.

The field has primarily focused on the role of descending propriospinal neurons following SCI since Bareyre et al. and others have shown their role in the formation of detour circuits [101,104]. However, little effort has been put forth to evaluate the role of ascending propriospinal neurons post-SCI. This lack of effort is surprising given that previous studies that produced small lesions in the intermediate gray matter of L2, where LAPN somata reside, resulted in locomotor deficits similar to those seen

following severe spinal contusions [92,93]. To date, only Shepard et al.[95] have evaluated the functional relevance of LAPNs post-SCI and found that silencing LAPNs chronically post-SCI improved locomotor function. These improvements were characterized by improved in intralimb coordination, increased number of plantar steps, improved hindlimb interlimb coordination, and normalized spatiotemporal gait measures. These findings indicate that LAPNs play a potentially detrimental role to recovered locomotion via injury-induced plasticity. Several mechanisms could explain the study's results including 1) formation of maladaptive ascending detour circuits to relay sensory information caudal to the injury, 2) aberrant sprouting of LAPN axons onto new targets, or 3) changes in myelination that alter the timing of LAPN action potentials to their targets.

Therapeutics for spinal cord injury

Spinal cord injuries are heterogeneous, as they occur at all levels of the spinal cord and vary in degree of severity. Broadly, SCI pathophysiology occurs in two phases: the primary injury followed by secondary injury. The primary injury is due to the initial trauma commonly associated with spinal fracture or dislocation and leads to overt and irreversible damage to white and gray matter at the injury site. The secondary injury results from a cascade of physiologic events leading to impaired cellular function, apoptosis, ischemia, edema, excitotoxicity, free radical production, and tissue disruption [105,106]. Both primary and secondary injuries affect multiple cell types, induce secondary signaling cascades [107], cause aberrant plasticity throughout the CNS [102,108] and impact other organ systems [109-111], likely making the development of a universal cure for SCI implausible.

Previous attempts at treatments have focused on mitigating the extent of secondary injury and minimizing complications. One common clinical course of action involves surgical decompression and spinal stabilization, preferably within 24 hours of injury [112,113] and mitigation of thrombotic events via low molecular weight heparin [114,115]. Additionally, maintenance of mean arterial pressure at >85mm Hg likely improves patient outcomes and is reflected in current treatment guidelines.[116] Outside of these treatments, little progress has been made to mitigate the extent of the secondary injury. Preclinical and clinical investigation of potential treatments is vast, and for discussion purposes here will be broadly divided into the following categories: neuroprotective strategies, stem cell therapies, and neuroregenerative pharmaceuticals.

Neuroprotective strategies

Following SCI there is frank irreversible tissue loss at the injury epicenter. However, penumbral tissue adjacent the injury, while damaged, might be salvageable and if successfully targeted tissue sparing might be increased. Most notably, high dose methylprednisolone was previously recommended, as it is a potent anti-inflammatory and is used to treat neuroinflammation in multiple sclerosis [106,117]. Preclinical studies on the methylprednisolone's efficacy for SCI show mixed results [118-121]. However, the majority of clinical data suggest that methylprednisolone does not improve patient outcomes. In fact, methylprednisolone is not United States Food and Drug Administration (FDA) approved for use in SCI and its side effects may outweigh potential benefits [122,123].

Minocycline, a second-generation tetracycline antibiotic, has also shown promise in preclinical studies for improving function post-SCI [124-126]. This is in part due to minocycline being more lipophilic than other tetracyclines allowing for greater concentrations to be achieved in the CNS [127]. Minocycline acts via binding to a ribosomal subunit, ultimately preventing amino acid elongation. Halting amino acid elongation positively impacts many mechanisms that contribute to the secondary injury including inhibiting inflammatory cascades [125], mitigating apoptosis [128], reducing oxidative stress[125], and reducing edema [128,129]. There are three phase I-III clinical trials that have assessed the use of minocycline for acute SCI (NCT00559494, NCT01828203, NCT 01813240), however, only the one of these trials is completed and has reported results. Reported results include an *n* of 24 for the treatment group and reported no difference in adverse events between groups, but also no differences in functional outcomes [130].

Riluzole, a sodium channel blocker that is FDA approved for use in amyotrophic lateral sclerosis has been shown to have anticonvulsant, sedative, and neuroprotective properties in vivo [131-133]. Following SCI, ion imbalances lead to an increase in intracellular levels of sodium which produces an influx of calcium and subsequently causes an increase in glutamate release which can lead to excitotoxity (30 and 31). Riluzole acts by blocking sodium channels, preventing the increase in intracellular sodium, preventing the excitotoxic cascade, and limiting cell death [134,135]. Preclinical studies in rodents have shown that post-SCI Riluzole can improve functional outcomes [136-138] and increase tissue sparing [139]. There are three clinical trials listed for the use of Riluzole in SCI populations.

After enrolling 193 patients, the most recent phase II-III multicenter trial was terminated in 2020 due to challenges in enrollment [134].

Lastly, investigation into the use of Naloxone to treat SCI both in preclinical studies and in clinical trials follows the same pattern of outcomes noted for the aforementioned neuroprotective treatments. Preclinical data have shown signs of efficacy [140,141] but when tested in clinical trials Naloxone is not efficacious [142].

Stem cell therapies

The potential treatments in the previous section were aimed at mitigating the secondary injury via neuroprotection, however, stem cell therapies may replace the cells lost during the primary injury or remyelinate demyelinated or regenerating axons. Stem cell therapies to treat SCI may also provide trophic support endogenous cells [143,144], guide/assist axon regeneration [145], and/or have immunomodulatory effects [146,147]. The stem cell literature related to SCI is vast and is not a primary focus of the work here. Because of this, a cursory overview of this literature will be provided here so that findings of this dissertation may be interpreted within the scope of spinal cord injury treatments; for scoping reviews see Ahuja et al 2020 and Silvestro et al 2020 [148,149]. Querying clinicaltrials.gov for “spinal cord injury” and “stem cells” returns 61 clinical trials, the earliest of which was completed in 2010. Of these 61 trials, only 3 are phase III trials; the most recent of which (NCT01676441) was terminated in 2021 for undisclosed reasons. The only completed phase III trial was completed in 2015 (NCT01873547) and was supported by a small phase I/II trial,[150] but no results have been reported for the phase III trial. The lack of successful clinical trials for stem cell therapies is at least in part

due to lack of preclinical evidence to support them. One striking example of this was seen by Anderson et al.[151], who in a clinically relevant rodent model tested the efficacy of two stem cell lines that were intended use in a phase II clinical trial (NCT02163876). They found that one of the cell lines tested was not efficacious, despite this the phase II trial used these cells and was terminated in 2016 due to lack of efficacy.

Neuro-regenerative therapies

Promoting neurite growth either collateral spouting or frank axon regeneration has been a therapeutic strategy to treat SCI as there is frank axon disruption due to the injury, which impacts circuitry throughout the neuroaxis [152,153]. Approaches to do so have included modification of cell extrinsic factors that inhibit growth such as perineural nets and the glial scar [154,155] or targeting cell intrinsic factors to promote growth [156,157]. Of these approaches, targeting the inhibitory neurite growth factor Nogo-A or targeting Rho which is a convergent signal for growth inhibition are the only potential treatments that have moved into clinical trials. Preclinical data are convincing that genetic deletion or therapeutic inhibition of Nogo-A induces axon regeneration and/or sprouting [158]. However, its effects on functional outcomes vary[158,159]. Despite this, two phase two trails were completed in 2022 (NCT03935321) and in 2023 (NCT03989440), but results from neither are currently available.

Similar to Nogo-A inhibition, inhibit of Rho also leads to enhanced neurite outgrowth [160] and there are numerous Rho antagonists that have been shown to enhance axon regeneration in vivo preclinically [156]. The majority of preclinical data suggest that Rho antagonists improve functional outcomes [156,161,162]. The clinical grade

Rho antagonist, Cethrin, readily crosses cell membranes in a nonspecific manner and is easily administered via direct application to the dura [158]. To date, two clinical trials have used Cethrin in acute SCI populations. The phase I/II trial (NCT00500812) was completed in 2009 and established safety in the patient population [157], however the subsequent phase II/III trial (NCT02053883) enrolled no patients and was withdrawn due to restructuring of the sponsor company.

Targeting the spinal cord for gene therapy

As the majority of phase II/III clinical trials mentioned above have either been withdrawn or lacked efficacy, the development of new therapeutics for spinal cord injury is paramount. Gene therapy approaches provide a flexible and promising new avenue for potential treatments, and there are currently two FDA approved gene therapies targeting the CNS. The first is Zolgensma that was approved in 2019 for treating spinal muscular atrophy [163] and second, Luxturna which was approved in 2017 for treating retinal dystrophy [164]. Both Zolgensma and Luxturna utilized adeno-associated viral vectors (AAVs), as AAVs provide a flexible platform that can be modified for targeted delivery. The AAV capsid can be modified which results in a different serotype. Capsid modifications can alter cellular tropism, impact rate of viral degradation, modify transgene expression, and if administered via direct injection alter spread at the injection site [164-169]. Additionally, the promoter selected can be ubiquitous for expression in all transduced cells, or cell specific to drive transgene expression in target cell populations [170,171]. Other advantages to using AAVs include long-term stable gene

expression in neurons, minimal toxicity at low doses, and high titer production for preclinical studies is easily [172-174].

Despite AAVs providing a flexible therapeutic platform, their use does not come without challenges. First, AAVs have a packaging capacity of 4.7 kilobases [175], which limits the size of potential therapeutic vectors. Second, while AAVs are commonly thought to cause little toxicity; high doses AAV delivered intravenously causes dorsal root ganglia toxicity [176,177] and slightly higher doses used in a clinical trial (NCT03199469) resulted in multiple patient deaths [178]. Lastly, production costs for the titers needed to target the CNS clinically are exceptionally high, as evident by the cost of Zolgensma at 2.1 million USD per dose. However, the high AAV dose used for Zolgensma, is required to as it is delivered intravenously. For IV delivery AAV dose must be high for 2 reasons: 1) most AAV serotypes in the bloodstream target and are expressed off target tissues such as the liver [179,180] and 2) most AAV serotypes do not readily cross the blood spinal cord (or blood brain) barrier (BSCB) to target neurons [181,182].

Other routes of administration such as intrathecal or intracerebroventricular AAV delivery bypass the BSCB but still confer transgene expression throughout the neuroaxis [183,184]. Focal targeting in the CNS is achievable via intraparenchymal injection but this involves invasive and potentially risky surgery. Given the benefits and disadvantages of each route of delivery, gene therapies utilizing AAVs to target the spinal cord would ideally have both ease of administration of intravenous delivery and the specificity of intraparenchymal injections. Two preclinical studies have, to some degree, achieved this and successfully targeted spinal segments adjacent to the lesion by IV injection of AAV9

within 3 hours of the injury while the BSCB is compromised [185,186]. While successful, this strategy has a limited time window for successful delivery and the viral dosages used exceeded those that caused patient deaths in a clinical trial (NCT03199469).

A potential approach to overcome the limitations of IV AAV delivery is the use of focused ultrasound plus IV microbubbles (FUS-MB). The microbubbles used are made a lipid monolayer, contain perfluorocarbon (a biologically inert gas), and are commonly used clinically to enhance contrast during ultrasound imaging [187,188]. Following IV microbubbles administration, low intensity ultrasound can be focused on the area of interest in the CNS and results in transient disruption of the BSCB (or BBB) without tissue damage allowing for a spatially and temporally restricted delivery of therapeutics to the target area [189]. Importantly, this temporary disruption of the BSCB is accompanied by a decrease in tight junction proteins and an increase in active transport proteins, both of which aid successful delivery of the therapeutic [189-191]. Numerous preclinical studies for Parkinson's diseases, Alzheimer's' disease, and Huntington disease have successfully delivered AAVs to the brain via this method [192,193], but only one study has attempted the spinal cord. Weber-Adrian et al [194] targeted the cervical spinal cord in rats and while expression of the AAV transgene is seen focally in the cervical spinal cord, the data are not convincing that neurons were successfully targeted. Additionally, they report off target expression in liver and skeletal muscle. Thus, this approach need be refined further if successful clinical translation is the goal.

Summary

As Shepard et al [83] surprisingly found that LAPNs post-SCI play a potentially detrimental role in recovered locomotion and that little is known about LAPN anatomy, a primary focus of this dissertation will be to characterize LAPNs pre- and post-SCI. To do so, target-defined labeling of LAPNs will be optimized (chapter 2) so that LAPN somata, dendritic, and axonal morphologies can be characterized in the non-pathologic spinal cord (chapter 3) and allow for the evaluation of SCI induced anatomic plasticity of LAPNs (chapter 3). Furthermore, as there is a clear need to develop treatments for SCI, the potential to non-invasively target the lumbar enlargement using ultrasound + intravenous microbubbles will be tested (chapter 4). Following optimization of this technique, it will be used to assess if spatially regulated and cell specific gene transfer to the lumbar enlargement is possible via intravenous delivery of adeno-associated viral vectors.

CHAPTER II

DUAL-VIRAL TRANSDUCTION UTILIZING HIGHLY EFFICIENT RETROGRADE LENTIVIRUS IMPROVES OF LABELING OF LONG PROPRIOSPINAL NEURONS.

The nervous system coordinates pathways and circuits to process sensory information and govern motor behaviors. Mapping these pathways is important to further understand the connectivity throughout the nervous system and is vital for developing treatments for neuronal diseases and disorders. We targeted long ascending propriospinal neurons (LAPNs) in the rat spinal cord utilizing Fluoro-Ruby (10kD rhodamine dextran amine, or RDA), and two dual-viral systems. Dual-viral tracing utilizing a retrograde adeno-associated virus (retroAAV), which confers robust labeling in the brain, resulted in a small number of LAPNs being labeled, but dual-viral tracing using a highly efficient retrograde (HiRet) lentivirus provided robust labeling similar to Fluoro-Ruby. Additionally, dual-viral tracing with HiRet lentivirus and tracing with Fluoro-Ruby may preferentially label different subpopulations of LAPNs. These data demonstrate that dual-viral tracing in the spinal cord employing a HiRet lentivirus provides robust and specific labeling of LAPNs and emphasizes the need to empirically optimize viral systems to target specific neuronal population(s).

Introduction

Understanding the complexity and specificity of neural pathways and circuits in the mammalian nervous system is a major goal for neuroanatomists and is vital to

understand and treat nervous system injuries and disorders [195-200]. The development and refinement of technologies such as functional near-infrared spectroscopy [201,202], diffusion weighted magnetic resonance imaging [203,204], and resting-state functional magnetic resonance imaging [200,205] have enhanced our understanding of macroscale connectomics, and improved patient treatments and outcomes [206-208]. Mesoscale connectomics – characterizing a single population of neurons and/or connectivity of those neurons – has made similar progress [196,197], but traditional tracers such as horseradish peroxidase, cholera toxin subunit B, (CTB) hydroxystilbamidine (known commercially as Fluoro-Gold) and conjugated dextran amines (which include biotinylated dextran amine, or BDA, and rhodamine conjugated dextran amine, or RDA, also known as Fluoro-Ruby or Mini Ruby depending on molecular weight) remain the most widely used technique. These traditional tracers allow for anterograde or retrograde tract-tracing and are valuable for revealing the locations of neurons projecting to or from an area of interest and have been widely used throughout the nervous system for more than 3 decades [195,209,210]. Despite their extensive use, each of these traditional tracers has limitations including the potential of labeling any/all neurons projecting to or from an area. More specifically, dextran amines can be taken up by axons damaged during injection procedures [211], long-term exposure to Fluoro-Gold can be neurotoxic [212], Fluoro-Gold and CTB can inadvertently be taken up by fibers of passage [213,214], and biotin conjugates of CTB can be transneuronal [215], all of which may hinder mesoscale connectomic analyses.

Targeted genetic manipulations and an improved understanding of neurotropic viruses have overcome some of the limitations of traditional tracers and allowed for precise targeting of pathways and evaluation of connectivity throughout the central nervous system (CNS) [216-219]. Since 1998, adeno-associated viruses (AAVs) have been widely used for CNS tract-tracing [172]. AAVs are neurotropic, permit long-term stable gene expression in neurons, cause little toxicity, and high titer production is easily achieved [172,173,220]. While viral-based tracing using AAVs or other vectors offers advantages over traditional tracers, there are numerous variables that must be understood and optimized if robust and specific tracing is to be achieved. For example, altering the AAV capsid, and therefore the serotype, impacts cellular tropism and changes the volumetric spread at the injection site [167,169,221,222] and AAV dosage - volume and titer - influences cellular tropism, transgene expression, and the direction of viral transport [171,223,224]. Even the purification method and route of delivery can alter AAV transduction [225,226]. Similarly, when using lentiviral vectors for CNS transduction, altering the viral envelope can impact transduction efficiency, immune response, and the direction of viral transport [227-230].

An improved understanding of viral vector transduction in the CNS, in combination with other technologies such as transgenic labeling and traditional tracers, has led to projects such as the Allen Mouse Brain Connectivity Atlas which has provided a high-resolution map of the mouse brain connectome [7]. However, viral-based tracing for targeting and mapping the spinal cord has not received as much attention. The main goal of the current study was to evaluate various tracing methods for targeting long ascending propriospinal neurons (LAPNs) in the rat. LAPNs are an ideal system for this

as, they have relatively long axons, they have been found in numerous species, and they have similar numbers of ipsi- and contra-lateral projections [82,87,91,94]. We utilized Fluoro-Ruby (FR), a 10kD rhodamine-conjugated dextran amine, as well as two dual viral systems for target-defined projection labeling (Figure 1 A,C,E) [198]. AAV2 containing a Cre-dependent flip-excision switch (FLEx) was injected at the level of the cell bodies, lumbar levels 2-3 (L2-3) [219]. For retrograde transduction and Cre delivery, either the retroAAV developed by Tervo et al. [173] or the HiRet lentivirus developed by Kato et al. [231], was injected at the level of LAPN axon terminals, cervical 5-6 (C5-6) (Figure 1). For either of these vectors to provide efficient retrograde transduction and subsequent FLEx recombination and labeling of LAPNs, the vector must readily infect axon terminals, undergo retrograde transport, and deliver its cargo to LAPN nuclei.

The process of quantifying labeled neurons in spinal cord tissue sections can be problematic. While the accuracy of manually counting is high, it is inefficient and introduces human error. To improve reproducible counting and reduce the time required for the quantification of large numbers of tissue sections, we developed a custom application using MATLAB® (ver. R2019a) to accurately count the number of labeled cells. The application developed allows for easy navigation through large numbers of tissue sections and lets users overlay anatomical maps or grids for more detailed quantification. The application can be downloaded at https://github.com/rachz18/CellCountingApplication.git, an instructional video for successful use of the application can be found here https://vimeo.com/485620502, and

details of the program along with written directions can be found in *supplemental document 1*.

Materials and Methods

Tracer and virus preparation

10% stocks of FR were made by dissolving 10 mg of FR dry powder in 100 μL of distilled water, and 10 μL aliquots were stored at -20°C. FR aliquots were thawed the morning of injection surgeries. 100 μL of AAV2-FLEx-GFP ($3.7x10^{12}$ vp/mL) and of retroAAV2-CAG-Cre ($5.3x10^{12}$ vg/mL) (referred to here as *retroAAV-Cre*) were ordered from the Gene Therapy Center Vector Core at the University of North Carolina at Chapel Hill. Ten μL aliquots of each were made, stored at -80°C, and thawed the morning of injection surgeries. HiRet-Cre ($1.6\text{-}2.0x10^{10}$ vg/mL) was produced by Zhigang He's laboratory (Boston Children's Hospital) using previously described methods [232]. Ten μL aliquots of Lenti-HiRet-Cre were stored at -80°C and thawed the morning of injection surgeries.

Stereotaxic spinal cord injection surgeries

This animal study was reviewed and approved by the University of Louisville Institutional Animal Care and Use Committee. A total of *N* = 12 female Sprague Dawley rats (200-220 g: Envigo) were evenly divided among the groups (*N* = 4 per group). Prior to surgical procedures, animals were housed two per cage with *ad libitum* food and water under 12 h light/dark cycle. Glass micropipettes for intraspinal injections were pulled from borosilicate glass capillaries (World Precision Instruments, Inc.) using a

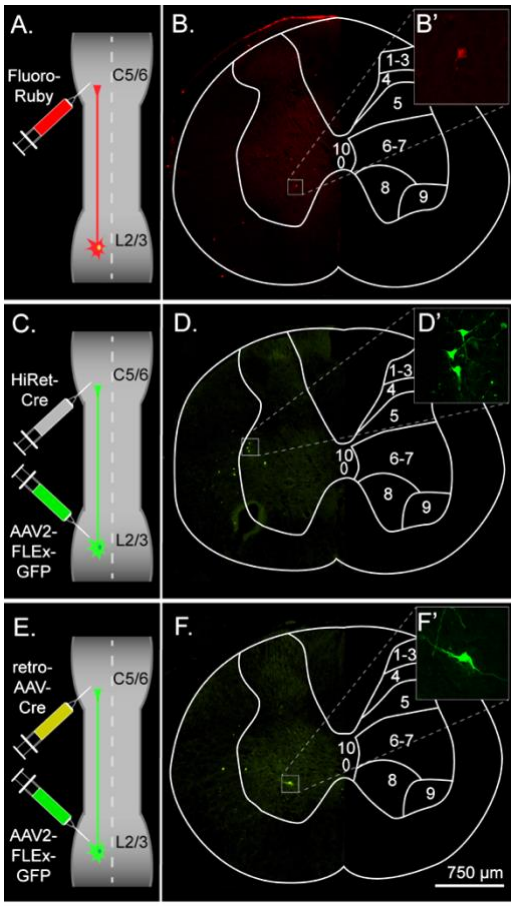

Figure 1. Experimental design and overview for labeling left ipsilateral long ascending propriospinal neurons (LAPNs) in the adult rat. (A) The chemical tracer Fluoro-Ruby was injected ipsilaterally at C5-6. (B) Lumbar spinal cord cross section showing labeled neurons from Fluoro-Ruby group. Inset shows 40x image of labeled LAPN. (C) HiRet-Cre was injected ipsilaterally at C5-6 and AAV2-FLEx-GFP ipsilaterally at L2-3. (D) Lumbar spinal cord cross section showing labeled neurons from the HiRet-Cre group. Inset shows 40x image of labeled LAPN. (E) retroAAV-Cre was injected ipsilaterally at C5-6 and AAV2-FLEx-GFP ipsilaterally at L2-3. (F) Lumbar spinal cord cross section showing labeled neurons from the HiRet-Cre group. (B',D',F') Maximum intensity projections of confocal z-stacks illustrate the intensity and detail of labeled cells.

micropipette puller (Sutter Instrument Co.) and the following parameters: heat = 600, pull = 29, velocity = 57, and time = 150. Pipettes were trimmed to an external diameter of 25 μm, beveled using a micropipette beveller (World Precision Instruments, Inc.), and sterilized with 100% ethanol prior to use. The morning of injection surgeries, individual tracers/viruses were loaded into pipettes and viral pipettes were kept on ice between surgeries to minimize viral degradation.

Animals were anesthetized with a mixture of ketamine, xylazine, and acepromazine (40 mg/kg, 2.5 mg/kg, and 1 mg/kg, i.p.), and supplemented with 1-2.5% isoflurane in 98% oxygen at a rate of 1L/minute as needed. For FR injections, animals were placed into a custom-built spinal stabilization unit [233] and received a C5-6 laminectomy and durotomy to expose spinal levels C5-6. Two, 0.25 μL boluses of FR were injected at same site into the left intermediate gray matter of C5-6 (0.55 mm mediolateral, 1.2 mm dorsoventral) using a stereotaxic device (World Precision Instruments, Inc.) [234]. Boluses were injected 2 minutes apart to allow FR to spread throughout the tissue, mitigate extravasation from the injection site, and minimize pressure exerted on the tissue at the injection site. This volume was used as the rostrocaudal spread within the spinal gray matter at the injection site was similar to the rostrocaudal spread of volume of virus(es) injected (data not shown).

For viral injections, animals were placed into the spinal stabilization unit, received a laminectomy and durotomy at thoracic vertebrae 12 to expose spinal L2-3, and a C5-6 laminectomy and durotomy to expose spinal C5-6. Two, unilateral injections of either of HiRet-Cre or retroAAV-Cre were injected into the left intermediate gray

matter of C5-6 (0.55 mm mediolateral, 1.2 mm dorsoventral, 1.3 mm rostrocaudal). The two injections were given in two, 0.25 μL boluses with 2 minutes between injections. AAV2-FLEx-GFP was injected into the intermediate gray matter of L2-3 (0.5 mm mediolateral, 1.35 mm dorsoventral, 1.3 mm rostrocaudal) using the same injection protocol as the C5-6 injections. Following injections, incision sites were sutured in layers and wounds closed with surgical staples. Gentamicin (20 mg/kg) and saline were given subcutaneously prior to animals waking, buprenorphine (10 mg/kg, s.c.) was administered every 12 hours for 48 hours post-surgery for pain management, and prophylactic doses of gentamicin (20 mg/kg, s.c.) were administered for 7 days. Animals were single housed until surgical staples were removed 7 days post-surgery.

Tissue processing, imaging, and manual quantification.

Two weeks following FR injections, and 3 weeks following viral injections, animals were anesthetized using a cocktail of ketamine, xylazine, and acepromazine (40 mg/kg, 2.5 mg/kg, and 1 mg/kg, i.p.), and transcardially perfused with phosphate-buffered saline (pH 7.4) followed by 4% paraformaldehyde. Spinal cords were harvested, post-fixed in 4% paraformaldehyde for 1-2 hours, and transferred to 30% sucrose for 3-4 days at 4°C. L1-4 spinal segments were isolated, embedded in tissue freezing medium, cryosectioned at 30 μm, slide mounted, and stored at -20°C. For coverslipping, slides were warmed, rinsed in PBS for 5 minutes, coverslipped with Fluoromount-G (SouthernBiotech), and air dried overnight.

Every other tissue section was imaged to avoid double counting labeled propriospinal neuron cell bodies. Images were acquired using a Nikon TiE 300 inverted

microscope (Nikon). A 10x objective was used to create a 3x3 stitched image using Nikon Elements Advanced Research software (Nikon). A Texas Red filter was used for FR labeled tissue and green fluorescent protein (GFP) filter used for GFP viral labeled tissue. Following acquisition, all images were converted to grayscale and manually counted by a single blinded individual. Lamina counts were performed by overlaying segmental lamina maps [235] onto each of the tissue sections in Illustrator (Adobe).

FR injected at C5-6 has the potential to retrogradely label any neuron with a projection at or near the injection site and we found labeled neurons at all spinal levels that were cryosectioned (L1-4). However, the rostrocaudal spread of labeled neurons at L2-3 in both viral labeled groups is limited by the rostrocaudal spread of the virus at the injection site(s) and the need for dual viral transfection to confer labeling. For equal comparison between groups, the number of quantified sections in the FR group was limited to 61 tissue sections per animal, the average number of sections quantified in the viral labeled groups. Additionally, 1 animal in the HiRet group was excluded from analyses for total and relative number of labeled neurons as the rostrocaudal spread of labeled neurons was half of that seen in all other virally labeled animals; this is likely attributable to an inaccurate or missed intraspinal injection.

MATLAB application development, quantification, and validation.

A custom application was built using MATLAB and incorporates the image processing techniques color thresholding and boundary determination to determine the number of labeled cells within a user-specified region of interest in the spinal cord. Of the cell detection methods utilized in the MATLAB program, the elimination of

background involves pixel-based thresholding, while cell counting is a combination of pixel and object-based detection based on image properties. First, the background of the image is eliminated using thresholding by labeling color and pixel value. Cells are then detected and counted based on the image region properties of pixel area and eccentricity. Pixel area is defined as the actual number of pixels within a region, while eccentricity is the ratio of the distance between the foci of the ellipse and its major axis length for each object region. The application was integrated into an interactive application and graphical user interface (GUI) created with MATLAB's AppDesigner. The GUI enables users to seamlessly navigate through a large number of images, while the semi-automated cell counting function eliminates variability between users and reduces quantification time. The application also allows user to easily overlay anatomical maps or grids for more detailed quantification. To validate the accuracy of the MATLAB application, the number of labeled somata counted using the application was compared to the number of somata counted manually and the correlation between the counting methods assessed. The application has been uploaded to an online data repository and can be accessed using this source code/DOI link for public use: https://github.com/rachz18/CellCountingApplication.git. The instructional video (https://vimeo.com/485620502) provides a step-by-step tutorial for the program, and written instructions are in *supplemental document 1*.

Statistical analyses.

Results for the total and relative number of somata labeled between groups were compared using an analysis of variance followed by Tukey HSD *post hoc* t-tests using

SPSS version 22 (IBM). Results for the percent of labeled somata by lamina were compared using a multivariate analysis of variance followed by Tukey HDS *post hoc* t-tests where appropriate in SPSS. P values for all analysis were considered statistically significant when $p. \leq 05$, and two-tailed p values are reported for *post hoc* t-tests. Pearson correlation was performed to evaluate the relationship between counting methods using RStudio version 1.2.5042. Results for the differences between counting methods by group were assessed using a one-way analysis of variance followed by a Tukey HSD *post hoc* t-test using SPSS.

Results

Tracing methods have different efficiencies

To understand the differences in efficiency between tracing methods, we evaluated the total number of neurons labeled and the number of neurons labeled per tissue section. The total number of labeled neurons (mean ± SD; FR: 135.5 ± 52.29, HiRet: 126.33 ± 45.79, retroAAV: 31.5 ± 10.15) was significantly higher in the FR and HiRet groups compared to the retroAAV group (Figure 2A). The relative number of labeled neurons was evaluated by normalizing the number of labeled neurons to the number of sections counted (mean of labeled neurons per section ± SD; FR: 2.12 ± 0.76, HiRet: 2.35 ± 0.47, retroAAV: 0.50 ± 0.13). After normalization, the same differences between groups were seen, with significantly fewer labeled cells in the retroAAV group compared to the FR and HiRet groups (Figure 2B). These results indicate that tracing LAPNs with FR or target-defined projection labeling utilizing HiRet lentivirus provide robust labeling of LAPNs, while target-defined projection labeling using retroAAV significantly reduced labeling of

LAPNs. Additionally, as seen in Figure 1B, D, F, the prominence, and detail of labeled neurons differed between FR and virally labeled neurons, with viral labeled neurons often being brighter and easier to identify. However, signal from both viral and FR labeled neurons can be amplified using immunohistochemistry and labeling with a lower molecular weight dextran amine can further improve signal as these dextran amines are more efficiently trafficked [236].

Specificity of labeling is influenced by tracing methods.

To evaluate differences in specificity of tracing and to determine whether tracing methods preferentially labeled a subset of ipsilateral LAPNs the laminar distribution of the labeled cells was assessed by comparing the percentage of labeled neurons in each lamina (Figure 3). For the absolute number of labeled neurons by animal and lamina see *Supplementary table 1*. In lamina 6-7, a greater percentage of neurons was found in the retroAAV group. The retroAAV group also had significantly fewer neurons labeled in lamina 9. In lamina 10, the percentage of neurons was significantly higher in the HiRet group compared to the other groups. These differences in laminar distribution indicate that tracing methods can impact the specificity of labeling either by preferentially targeting a subset of the neuronal population of interest or by random chance. MATLAB application was assessed. Cell counts using either method were highly correlated with one another (Figure 4A), indicating that the MATLAB application is as accurate as manual counting.

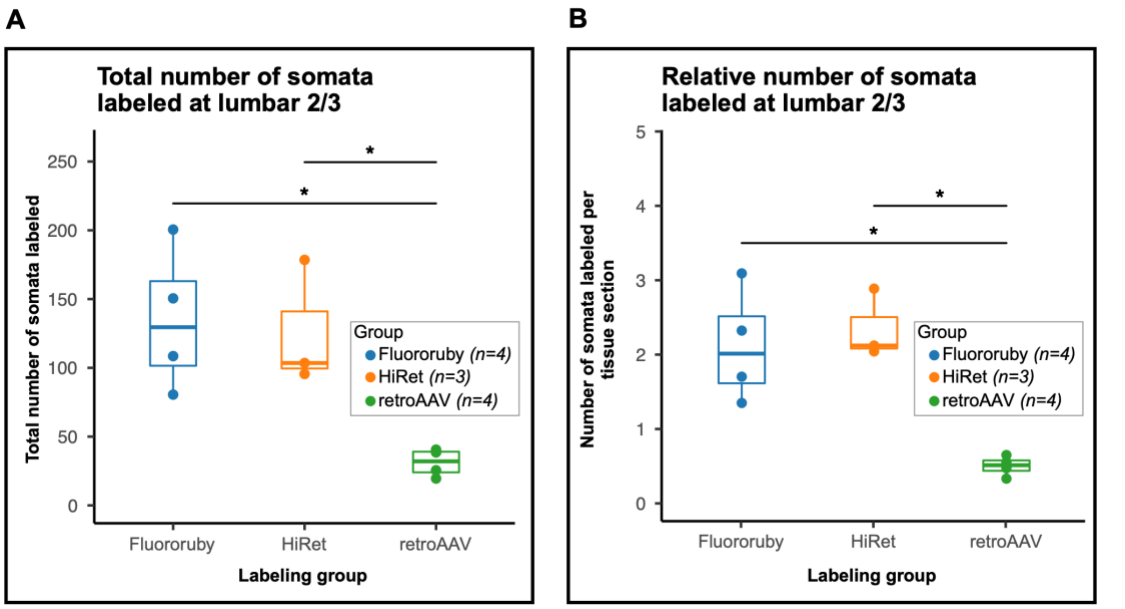

Figure 2. The number of labeled neurons in the lumbar spinal cord is significantly impacted by the tracing method(s) used. (A) The total number of labeled neurons differed between groups (One-way Analysis of Variance (ANOVA), F = 13.5, df = 2,8, p = .003) and was lower in the retroAAV group (Tukey's Honest Significant Difference (HSD) post hoc, FR vs. retroAAV, p = .015; HiRet vs. retroAAV, p = .034). (B) When normalized to the number of tissue sections counted the number of labeled neurons differed between groups (One-way ANOVA, F = 8.6, df = 2,8, p = .01) and was significantly lower in the retroAAV group (Tukey's HSD post hoc, FR vs. retroAAV, p = .006; HiRet vs. retroAAV p = .005). (A,B) Tukey style box plots. Bold center line shows median, upper hinge shows 75th percentile, lower hinge shows 25th percentile, whiskers represent 1.5 times the interquartile range. Individual data points shown for clarity. (p < .05*, ANOVA and Tukey's HSD post-hoc t-tests).

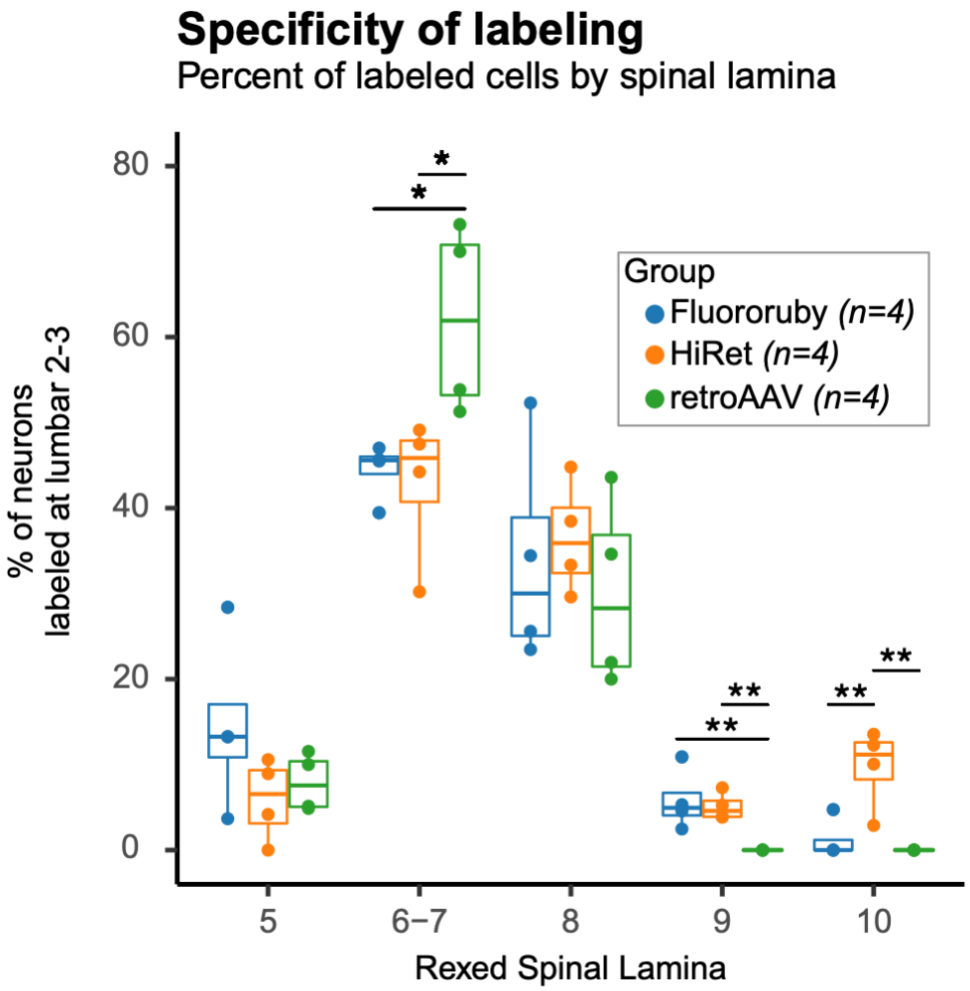

Figure 3. Specificity of labeling is impacted by the tracing method used. Percentages of labeled neurons in Rexed spinal lamina differed between lamina and groups. The retroAAV group had a significantly higher percentage of labeled neurons in lamina 6-7 (Multivariate Analysis of Variance (MANOVA), F = 6.6, df = 2,9, p = .017; Tukey's HSD post hoc, retroAAV vs. FR, p = .037; retroAAV vs. HiRet, p = .024) and a significantly lower percentage of labeled neurons in lamina 9 (MANOVA, F = 7.7, df = 2.9, p = .01; Tukey's HSD post hoc, retroAAV vs. FR, p = .014; retroAAV vs. HiRet, p = .028). The HiRet group had a significantly higher percentage of labeled neurons in lamina 10

(MANOVA, F = 7.7, df = 2.9, p = .01; Tukey's HSD post hoc, retroAAV vs. FR, p = .014; retroAAV vs. HiRet, p = .028). Tukey style box plot. Bold center line shows median, upper hinge shows 75th percentile, lower hinge shows 25th percentile, whiskers represent 1.5 times the interquartile range. Individual data points are shown for clarity. Data points falling outside of whiskers are outlying points that are < or > 1.5 times the interquartile range. (p < .05*, p < .01**, MANOVA and Tukey's HSD post hoc t-tests). Mean percentage +/- standard deviation for each lamina and group (FR, HiRet, and retroAAV): lamina 5 (14.6 +/- 10.2, 5.9 +/- 4.8, 7.9 +/- 3.4), lamina 6-7 (44.4 +/- 3.4, 42.8 +/-8.6, 62.1 +/- 11.1), lamina 8 (33.9 +/- 13.1, 36.6 +/- 6.6, 30.0 +/- 11.1), lamina 9 (5.8 +/- 3.6, 5.1 +/- 1.6, 0.0 +/- 0.0), and lamina 10 (1.2 +/- 2.4, 9.7 +/- 4.8, 0.0 +/- 0.0)

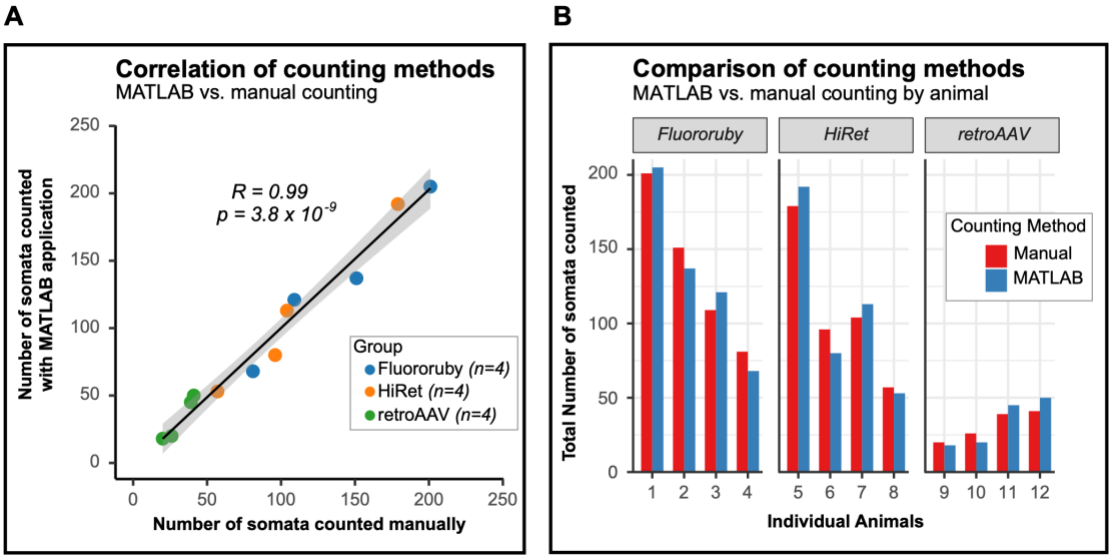

Figure 4. The number of labeled neurons counted with the MATLAB program and manually counting are similar and correlated. (A) The number of neurons counted is highly correlated between the MATLAB program and manual counting. Black line indicates line of best fit, gray outline indicates 95% confidence interval. (Pearson correlation: R = 0.99 and p = 3.8×10^{-9}) (B) Animal-by-animal comparison of the number of labeled neurons in the lumbar spinal cord, the difference between counting methods was similar between groups (One-way ANOVA, F = 1.7, df = 2,9, p = .247).

As previously noted, the prominence and detail of labeled neurons differed between FR labeled and virally labeled neurons, with viral labeled neurons being brighter. The poor cellular filling of FR labeled LAPNs may make it difficult for the MATLAB application to detect these neurons. To evaluate potential errors of the MATLAB application in identifying chemically versus virally labeled neurons, absolute differences in the number of neurons counted using each method were calculated and compared between the groups (mean difference scores ± SD; FR: 10.75 ± 4.67, HiRet: 10.50 ± 5.20, retroAAV: 5.75 ± 2.87). These differences were not significant between groups and are visualized animal-by-animal in Figure 4B. Taken together, these results show that the MATLAB application is as accurate as manual counting for quantifying labeled propriospinal neurons and that the application reliably identifies both virally- and chemically-labeled neurons.

Discussion

Efficiency of labeling methods.

Traditional tracers, such as CTB, Fluoro-Gold, and various dextran amines have been extensively characterized in multiple species for tract-tracing throughout the CNS [195,209]. However, each of these tracers comes with its own caveats. Dextran amines may inadvertently label damaged fibers of passage [211], Fluoro-Gold is neurotoxic [212], and Fluoro-Gold and CTB can label fibers of passage. [213,214]. To circumvent these potential limitations and gain a better understanding of viral tropism in the spinal cord, we targeted left ipsilateral LAPNs using target-defined projection labeling [198]. For cell body transduction, AAV2 was chosen over other serotypes as: 1) AAV2 has high neuronal

tropism [167,237,238], 2) AAV2 has minimal volumetric spread at the injection site [167,221], 3) unlike other serotypes, AAV2 has little potential for retrograde transduction [223,239,240], and 4) AAV2 does not spread transsynaptically like AAV1 and AAV9 [218]. These AAV2 characteristics allow precise targeting of the neuronal cell bodies at the injection site. For retrograde transduction and Cre delivery, we utilized the retroAAV serotype developed by Tervo et al. [173] and the HiRet lentiviral vector developed by Kato et al. [231]. While we found similar numbers of labeled neurons at L2-3 in the FR and HiRet groups, the retroAAV group showed a 76% decrease in the number of labeled neurons. This is somewhat surprising, as Cre activity is catalytic [241,242]. Thus, little Cre expression is needed for FLEx-switch recombination, subsequent transgene expression, and neuronal labeling. One potential explanation for these findings is poor infectivity of LAPN axon terminals. The retroAAV serotype was developed via directed evolution for optimal retrograde transduction of mouse corticopontine neurons [173], but its retrograde transduction of rat LAPNs was modest. RetroAAV has also shown preferential tropism for layer 5 of the cortex when compared to other viral tracers [243]. As the receptor/co-receptor for this serotype are currently unknown, this modest labeling may result from poor viral uptake at LAPN axon terminals due to little expression of the requisite receptor and/or co-receptor for internalization of retroAAV virions.

Previous studies have shown that changes to the AAV capsid impact the rate of viral degradation and subsequent transgene expression [165,166,244]. It is possible that a similar phenomenon is responsible for the poor labeling in the retroAAV group here, as the VP1 region of the AAV2 capsid was altered to produce the retroAAV [173]. These

mutations may result in increased phosphorylation of viral particles, subsequent ubiquitination, and proteasomal degradation of retroAAV in propriospinal neurons [244-246]. Lastly, the poor labeling in the retroAAV group may reflect a length-dependent issue, as rat LAPN axons are 6.2-7.6 cm long [247], approximately 10 times longer than the mouse corticopontine axons (6-7 mm) the retroAAV was developed to target [7,173]. This may result in poor retrograde trafficking of endosomes containing retroAAV virions. However, Weiss et al. [248] recently showed successful retrograde transduction of numerous cortical regions in rhesus macaque following intra-caudate and intra-putamen injections. Therefore, we do not believe the poor labeling by retroAAV here is a length-dependent issue. Rather, that this is due to poor uptake and infectivity of retroAAV at propriospinal axon terminals, which may reflect little to no expression of the receptor/co-receptor needed for the retroAAV serotype binding at propriospinal axon terminals.

Specificity of labeling methods.

The current data corroborate previous findings that LAPNs in the rat are positioned throughout the intermediate gray matter of the lumbar spinal cord, with the majority residing in laminae 6-8 [85,94,234]. This finding was consistent irrespective of the tracing method utilized. We found a higher percentage of labeled neurons in lamina 10 in the HiRet group. Previous studies found that 12.6% of L2-3 LAPNs reside in lamina 10 [94], and that large number of LAPNs are located in lamina 10 [85]. The higher percentage seen in the HiRet group here likely reflects the superior retrograde transduction efficiency of HiRet vectors and its ability to efficiently infect LAPN axon terminals compared to retroAAV. Additionally, in the retroAAV group, there was a greater

percentage of labeled neurons in lamina 6-7 and fewer in lamina 9 compared to the other groups. These differences reflect either preferential retrograde transduction - or lack thereof - of LAPN sub-populations or are due to a small number of neurons in any lamina resulting in a large percentage change in this group. LAPNs are a heterogenous population of neurons that project ipsi- and contra-laterally [91,94], have both excitatory and inhibitory neurotransmitter phenotypes [82,94], and have varied soma sizes (unpublished data). Future studies may evaluate the neurotransmitter phenotype and soma size of neurons labeled by these tracing methods to determine if differences in the laminar distributions are due to preferential labeling or random chance.

We previously used CTB to retrogradely label LAPNs and found a significantly higher percentage of labeled LAPNs in lamina 5 compared to target-defined projecting labeling with a HiRet vector [94]. As CTB can be taken up by fibers of passage [213], we attributed this difference to inadvertent labeling of lumbar spinocerebellar neurons, a majority of which reside in lumbar lamina 5 [249]. While we do not report the same finding with Fluoro-Ruby here, it is important to note that the uptake of dextran amines - such as Fluoro-Ruby - by damaged axons is more efficient than its uptake by axon terminals [211]. Thus, when injecting dextran amines, the procedures should minimize damage to the tissue that may occur from osmotic or mechanical pressures.

Validation of MATLAB Application.

Our MATLAB application has semi-automated the quantification of spinal cord labeling, which reduces time, minimizes human error, and allows for anatomical diagrams, such as spinal cord Rexed laminae maps to be easily overlaid on tissue

sections for further anatomic characterization. The strong correlation between manual cell counts and those from the MATLAB application (Figure 4A), in conjunction with there being no difference in the error between counting methods for all labeling methods (Figure 4B), emphasizes the accuracy of the MATLAB application for various tracing methods. The detection and counting methods employed in the MATLAB application are effective for small populations of labeled neurons whose boundaries are well defined such as LAPNs, it may not be as effective for larger neuronal populations with more densely packed cells. To accurately detect densely packed cells more advanced object-based detection methods such as edge detection and watershed algorithms might be needed. The program also only extracts either red or green color channels, and if multiple channels are to be detected the images would have to be analyzed twice with each color being counted separately. The application is freely available (https://github.com/rachz18/CellCountingApplication.git) and aims to provide a user-friendly application that allows for easy navigation through large numbers of images and the option to overlay anatomical diagrams for further analysis.

Target-defined projection labeling utilizing HiRet vectors showed improved retrograde transduction efficiency compared to retroAAV in the population of propriospinal neurons studied here. This provides the framework for more advanced mesoscale connectomics. This target-defined dual viral approach might also be adapted for exogenous gene expression for therapeutics targeting an anatomically defined set of propriospinal neurons. For these therapeutic approaches to be viable the immune response reported when using lentiviral HiRet vectors must be mitigated [228]. Tanabe et

al. [228] found that lentiviral NeuRet vectors which utilize the fusion E glycoprotein, rather than the fusion B2 glycoprotein used in HiRet vectors, produced no immune response in the primate brain. However, others have reported poor retrograde transduction efficiency of NeuRet vectors when targeting hindbrain and spinal motoneurons [227]. Prior to use as a therapeutic for targeting anatomically defined neuronal populations, the retrograde transduction efficiency and immune response of the vectors used should be evaluated. Collectively, the current findings emphasize the need to empirically evaluate and optimize the transduction efficiency of viral vectors and their respective transport properties to target specific neuron population(s).

CHAPTER III

LONG ASCENDING PROPRIOSPINAL NEURONS ARE HETEROGENOUS AND SUBJECT TO SPINAL CORD INJURY INDUCED ANATOMIC PLASTICITY

Long ascending propriospinal neurons (LAPNs) are an anatomically defined subset of spinal interneurons that provide direct connectivity between the lumbar and cervical enlargements. Previous studies showed that silencing LAPNs in awake and freely moving animals disrupted coordination interlimb coordination of the hindlimbs, forelimbs, and contralateral limb pairs. Surprisingly, despite a proportion of LAPNs being anatomically intact post- spinal cord injury (SCI), silencing them improved locomotor function but only impacted coordination of the hindlimb pair. Given the functional significance of LAPNs pre- and post-SCI, we characterized LAPN anatomy and evaluated SCI induced anatomic plasticity of LAPNs. This detailed anatomical characterization revealed three morphologically distinct subsets of LAPNs that differ in soma size, neurite complexity, and/or neurite orientation. Following SCI there was a marked shift in neurite orientation in 2 of the LAPN subpopulations to a more dorsoventral orientation, and collateral densities decreased in the cervical enlargement but increased caudal to the injury epicenter. These anatomical changes post-SCI likely reflect maladaptive plasticity involving LAPNs and are likely an effort to seek out new functional inputs from sensory afferents that sprout post-SCI in an effort to achieve homeostasis of the circuitry post-

SCI. Further characterization of LAPN transcriptional profiles at various timepoints post-SCI may provide potential therapeutic targets.

Introduction

Propriospinal neurons (PNs) have their somata and axon terminals wholly contained within the spinal cord. Broadly, PNs can be divided into subsets of "short" and "long" PNs, the former having axonal projection(s) spanning 3 or fewer spinal segments and the latter projecting 4 or more spinal segments [322]. PNs can further be divided into subpopulations based on embryonic lineage, neurotransmitter phenotype, electrophysiologic characteristics, connectivity, morphologically, or anatomically [323].Here, we have focused on a subset of long ascending propriospinal neurons (LAPNs) that are anatomically defined by having somata at lumbar level 2/3 (L2/3) and axon terminal(s) at cervical level 5/6 (C5/6).

The majority of LAPN somata are found in the intermediate gray matter of L2/3, have axons which ascend in the outer rim of the spinal white matter via the ventrolateral funiculus (VLF), and project to C5/6. 46% of LAPNs project ipsilaterally while 54% have axons that cross mid-line at or near the level of the cell body and ascend in the contralateral VLF [91,288,324]. The importance of L2, where LAPN somata reside, was shown by kainic acid injections into the intermediate gray matter. Independent of motoneuron loss, kainic acid injections at L2 resulted in severe locomotor impairments, indicating that somata at L2 are important to locomotor function [94]. To further elucidate the role of LAPNs in locomotor function Pocratsky et al 2020 and Shepard et al 2021 used a dual-viral system to reversibly silence LAPNs in awake and freely moving rats and found that

LAPNs are involved in the coordination of the contralateral forelimb-hindlimb pairs and in the left-right forelimb and hindlimb pairs [94,95]. Interestingly, LAPNs were primarily involved limb pair coupling during non-exploratory overground locomotion on a high friction surface, indicating that LAPNs are a flexible, task-specific network of neurons involved in securing interlimb coordination.

Clinically and in animals models, SCI bidirectionally disrupts the propagation of signals past the injury epicenter leading to functional deficits. However, even if SCI patients are classified as neurologically complete, most SCIs are anatomically incomplete [325]. This spared tissue may provide a means of relaying top-down or bottom-up signals to targets rostral or caudal the injury. As LAPN axons ascend in the most superficial layers of the VLF, where tissue sparing is most likely to occur, they are anatomically situated to allow involvement in such injury-induced plasticity. Bareyre et al. & Filli et al. showed that long descending propriospinal neurons with axons projecting caudal to the injury are increasingly contacted by higher motor centers, to form detour circuits post-SCI [100,102]. This post-SCI rewiring is believed to be an effort to relay top-down signals to spinal levels caudal to the injury. It is conceivable that LAPNs are involved in similar injury-induced plasticity.

Functionally, Shepard et al. showed that silencing LAPNs at 6 weeks post-SCI surprisingly improved locomotor function [95]. These improvements were characterized by an increase in the number of plantar steps, improved hindlimb interlimb coordination, normalized spatiotemporal gait indices, and improved hindlimb intralimb coordination. These data suggest that post-SCI, LAPNs play a detrimental role related to locomotor

function and are likely involved in injury-induced maladaptive plasticity. These maladaptive changes may result from a change in LAPN inputs and/or changes in the areas targeted by LAPN axons. However, as English et al. the only study to anatomically classify LAPNs based on morphology and did so qualitatively in cats, our goal was to anatomically and morphologically characterized LAPNs in rats before and after SCI to evaluate SCI induced neuroplasticity [84].

Methods

All animal procedures were reviewed and approved by the University of Louisville Institutional Animal Care and Use Committee and Institutional Biosafety Committee. A total of N=8 female Sprague Dawley rats (200–220 g: Inotiv Maryland Heights, MO) were evenly divided among groups (N=4 per group). Prior to surgical procedures animals were housed two per cage with *ad libitum* food and water light/dark cycle and were handled by researchers daily prior to any testing.

Stereotaxic injections

Glass micropipettes for stereotaxic spinal cord injections were pulled from borosilicate glass capillaries (World Precision Instruments, Inc., Sarasota, FL) using a micropipette puller (Sutter Instrument Co., Novato, CA), were trimmed to an external diameter of 25 µm, beveled using a micropipette beveller (World Precision Instruments, Inc., Sarasota, FL), and sterilized with 100% ethanol prior to use. The morning of injection surgeries, individual viruses were loaded into pipettes and were kept on ice between surgeries to minimize viral degradation.

Animals were anesthetized with a mixture of ketamine, xylazine, and acepromazine (40, 2.5, and 1 mg/kg, i.p.), and supplemented with 1–2.5% isoflurane in 98% oxygen at a rate of 1 L/min as needed. Prior to surgical openings, animals were given 5 mL of saline (s.c.), buprenorphine (10 mg/kg, s.c.), and meloxicam (1.5 mg/kg, s.c.). A laminectomy and durotomy were performed at thoracic vertebrae 12 to expose spinal L2/3. Animals were then placed in a custom-built spinal stabilization unit to stabilize the thoracic spine, and a laminectomy and durotomy were performed at cervical vertebrae 5 and 6 to expose spinal C5/6 [233]. Using a stereotaxic device (World Precision Instruments, Inc.) HiRet-Lenti-Cre (produced by Boston Children's, titer = 1.18 x 10^{12} gc/mL) was injected bilaterally into the intermediate gray matter of C5/6 (0.55 mm mediolateral, 1.2 mm dorsoventral, 1.3 mm rostrocaudal). Two injection sites on each side spinal cord were targeted; at each site two, 0.25 µL boluses were injected with 2 minutes between to allow viruses to spread through the tissue, mitigate extravasation from the injection site and minimize pressure exerted on the tissue (Figure 5A, only unilateral injections shown). Following cervical injections, spinal stabilizers were moved to T12 for lumbar injections. AAV2-CAG-FLEx-GFP (produced by UNC Vector Core, titer = 4 x 10^{12} gc/mL) was injected bilaterally into the intermediate gray matter of L2-3 (0.5 mm mediolateral, 1.35 mm dorsoventral, 1.3 mm rostrocaudal) following the same procedures as cervical injections (Figure 5A, only unilateral injections shown). Incision sites were sutured in layers and wounds closed with surgical staples. Post-surgery, animals were single housed for 7 days, administered saline 2x/day for 3-5 days,

buprenorphine 3x/day for 3 days, and meloxicam 1x/day for 3 days at previously mentioned dosages.

Behavioral assessments

Three weeks following intraspinal injections, animals underwent baseline testing. To assess gross hindlimb locomotor function the Basso, Beattie, Bresnahan locomotor rating scale (BBB) was used by blinded testers [326]. Overground gait analyses and interlimb phase calculations were performed as previously described [94,95,288]. Phase values from overground recordings were converted to a linear scale to eliminate any lead limb preferences and allow for linear plotting. Thermal nociceptive thresholds were assessed using radiant heat tail flick device [327]. Animals were briefly wrapped in a small towel with the tail exposed and placed on the device. Once the tail was flat and immobile, the heat source was started, tail movement exceeding 0.5 cm terminated the heat source, and latency was recorded. A minimum of 2 minutes separated trials. Thermal nociceptive thresholds of the hind paws were tested using the Hargreaves test, where animals were placed a warmed glass surface (32°C) and allowed to acclimate to the environment for 10 -15 minutes. Infrared light was shone onto the plantar surface of the foot and latency recorded. At least 2 minutes elapsed between trials.

Spinal cord injury surgeries

Animals were re-anesthetized with the same anesthesia used for intraspinal injections and given the same pre-operative drugs. T9-10 was stabilized in custom-built spine stabilizers, and a T9 laminectomy performed to expose spinal T10. The Infinite Horizons Impactor (PSI., Fairfax Station, VA) was centered in the laminectomy window

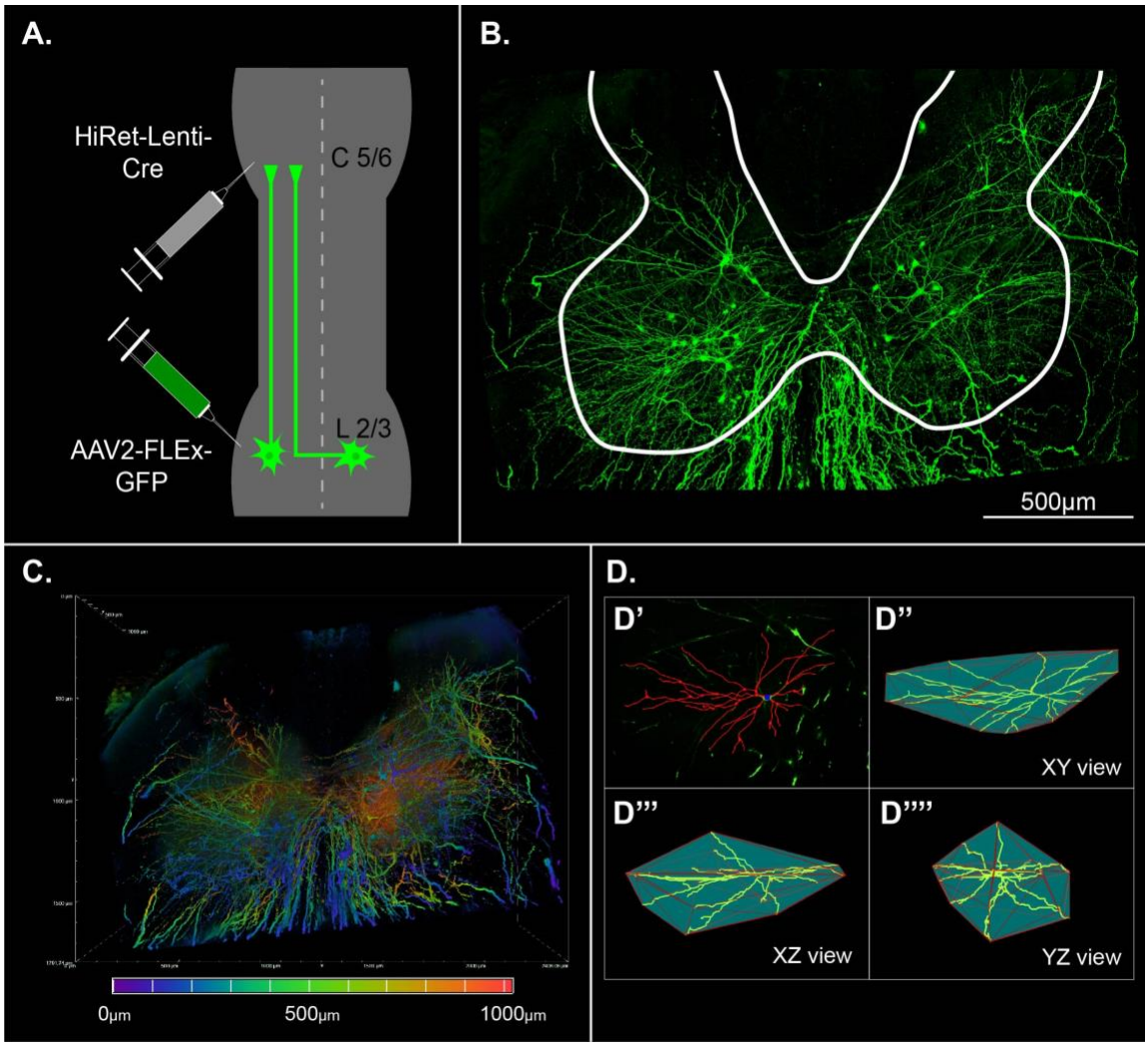

Figure 5. Experimental design and overview for labeling and reconstruction of long ascending propriospinal neurons (LAPNs) A. HiRet-Lenti-Cre injected bilaterally at cervical 5-6 and AAV2-FLEx-GFP bilaterally at lumbar 2-3 (only ipsilateral injections shown for illustration) to label both ipsilateral and contralateral projecting LAPNs B. Maximum intensity projection of LAPN cell bodies and neurites at L2-3, following viral labeling and iDISCO tissue clearing. White lines depict edges of gray matter. C. Volume rendering of L2-3 confocal image depth coded to visualize rostrocaudal location of

viral labeled LAPN somata and neurites. D. D’ traced LAPN (red) overlaid on maximum intensity projection D’’-D’’’’ Visualization of traced neuron (yellow) in multiple planes with convex hull (blue).

and the spinal cord impacted with 150 kdyn of force [328]. Sham animals underwent same procedures minus the SCI. Surgical closure and post-operative care were the same as following intraspinal injections, with the addition of manual bladder expression as needed. One-week post-SCI BBB were performed to functionally confirm injury. 5-weeks post-SCI, all previously described behavioral assessments were performed.

Tissue processing and microscopy

Following week 5 behavioral assessments, animals were anesthetized using a cocktail of ketamine, xylazine, and acepromazine, (40, 2.5, and 1 mg/kg, i.p.) and transcardially perfused with chilled phosphate-buffered saline (pH 7.4) (PBS) followed by 4% paraformaldehyde. Spinal cords and brains were harvested. Spinal cords were post-fixed in 4% paraformaldehyde for 1-2 hours, brains post-fixed for 3-4 hours, and all tissue transferred to 30% sucrose for 3-4 days at 4°C. C5-6, T9-T11 spinal segments, and brainstems were isolated, embedded in tissue freezing medium, cryosectioned at 30 µm, slide mounted in sets, and stored at −20°C.

To evaluated spared white matter, injury epicenters (T10) were stained using FluoroMyelin (Invitrogen, F34652, Waltham, MA) following the manufactures protocol, at a dilution of 1:150, for 60 minutes at room temperature and coverslipped with Fluoromount G (Southern Biotech, 0100-01, Birmingham, AB).

For assessment of LAPN axons/sprouts, GFP from viral labeled LAPN axons was enhanced using immunohistochemistry in thoracic spinal cord sections immediately rostral (T9) and caudal (T12) to the injury epicenter. Sections were heated at 37°C for 30 min, rehydrated in room temperature PBS for 10 min, incubated in a blocking solution

made of nine parts milk solution (bovine serum albumin [BSA]), 0.75 g of powdered skim milk, and 14.25 ml 0.1% of PBS with Tween 20 (PBST) and one part 10% normal donkey serum (NDS) for 60 minutes. Blocking was followed by a 10 min wash in PBS and an overnight incubation at 4°C with rabbit anti-GFP at 1:500 (Abcam, ab290, Waltham, MA). Tissue was then washed 3 times alternating between PBS and PBST for 10 minutes each, followed by secondary antibody (Donkey anti-rabbit Plus 488, Thermofisher, A32790, Waltham, MA) incubation at 1:200 at room temperature for 1 hour. Tissue sections were washed 3 more times alternating between PBS and PBST for 10 minutes each and coverslipped with Fluoromount-G (Southern Biotech, 0100-01, Birmingham, AB). Brainstem sections were stained in the same manner but prior to coverslipping were incubated at room temperature with fluorescent Nissl (NeuroTrace 640/660, ThermoFisher, N21483, Waltham, MA) in PBS at 1:100 for 1 hr and washed 3 times with PBS for 10 minutes each.

Spinal levels L2-3 (where LAPN somata reside) were used for tissue clearing and large volume imaging. Prior to tissue clearing, the rostral half of the lumbar enlargement was cut coronally into 1.5 mm segments using a spinal cord matrix (Alto Scientific, Eatonton, GA). iDISCO (updated protocol December 2016, https://idisco.info/idisco-protocol/update-history/) was used to clear individual segments [329]. Segments were incubated in primary (Chicken anti-GFP, Aves, GFP-1020, Davis, CA) and secondary (Goat anti-chicken 488+, Invitrogen, A32931) antibody solutions for 3 days each, and mounted in custom built silicone slide chambers.

Imaging

Widefield fluorescent images of thoracic spinal cords and brainstem sections were acquired using a Nikon (Melville, NY) Ti2E inverted microscope with SOLA SE LED white light engine, Hamamatsu Orca Fusion Gen III camera, and DAPI, GFP, and Cy3 filters. For thoracic spinal cords, one slide from each set was imaged, and stitched images were acquired using a CFI60 Plan Apo λ 10X NA lens, with the appropriate filter(s). Injured thoracic tissue was imaged with the same equipment using a CFI Plan Fluor 4X NA lens.

Cleared lumbar segments were imaged with a Nikon C2+ confocal microscope with intelligent acquisition, LUN4 solid state laser launch (405, 488, 561, and 640 nm), DUVb high-sensitivity GaAsP detectors, and an ORCA-Fusion Gen-III sCMOS monochrome camera. Large volume images were acquired with a custom-built JOBS program in NIS-Elements AR (Nikon, version 5.30.05) using CFI60 Plan Apo λ 10X NA lens with the 488 laser and post-acquisition, volumes were stitched in Nikon Elements (Figure 5B-C).

Microscopy quantification

Spared white matter spanning 1.5 mm rostrally and 1.5 mm caudally to the injury epicenter were quantified to confirm injury severity. The total cross-sectional area of the spinal cord and the lesion boundary were quantified and analyzed. The epicenter of each injury was determined based on the section with the least amount of spared white matter.

For quantification of LAPN axon collaterals in thoracic and cervical spinal cords heatmaps were generated from 15 sections from each animal, covering 1.7 mm

rostocaudally. Heatmaps were generated and quantified using a custom built MatLab (Mathworks, Natick, MA) program to determine the percentage of positive pixels in the spinal gray matter.

To analyze LAPN axon collaterals and sprouting in the brainstem, images were imported into ImageJ and the appropriate anatomic map (Rat Brain Atlas) overlaid. Relevant brainstem nuclei were selected as regions of interest and the number of positive pixels and percent of positive area for each nuclei quantified. Tissue from 2 animals (one from each group) were not analyzed due to tissue artifact.

For soma and neurite reconstructions of viral labeled LAPNs, the Simple Neurite Tracer (SNT) plugin in ImageJ was used. Cells were reconstructed using a single point for the soma and neurites manually traced for each cell (Figure 5D). Following tracing, the following neurite measures were exported; 1) neurite length which gives a cumulative measure the length of all traced neurites, 2) convex hull which is the minimum 3-dimensional geometric space needed to contain all neurites, 3) z-projection depth which measures the rostrocaudal distance the cell's neurites span, and 4) complexity index which provides as calculated measure of branching complexity [330]. Soma volumes were measured using the "Fill Manager" in SNT and neurite/trace proprieties were exported to a CSV file. CSV files were analyzed using a custom built MatLab program to quantify neurite directionally of each cell.

Statistical analyses

Agglomerative hierarchical clustering of LAPNs and production of parallel plots were performed in R (Posit Software, version 2023.03.1). Input variables were

normalized using min-max scaling, Ward's clustering method was used, and the number of clusters was determined using the elbow method. Comparison of LAPN cluster morphologic characteristics were compared using one-way ANOVAs followed by Tukey's HSD *post hoc* where appropriate in Prism 9 (GraphPad Software, Version 9.5.1). Analysis of LAPN cluster neurite directionality both pre- and post-SCI Kruskal-Wallis test followed by Dunn's test where appropriate were performed in Prism 9.

BBB scores were compared using a two-way ANOVA followed by Bonferroni's multiple comparisons test where appropriate in Prism 9. Tail flick and Hargreave's test outcomes were compared using unpaired *t*-tests in Prims 9. Binomial Proportion Test was used to evaluate differences in the proportion of abnormal phase values, defined as greater than 2 standard deviations from baseline measures and regression analyses were performed in Prism 9 for spatiotemporal gait indices.

For comparison, morphologic characteristic of sham versus SCI LAPN clusters unpaired *t*-tests were performed in Prism 9. Kruskal-Wallis test followed by Dunn's test where appropriate were used to analyze axon collateral densities at thoracic spinal levels, and for cervical and brainstem collateral comparisons unpaired - tests used all performed in Prism 9. *P* values for all analysis were considered statistically significant when $p \leq 0.05$, and two-tailed p values are reported for post hoc t-tests.

Results

LAPNs differ based on soma and dendrite morphology

Hierarchical cluster analysis based of 11 morphologic characteristics from 572 reconstructed LAPNs revealed that LAPNs group into three distinct clusters (Figure 6A).

Of the resultant clusters, cluster 1 contained 171 cells, cluster 2, 198 cells, and cluster 3, 203 cells. LAPNs in cluster 1 (Figure 5B & B') are larger, more complex neurons than clusters 2 and 3. This is evident as soma volume (Figure 6E), total neurite length (Figure 6F), convex hull volume (Figure 6G), z-projection depth (Figure 2H), and complexity index (Figure 6I), are all significantly greater for cluster 1 compared to clusters 2 and 3. Overall size and complexity of LAPNs in clusters 2 and 3 did not differ, however neurite directionality did (Figure 6A, C, D). Cluster 2 LAPNs orient the greatest percentage of neurites medially and laterally and cluster 3 the lowest percentage. However, cluster 3 LAPNs have the highest percentage of neurites oriented ventrally and a higher percentage oriented dorsally than cluster 2 (Figure 6J). These resultant clusters reflect three distinct subsets of LAPNs based on soma and neurite morphologies.

Mild SCI causes minimal functional deficits

Mild T10 contusive SCI (150 kDyn) was confirmed in each animal by quantifying the percent of spared white matter (Figure 7A-B). Additionally, assessment of gross locomotor function using the BBB confirmed functional deficits at 1-week post-SCI (mean score ± SD; sham: 20.5 ± 1.0, SCI: 13.3 ± 3.0) compared to baseline scores (mean score ± SD; 21.0 ± 0) and week 1 sham scores. However, by week 5 BBB scores were similar between sham and SCI groups (mean score ± SD; sham: 20.3 ± 0.5, SCI: 19.75 ± 1.0) (Figure 7C). Sensory testing for thermal hypersensitivity via tail flick response (mean percent change from baseline ± SD; sham: -12.37 ± 1.4, SCI: 1.4 ± 9.1) and Hargreaves' test (mean percent change from baseline ± SD; sham: 2.0 ± 26.4, SCI: 36.6 ± 34.4) showed no change from baseline testing in either group at week 5. It is not surprising

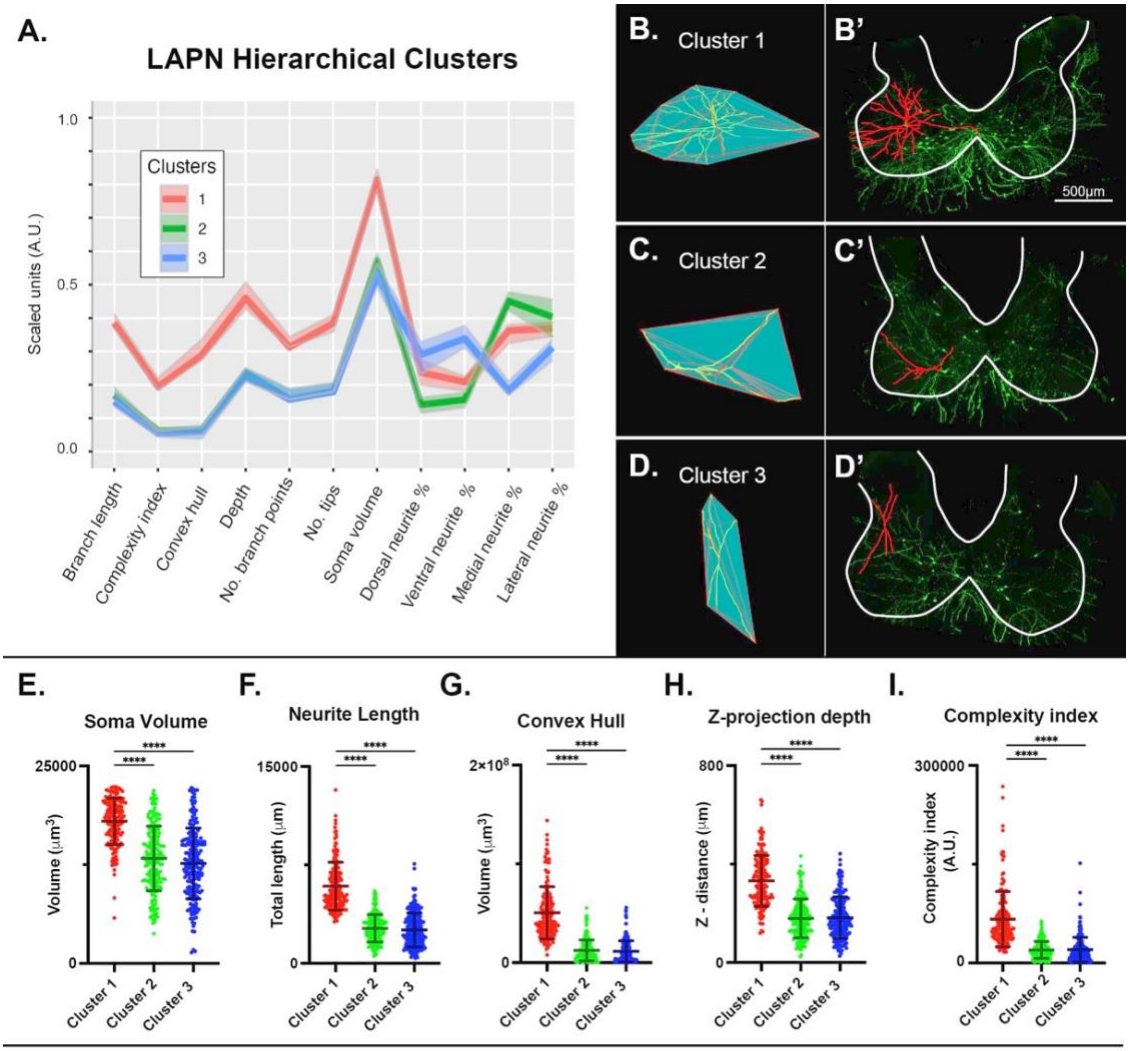
A.
LAPN Hierarchical Clusters
Scaled units (A.U.)
1.0
0.5
0.0
Clusters
1
2
3
Branch length
Complexity index
Convex hull
Depth
No. branch points
No. tips
Soma volume
Dorsal neurite %
Ventral neurite %
Medial neurite %
Lateral neurite %
B. Cluster 1
B'
500µm
C. Cluster 2
C'
D. Cluster 3
D'
E.
Soma Volume
Volume (µm³)
25000
0
F.
Neurite Length
Total length (µm)
15000
0
G.
Convex Hull
Volume (µm³)
2×10⁸
0
H.
Z-projection depth
Z - distance (µm)
800
0
I.
Complexity index
Complexity index (A.U.)
300000
0
****
***
*
Cluster 1
Cluster 2
Cluster 3
J.
Neurite directionality by cluster
Dorsal
Ventral
Medial
Lateral
% total neurite length
100%
0%

Figure 6. LAPNs differ anatomically based on soma and neurite characteristics. **A.** Parallel plot with confidence intervals show LAPN clusters from hierarchical cluster analysis based on morphologic characteristics. Dark lines indicate medians for each cluster and lighter bands represent confidence intervals. **B, C, D.** 3-dimensional rendering of representative LAPNs from each cluster (not shown to scale, for ease of visualization). **B', C', D'.** Representative traced LAPNs (red) overlaid on maximum intensity projections of L2-3. **E-I.** LAPNs clusters differ morphologically (one-way ANOVAs, p<.0001) based on neurite length (Tukey's HSD *post hoc*, cluster 1 vs. cluster 2, p<.0001; cluster 1 vs. cluster 3, p<.0001), z-projection depth (Tukey's HSD *post hoc*, cluster 1 vs. cluster 2, p<.0001; cluster 1 vs. cluster 3, p<.0001), convex hull (Tukey's HSD *post hoc*, cluster 1 vs. cluster 2, p<.0001; cluster 1 vs. cluster 3, p<.0001), soma volume (Tukey's HSD *post hoc*, cluster 1 vs. cluster 2, p<.0001; cluster 1 vs. cluster 3, p<.0001), and neurite complexity (Tukey's HSD *post hoc*, cluster 1 vs. cluster 2, p<.0001; cluster 1 vs. cluster 3, p<.0001). **J.** LAPN clusters differ (Kruskal-Wallis tests, p <.0001) based on dorsal (Dunn's test *post hoc*, cluster 1 vs. cluster 2, p<.0001; cluster 2 vs. cluster 3, p<.0001), ventral (Dunn's test *post hoc*, cluster 1 vs. cluster 2, p<.0001; cluster 2 vs. cluster 3, p<.0001), medial (Dunn's test *post hoc*, cluster 1 vs. cluster 2, p<.0001; cluster 1 vs. cluster 3, p<.0001; cluster 2 vs. cluster 3, p<.0001), and lateral (Dunn's test *post hoc*, cluster 1 vs. cluster 2, p<.005; cluster 1 vs. cluster 3, p<.0001; cluster 2 vs. cluster 3, p<.05) neurite directionality. **E-J.** Large center lines show group means and error bars are standard deviations. **p*<.05, ***p*<.01, ****p*<.001, **** *p*<.0001.

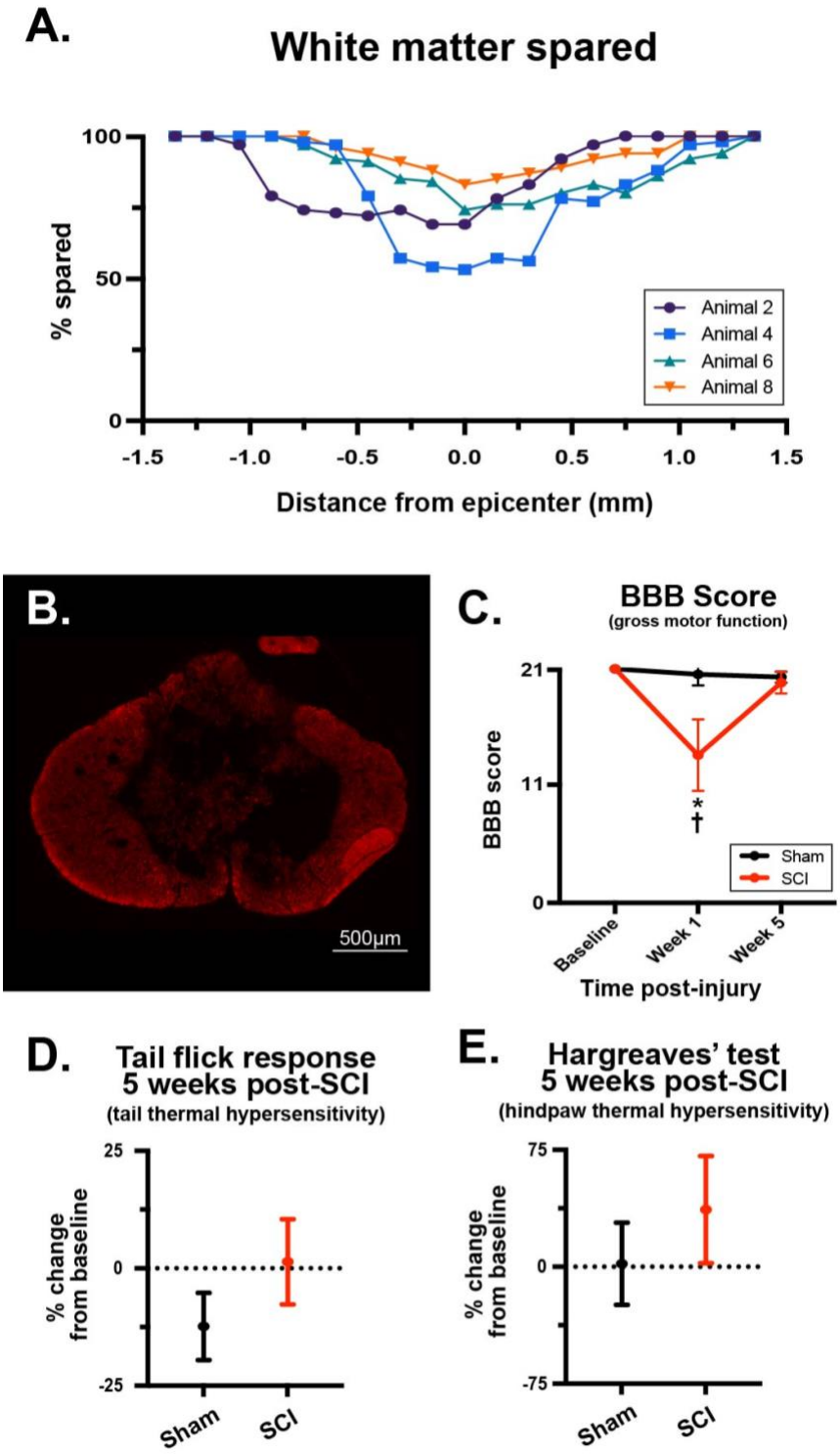

Figure 7. 150kdyn T10 SCI produces no gross functional deficits at 5 weeks post-SCI **A.** Spared white matter by animal following 150kdyn contusive SCI. **B**. Representative

injury epicenter (T9) cross section stained with Fluoromyelin (red). **C.** Basso, Beattie, Bresnahan locomotor rating scale (BBB) scores for sham and SCI groups. BBB scores decrease (two-way ANOVA, interaction, p=.0001; column factor, p=.0021; group factor, p= .011) at 1-week post-SCI (Bonferroni's multiple comparisons test, p=.04, sham week 1 20.5 ± 1.0 vs. SCI week 1 13.25 ± 3.2; p<.0001, SCI baseline 21.0 ± 0.0 vs. SCI week 1 13.25 ± 3.2; p <.0001, SCI week 1 13.25 ± 3.2 vs. SCI week 5 19.75 ± 0.96) but recover by week 5. **D.** Tail flick response and **E.** Hargreaves thermal sensitivity test show now difference between sham and SCI groups. **C-D.** Circles represent group means error bars standard deviations. *p<.05 for group interaction, †p<.05 for column interaction.

that there was no difference in these gross functional measures at week 5 given the mild injury severity.

For a more in-depth analysis of locomotor function than the BBB provides, overground gait kinematics were assessed. Coupling patterns of each limb pair was determined by dividing the initial contact time of one limb by the stride time of the other limb. Resulting phase values of 0 or 1 indicate synchrony and values of 0.5 alternation of the limb pair. To eliminate discrepancies in of the lead limb selection and for ease of visualization, phase values were converted to a linear scale of 0.0 - 0.5 or 0.5 – 1.0. Mean phase values of the limb pairs were calculated at baseline and any value >2 standard deviations from these means were considered 'irregular', as indicated by the blue boxes (Figure 8A-D). SCI had no impact on left-right alternation of the hindlimb (Figure 8A) or forelimb pairs (Figure 4B). However, at 5 weeks post-SCI ipsilateral and contralateral phase values were altered, with ipsilateral limb pairs showing more synchrony (Figure 8C) and contralateral limb pairs showing more alternation (Figure 8D). No difference was seen between groups for speed-dependent gait indices of swing time (Figure 8 E, J, O), stance time (Figure 8K ,P), stride frequency (Figure 8G,L,Q), stride time (Figure 8H,M,R), or stride length (Figure 8I,N,S). Together, these data suggest that mild contusive T10 SCI only impacts coupling of the ipsilateral and contralateral limb pairs during overground locomotion.

Post-SCI LAPNs resemble uninjured LAPNs but differ in neurite directionality

Hierarchical cluster analysis using 11 morphologic characteristics from 535 reconstructed LAPNs revealed that post-SCI LAPNs can be divided into three distinct

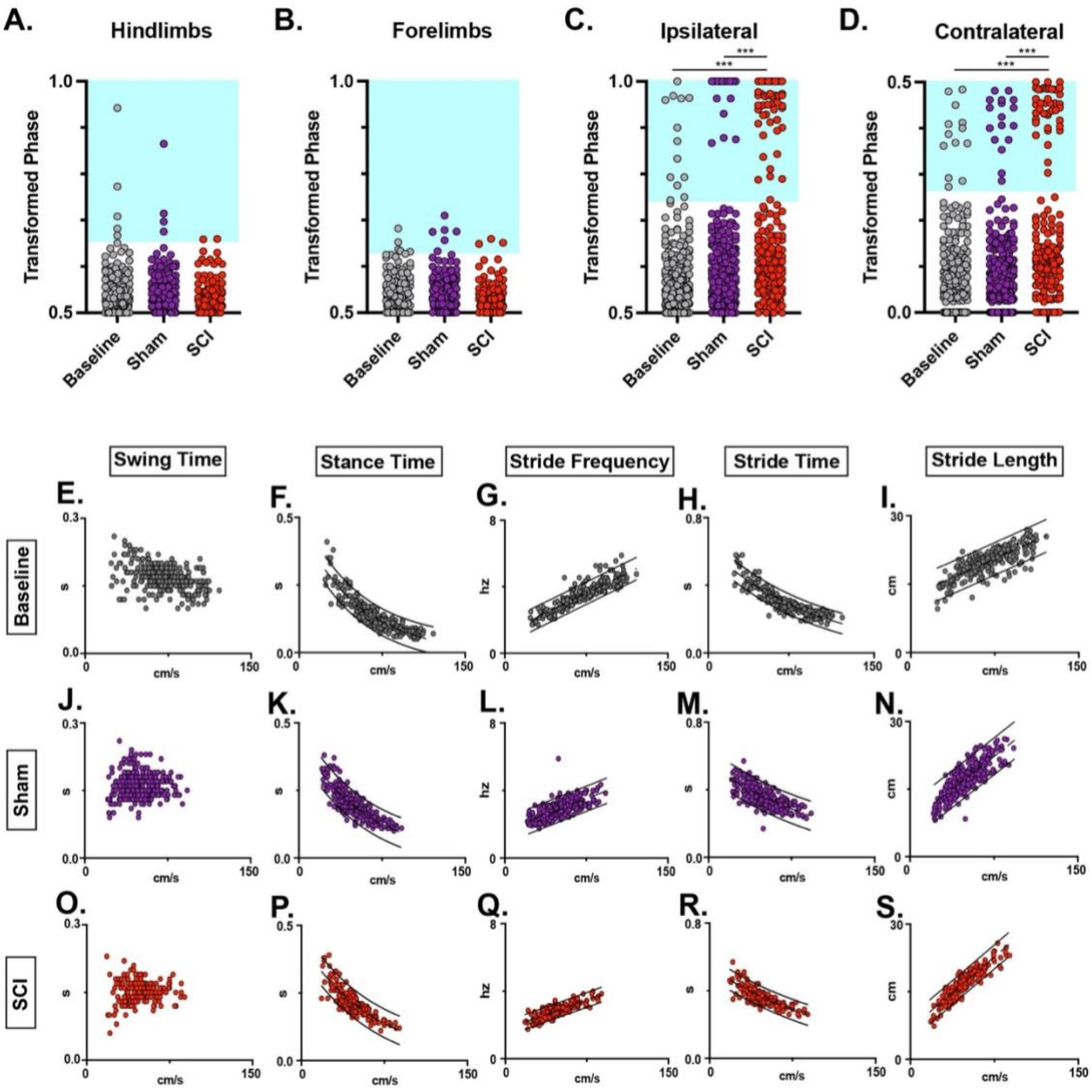

Figure 8. 5 weeks post-SCI limb coupling is impaired but other key features of locomotion are unaltered. **A-D.** Transformed phase values for limb pairs. There is no disruption in the forelimb (**A**) or hindlimb (**B**) pairs, but the SCI group shows disrupted phase values for ipsilateral (**C**) (binomial proportion test, baseline, *n* = 12/262 vs. SCI, *n* = 42/191, *p*<.001; Sham, *n* = 16/253 vs. SCI, *n* = 42/191, *p*<.001) and contralateral (**D**) (binomial proportion test, baseline, *n* = 13/259 vs. SCI, *n* = 41/178, *p*<.001; Sham, *n* =

17/240 vs. SCI, *n* = 41/178, *p*<.001) limb pairs**. E-S.** Relationships between swing time, stance time, stride time, and stride distance are plotted against speed. An exponential decay line of best fit is displayed for stance time (baseline R^2 =0.749 vs. sham R^2 =0.824 vs. SCI R^2=0.733) and stride time (baseline R^2 =0.826 vs. sham R^2 =0.535 vs. SCI R^2=0.650), and a linear line of best fit shown for stride frequency (baseline R^2 =0.801 vs. sham R^2 =0.496 vs. SCI R^2=0.682) and stride length (baseline R^2 =0.626 vs. sham R^2 =0.662 vs. SCI R^2=0.832). Dotted lines indicate line of best fit and solid lines indicate 95% prediction intervals. ****p*<.001

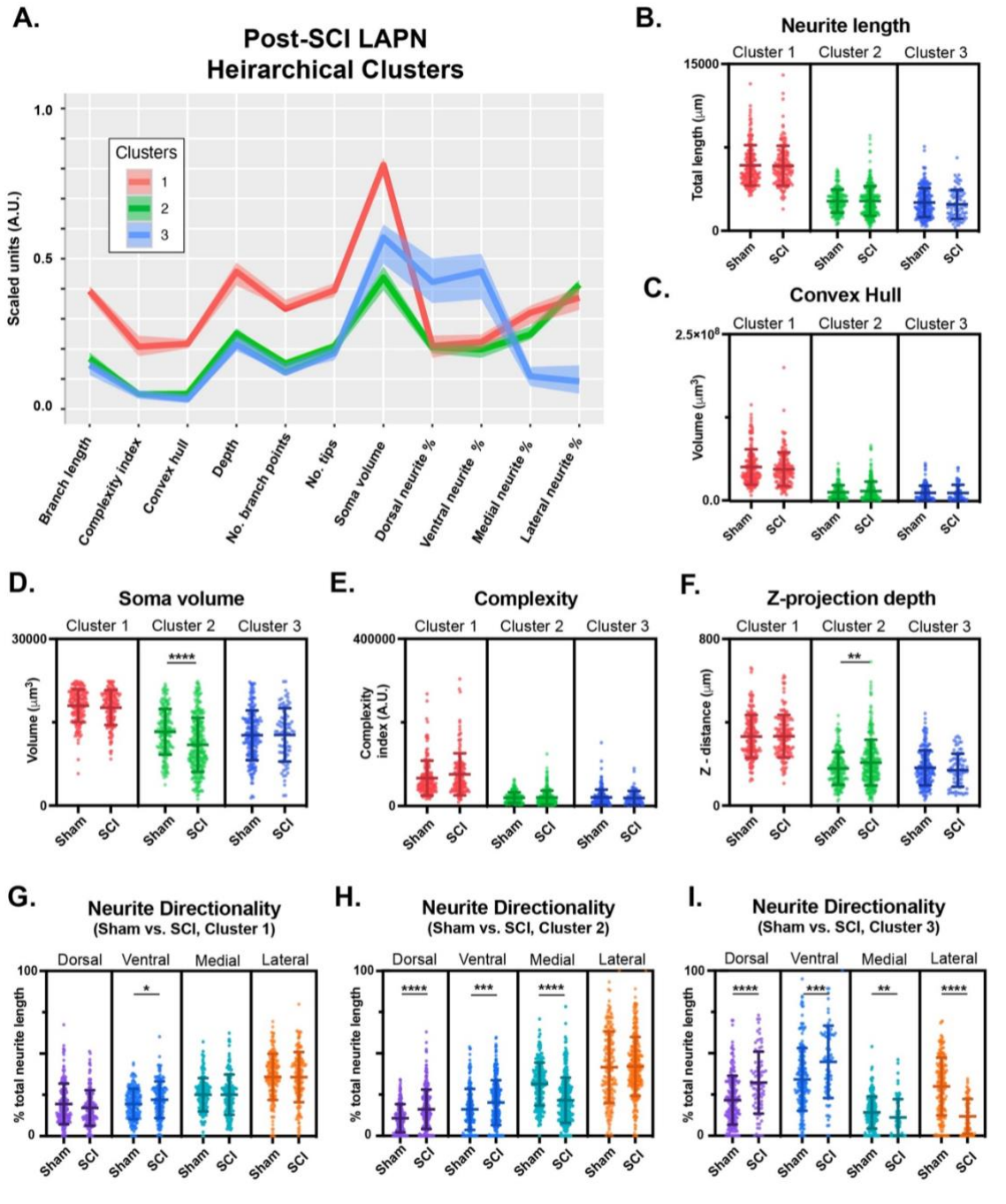

Figure 9. 5 weeks post-SCI LAPNs morphologically group into 3 clusters, and post-SCI LAPNs morphologically differs from uninjured LAPNs. **A.** Parallel plot with confidence intervals shows that post-SCI LAPN clusters from hierarchical cluster analysis based on

morphologic characteristics. Dark lines indicate medians for each cluster and lighter bands represent confidence intervals. **B-F.** Uninjured and post-SCI LAPN clusters are similar based on neurite length (**B**), convex hull (**C**), and complexity (**E**) but post-SCI cluster 2 LAPNs differ from uninjured LAPNs in soma volume (unpaired *t* test, $p<.0001$, sham 13294 ± 4095 vs. SCI 10931 ± 4880) and z-projection depth (unpaired *t* test, $p=.002$, sham 179 ± 78.0 vs. SCI 206.8 ± 109.7). **G-I.** Post-SCI LAPN neurite directionality differs from uninjured LAPNs. For cluster 1 LAPNs, ventral (Mann-Whitney test, $p=.022$, sham 0.19 ± 0.09 vs. SCI 0.22 ± 0.11) neurite orientation differs post-SCI (**G**). For cluster 2 LAPNs dorsal (Mann-Whitney test, $p<.0001$, sham 0.11 ± 0.16 vs. SCI 0.16 ± 0.12), ventral (Mann-Whitney test, $p=.0009$, sham 0.16 ± 0.12 vs. SCI 0.20 ± 0.14), and medial (Mann-Whitney test, $p<.0001$, sham 0.31 ± 0.13 vs. SCI 0.22 ± 0.14) neurite orientations differ post-SCI (**H**). For cluster 3 LAPNs dorsal (Mann-Whitney test, $p<.0001$, sham 0.22 ± 0.15 vs. SCI 0.32 ± 0.19), ventral (Mann-Whitney test, $p<.0001$, sham 0.34 ± 0.19 vs. SCI 0.45 ± 0.22), medial (Mann-Whitney test, $p=.0051$, sham 0.14 ± 0.09 vs. SCI 0.11 ± 0.11), and lateral (Mann-Whitney test, $p<.0001$, sham 0.30 ± 0.18 vs. SCI 0.12 ± 0.11) neurite orientations differ post-SCI (**I**). Large center lines show group means and error bars are standard deviations. *$p<.05$, **$p<.01$, ***$p<.001$, **** $p<.0001$.

clusters (Figure 9A). Based on parallel plots, the pattern of clustering is similar between LAPN clusters in sham and SCI animals (Figure 7A & Figure 9A), with cluster 1 consisting of larger more complex cells, and clusters 2 and 3 consisting of smaller, less complex LAPNs that differ in neurite directionality. Comparing morphometrics of sham and SCI clusters showed that the clusters are similar based on neurite length (Figure 9B), convex hull (Figure 9C), and complexity (Figure 9E). The only differences between sham and SCI clusters were for cluster 2 LAPNs, where SCI LAPNs had smaller soma volumes (Figure 9C) and greater z-projection depths (Figure 9F).

Neurite directionality of the largest and most complex LAPNs, cluster 1, was similar between groups with only a modest increase in the percentage of ventral oriented neurites in the SCI group (mean ± SD; sham: 19.4 ± 9.3, SCI: 22.0 ± 11.1) (Figure 9G). Cluster 2 LAPNs in both the sham and SCI groups oriented most neurites mediolaterally. However, SCI LAPNs have a higher percentage of dorsal (mean ± SD; sham: 10.7 ± 8.5, SCI: 16.1 ± 12.0) and ventral (mean ± SD; sham: 16.1 ± 12.4, SCI: 20.1 ± 13.7) oriented neurites and a lower percentage of medially (mean ± SD; sham: 31.2 ± 13.0, SCI: 21.6 ± 13.7) oriented neurites (Figure 9H). Cluster 3 LAPNs in both groups have neurites predominantly oriented dorsoventrally. In the SCI group there was a higher percentage oriented both dorsally (mean ± SD; sham: 21.5 ± 14.8 , SCI: 32.2 ± 18.7) and ventrally (mean ± SD; sham: 34.2 ± 19.0, SCI: 44.8 ± 21.9), and a lower percentage oriented medially (mean ± SD; sham: 14.11 ± 9.7, SCI: 11.1 ± 11.1) and laterally (mean ± SD; sham: 29.9 ± 17.5, SCI: 11.8 ± 10.5) (Figure 5I). As there were minimal differences in

other morphometrics between sham and SCI LAPN clusters the differences in neurite directionality likely represent injury induced plasticity of LAPN subpopulations/clusters.

SCI alters LAPN axon collateral targets

Here, LAPNs have been defined as having somata at L2/3 and axon terminals at C5/6. However, this does not exclude the possibility of LAPNs having axon collaterals targeting other spinal levels. As expected, LAPN collaterals were seen at C6 (Figure 10A, top left panel) and concentrated in lamina IX. Surprisingly, LAPN collaterals were also found at T9 (Figure 10A, top middle panel) and T12 (Figure 10A, top right panel) primarily in the intermediate gray matter. As LAPN axons ascend in the VLF, their axons likely remain intact following SCI, but the insult may induce changes in collateral densities and target areas. In the SCI group, collateral densities rostral to the injury at C6 (mean ± SD; sham: 10827 ± 8171, SCI: 7259 ± 7087) (Figure 10B). In the thoracic spinal cord collateral densities in the sham group were similar at T9 (mean ± SD; 2965 ± 2529) and T12 (mean ± SD; 3505 ± 2941) and a similar density was found in the SCI group at T9 (mean ± SD; 4149 ± 4169) (Figure 10C). However, there was an increase caudal to the injury at T12 in the SCI group (mean ± SD; 6317 ± 3494) compared all other spinal levels and groups (Figure 10C).

By definition, propriospinal neurons are wholly contained within the spinal cord. However, as there were fewer LAPN collaterals at C6 in the SCI group, we anticipated that LAPN axons may target other motor centers. Surprisingly, in both the sham and SCI groups, LAPN collaterals were seen in the reticular formation (Figure 11A). Collaterals were quantified in the caudal gigantocellular reticular nucleus (Gi) and lateral

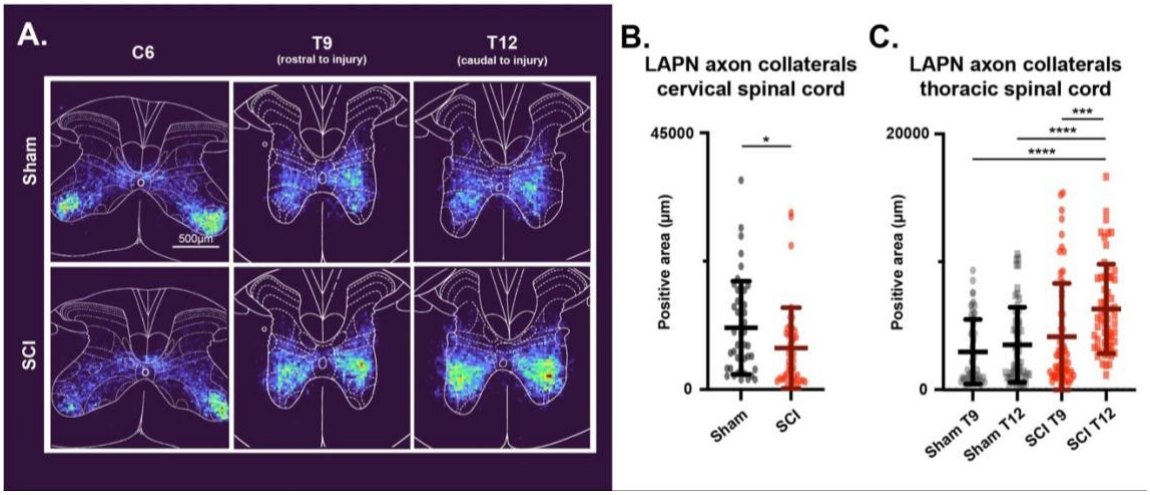

Figure 10. 5 weeks post-SCI LAPN axon collaterals densities differ by target. **A.** Heatmaps depicting LAPN axon densities at T9, T12, and C6. **B.** LAPN axon collaterals in the thoracic spinal cord differ post-SCI (Kruskal-Wallis test, $p<.0001$) with an increase in collaterals caudal to the injury at T12 (Dunn's test, $p<.0001$, sham T12 3505 ± 2941 vs. SCI T12 6317 ± 3494; $p<.0001$ sham T9 4149 ± 4169 vs. SCI T12 6317 ± 3494; $p=.0002$ SCI T9 4149 ± 4169 vs. SCI T12 6317 ± 3494).**C.** LAPN axon collaterals in cervical spinal cord decrease at 5 weeks post-SCI (unpaired *t*-test, $p=.03$, sham 10827 ± 8171 vs. SCI 7259 ± 7087). Large center lines show group means and error bars are standard deviations. *$p<.05$, ***$p<.001$, **** $p<.0001$.

paragigantocellular nucleus (LPGi), but no differences were seen between groups (Figure 11B-C).

Discussion

LAPN morphology is heterogenous

Previous studies have traced LAPNs in multiple species and characterized the number of ipsi- and contralateral projecting LAPNs [84-86,91]. However, this is the first study to quantify LAPN soma and neurite morphologies and unbiasedly cluster LAPNs based on these measures. Hierarchical cluster analysis grouped LAPNs into three distinct clusters that differed based on soma size and/or dendrite orientation. Cluster 1 LAPNs had large somata with extensive neurite length and complexity. Total length and complexity of neurite arbors directly relates to the number of inputs, cluster 1 LAPNs likely receive more inputs than cluster 2 and 3 neurons. Additionally, larger somata have lower input resistances requiring more input to reach threshold potential and are associated with larger diameter, faster conducting axons [331-333]. These properties mean that cluster 1 LAPN are more likely to be recruited when faster conduction velocities are required for interlimb coordination during high-speed locomotion. Cluster 2 and 3 LAPNs had smaller somata and less extensive neurites compared to cluster 1 LAPNs but differed in neurite directionality. Cluster 2 LAPNs were oriented mediolaterally which may reflect that the primary inputs of these cells are axons from the lateral and ventral funiculus [286,334], which includes the descending reticulospinal tract, vestibulospinal tract, and other propriospinal neurons all of which are involved in locomotor output [335]. Afferent sensory projections from the dorsal root ganglia enter the dorsal horn of the

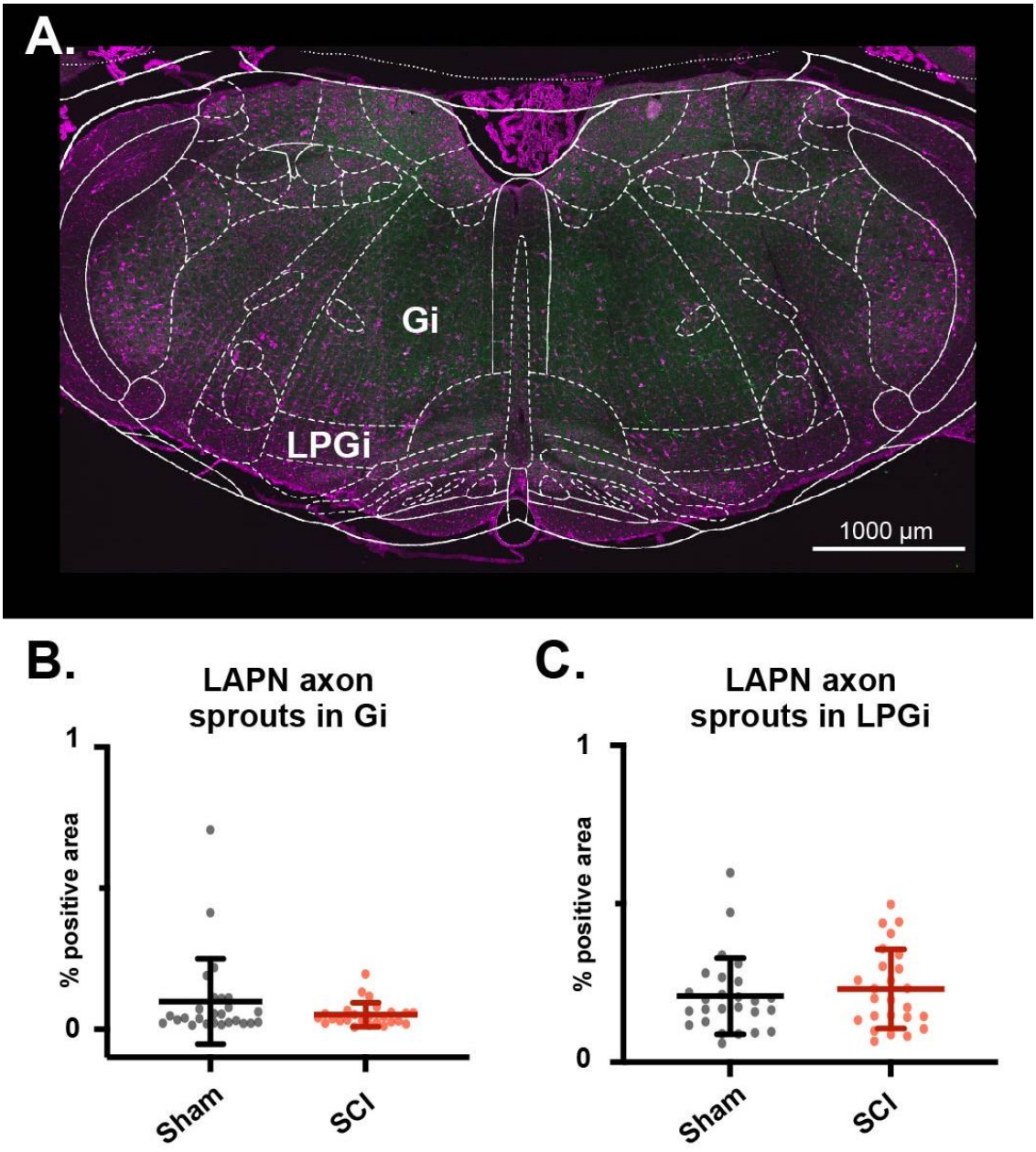

Figure 11. SCI does not alter LAPN axon collaterals in the reticular formation. **A.** Brainstem cross section stained with fluorescent Nissl (magenta) and viral labeled LAPN axon collaterals (green). White overlay is an anatomical map showing the gigantocellular nucleus (Gi) and lateral paragigantocellular nucleus (LPGi). **B.** Percent positive area for LAPN axon collaterals in the Gi are unaltered post-SCI. **C.** Percent

positive area for LAPN axon collaterals in the LPGi are unaltered post-SCI. Large center lines show group means and error bars are standard deviations.

spinal cord and penetrate into the spinal gray matter, given the dorsoventral orientation of cluster 3 LAPNs, it is likely they receive input from sensory afferents and are involved in the integration and processing of incoming sensory signals [336-338].

LAPN neurites primarily project coronally with minimal rostrocaudal spread (z projection distance). This morphologic characteristic seems to be conserved among other propriospinal populations as Deng et al. found the same morphologic characteristic in long descending thoracic PNs [216]. Additionally, in multiple species neurons located in the intermediate gray matter, where LAPN somata primarily reside, also have coronal neurite orientations [339-341], and thus this characteristic seems conserved and may represent a morphology that is sufficient for the execution of movement without input from the forebrain [342].

Minimal functional deficits following mild T10 contusive SCI

Clinically, most SCIs are contusion injuries and even if classified as clinically complete there is some level of tissue sparing [96,97]. To reflect this, we used a mild contusive SCI that spared a high level of tissue, which included the VLF where LAPN axons ascend. The injury caused a transient drop in gross locomotor function and resulted in no differences in sensory function. However, as BBB scoring is a crude measure of locomotor function, overground gait kinematics were assessed for precise locomotor analysis. Mild contusive T10 SCI disrupted interlimb coordination of the ipsi- and contralateral forelimb-hindlimb pairs but had no effect on the hindlimb or forelimb pairs or spatiotemporal gait indices. Previous studies have shown morphologic changes in spared spinal neurons correlates with function [216,343]. As Pocratsky et al and Shepard

et al both showed that LAPNs play a vital role in interlimb coordination pre-SCI and impair interlimb coordination post-SCI, and the deficits seen here are restricted to interlimb coordination, the neuroanatomical changes seen are likely related to the functional deficits seen [94,95].

LAPNs differ morphologically following SCI

LAPN somata are multiple spinal levels caudal of the injury and their axons ascend in the outer rim of the spared white matter, leaving them anatomically intact following SCI. However, since injury-induced neuroplasticity is seen throughout the neuroaxis we hypothesized that LAPN morphology would differ post-SCI [102,108]. At 5 weeks post-SCI, hierarchal cluster analysis grouped LAPNs into three distinct clusters that were similar to sham clusters (Figures 6A & 9A), but there were marked differences in neurite orientation. Cluster 2 and 3 LAPN neurites oriented more dorsoventrally in the SCI group, likely reflecting injury-induced plasticity. Post-SCI shifts in orientation are also seen in long descending thoracic PNs, but these PNs assume a more mediolateral orientation which opposes the dorsoventral shift of LAPNs here [216]. As functional synaptic inputs influence neurite orientation, the shifts in both of these PN populations are likely a compensatory response to seek out new inputs post-SCI. The difference in orientation shifts between LAPNs and descending thoracic PNs is likely a consequence of soma location relative to the injury epicenter [344-347]. The mediolateral shift in thoracic PNs is advantageous as descending PNs are involved in the formation of detour circuits in an effort to relay commands to targets caudal to the injury [100,102]. However, descending input to LAPNs are disrupted post-SCI and the dorsoventral shift in LAPN

neurites may be an attempt to create functional inputs with sensory afferents that sprout caudal to the injury [348,349]. Interestingly, the changes in LAPN morphology closely resemble those seen in pyramidal neurons of the barrel cortex following deafferentation. In both cases, neurite orientation is altered but there are no changes in convex hull or total neurite length. This suggests that orientation differences are not just a consequence of neurite degeneration/loss but also of neurite growth in new directions. Such plasticity is referred to as homeostatic structural plasticity, in which synapses and resultant circuitry self-organize to assure network stability [350]. Furthermore, aspects of development are recapitulated post-SCI [351], and LAPN neurites may go through the growth and stabilization phases of dendrite development. During the growth phase, the neurites increase in number, length, and complexity and form NMDA receptor mediated synapses. Subsequently, active synapses increase have an increase in AMPA receptors. These neurites and synapses are maintained while neurites that fail to increase the ratio of AMPA/NMDA receptors are retracted [352-354]. A shift to the stabilization phase then occurs when CaMKII expression increases (which occurs 3-14 days post-SCI) resulting in decreased new branch formation retraction [355]. Given this, it is plausible that LAPNs are seeking out new functionally active inputs post-SCI in an effort to achieve homeostatic plasticity.

While there were drastic differences in neurite orientations for cluster 2 and 3 LAPNs, the large complex LAPNs in cluster 1 showed little difference between groups as only a modest increase in ventral neurites was seen in the SCI group. This is counterintuitive as larger cells are often more susceptible to injury and disease [356-358].

The seeming resistance to injury induced plasticity may reflect differences in transcriptional profiles which alter a cells potential to respond to injury [359-361]. It would be interesting for future studies to compare the transcriptional profiles of cluster 1 LAPNs with cluster 2 and 3 LAPNs following SCI, as this may provide therapeutic targets.

LAPN collateral targets differ post-SCI

In both groups, LAPN collateral densities in the cervical spinal cord were greatest in lamina IX, suggesting that LAPNs target motoneurons both pre- and post-SCI. Despite LAPN axons ascending in the intact VLF, LAPN collateral densities were lower at C6 in the SCI group. This may result target disconnection as motoneurons rostral to the injury can die or atrophy [362,363]. Here, LAPNs are defined as having somata at L2/3 and axon terminals at C5/6 however we unexpectedly found collaterals in the gray matter of the thoracic spinal cord. In both groups, at T9 and T12, LAPN collateral densities were highest in lamina VII which contains GABA-ergic premotor interneurons and spinocerebellar neurons and is known to integrate sensory and motor inputs [79,364-368]. This is significant as it shows LAPNs likely contact ensembles of thoracic premotor neurons to coordinate and execute whole body movements such as locomotion. This coincides with electrophysiologic data from Juvin et al which show that activation and coupling of thoracic circuity ensures effective interenlargement coordination [90]. Furthermore, these findings provide anatomical substrates that at least partially explain the findings of Shepard et al, which showed that silencing of LAPNs post-SCI only improved interlimb coordination of the hindlimbs but no longer had an impact on contralateral or forelimb interlimb coordination following injury [95]. The increase in

collateral density caudal to the injury may represent aberrant plasticity that when silenced, allows the lumbar circuitry to function appropriately via removal of excess 'noise' from the hindlimb locomotor system.

We further investigated whether LAPNs projected to supraspinal centers involved in locomotion. In the sham group, LAPN collaterals were present in the gigantocellular (Gi) and lateral paragigantocellular (LPGi) nuclei of the reticular formation. Importantly, this means that this population of "propriospinal" neurons are not wholly contained within the spinal cord, and therefore by definition are not truly propriospinal neurons. As there were differences in collateral densities at C6, we anticipated differences in the reticular formation as well. However, we found no differences in either the Gi or LPGi. Given that at least some LAPNs are also part of the spinoreticular system, they likely respond to noxious input from the hindlimbs [367,369,370]. For survival and relay of noxious stimulus rostral to the injury it would functionally be more beneficial to maintain this connectivity post-SCI than the ability to coordinate contralateral limb pairs. As there were no differences in collaterals at T9, Gi, or LPGi, but a decrease at C6 and an increase at T12, it appears that LAPN collaterals are retracted from some target areas but retain or increase connectivity to other targets. Similar to the changes seen in neurite orientations, this is likely another example of homeostatic plasticity following injury.

Functional and clinical implications of LAPN plasticity

At 5 weeks post-SCI, Shepard et al. showed that conditional silencing of LAPNs improved gross locomotor function and normalized interlimb coordination [95]. These findings were counterinitiative, as silencing an anatomically intact pathway was

hypothesized to exaggerate locomotor deficits. However, current data found shifts in LAPN neurite orientation and differences in collateral densities post-SCI which support these findings. Following an insult such as an SCI, the CNS undergoes an intense period of injury-induced plasticity which includes changes in synaptic boutons, receptor densities, and circuit reorganization [371]. Formation and maintenance of synaptic connectivity is dependent on functional inputs, and LAPNs likely seek new functional inputs post-SCI to maintain homeostasis. However, our findings and those of Shepard et al. suggest that post-SCI, LAPN homeostatic plasticity is maladaptive [95]. This is likely a consequence of a combination of: 1) disruptions in descending motor pathways that previously targeted LAPNs and 2) sprouting sensory afferents caudal to the injury. As there is little meaningful sensory and motor input to guide the formation of circuitry caudal to the injury during the intense period of acute post-injury plasticity, the resultant circuity is hyperexcitable and overactive which impairs the ability of the locomotor circuity to produce meaningful output [286,351,372]. In agreement with this, Kathe et al showed that epidural stimulation, which improves locomotor function post-SCI, decreased overall neural activity in the lumbar enlargement, but also resulted in an increase in activity of a PN subpopulation which are responsible for the improved functional outcomes [286].

During the acute and subacute phases of SCI, patients are often immobile while polytrauma is being treated, resulting in poor afferent sensory input being provided to the cord below the level of the lesion. Unfortunately, this coincides with the intense period of injury induced neuroplasticity, and maladaptive circuits form [373-377].

Chronically, activity-based therapy coupled with epidural stimulation improves function, but patient outcomes might be further improved if the circuitry was more receptive and plastic to the meaningful inputs therapy provides. Therefore, finding a way to recapitulate the high level of plasticity seen acutely and subacutely might be beneficial if the correct input(s) are provided via activity-based or other rehabilitative strategies. Potential approaches to do so include eliciting low levels of inflammation, modifying perineural nets, upregulating plasticity associated genes, or intermittent hypoxia [322,378-380].

Conclusions

This is the first study to quantitively characterize any population of ascending propriospinal neurons and showed that LAPNs are morphologically heterogenous. This heterogeneity suggests LAPNs have diverse synaptic inputs and potentially differing roles in locomotion. The coronal orientation of LAPN neurites is conserved among propriospinal neuron populations and among species and represents a morphology that is advantageous for locomotor output. Additionally, LAPN neurite orientation and collateral targets are altered post-SCI indicating that despite being anatomically spared, LAPNs exhibit SCI induced plasticity that appears maladaptive. This plasticity is likely triggered by a loss of descending inputs and increased input from sensory afferents which sprout caudal to the injury. Further characterization of LAPN transcriptional profiles at various timepoints post-SCI may provide potential therapeutic targets.

Limitations

The cluster analyses used here are unbiased and clustered LAPNs into distinct clusters both in the sham and SCI groups. For comparisons between sham and SCI groups, we compared individual clusters with one another. Though the morphometrics of the clusters were similar to one another, there is no way to confirm that the LAPNs in each cluster are part of the same subgroups of LAPNs in the sham and SCI groups.

CHAPTER IV

FOCUSED ULTRASOUND AND INTRAVENOUS MICROBUBBLES CONFER FOCAL CELL SPECIFIC GENE TRANSFER IN THE RODENT LUMBAR SPINAL CORD

The semi-selective permeability of the blood spinal cord barrier (BSCB) is vital in maintaining a homeostatic environment. However, this property of the BSCB makes it challenging to successfully target the spinal cord with therapeutics. Here, we demonstrate that focused ultrasound plus intravenous microbubbles (FUS+MB) can be used for transient, focal permeabilization of the BSCB in the lumbar enlargement and can be optimized to minimize histopathology. Following BSCB permeabilization, we delivered low-dose ($3.5x10^{12}$ vg/kg) adeno-associated virus 9 (AAV9) with a neuronal-specific promoter (scAAV9-hsyn-NLS-EGFP) to evaluate gene transfer in neurons at the target site. Gene transfer was highly neuron-specific with >90% of viral expressing cells being neuronal and resulted in little functional deficits. FUS+MB and systemic AAV delivery may provide a non-invasive means of targeting spinal segments and allow for the development of safe and effective gene therapies to treat spinal cord injury.

Introduction

The blood brain barrier (BBB) and blood spinal cord barrier (BSCB) are comprised of pericytes, endothelial cells, and astrocytic end feet and provide a selective semi-

permeable membrane that regulates the movement of molecules and ions between the blood and CNS [250]. These functions are vital to maintain a homeostatic environment, minimize pathogen exposure, and regulate nutrient trafficking to the CNS [251]. However, this tightly regulated trafficking of molecules across the BBB/BSCB makes it difficult to successfully target the CNS with therapeutics, as evident by the inability of 100% of large molecule and >98% of small molecule drugs to cross the BBB/BSCB and enter the parenchyma from the blood stream [252]. To bypass the BBB/BSCB for therapeutic delivery to the CNS, intrathecal or intracerebroventricular delivery via injection or catheter implantation can be used [253]. These routes of administration allow CNS wide targeting which may not be desirable depending on the disease pathology [254-257]. Hyperosmotic agents can be delivered intravenous to cause a shrinkage of the endothelial cells of the BBB/BSCB allowing for passage into the parenchyma, but effects are seen throughout the CNS transiently [258,259]. Focal targeting within the CNS can also be achieved through direct intraparenchymal injection. However, this involves invasive and potentially risky surgery. Given the benefits and disadvantages of each route of administration, ideal therapeutic delivery to the CNS would be as minimally invasive as intravenous (IV) delivery and provide the focal targeting of intraparenchymal injection.

IV administration of various adeno-associated viral (AAV) vectors has successfully targeted the CNS and provides a promising platform for noninvasive delivery of gene therapies to the CNS [260,261]. Most notably, in 2019 Zolgensma was approved for treating spinal muscular atrophy (SMA) and uses a self-complimentary (sc) AAV9 to express the survival motor neuron 1 gene allowing for widespread gene transfer throughout the CNS

[262,263]. However, this treatment requires high doses (1.1 x 10^{14} vg/kg) of clinical grade vector which costs 2.1 million USD per patient. While no serious adverse events were reported during early clinical trials, two patients receiving this treatment recently died from acute liver failure related to AAV delivery [264]. The same was reported for 4 patients in a phase 2 clinical trial for that delivered 3 x 10^{14} vg/kg of AAV8 via IV injection to treat X-linked Myotubular Myopathy [265]. Furthermore, pre-clinical studies using similar doses in nonhuman primates and piglets found hepatic toxicity, dorsal root ganglia pathology, proprioceptive deficits, and/or ataxia in treated animals [266,267]. Therefore, for safe and effective targeting of the CNS via IV administration, gene transfer must be more efficient allowing for lower viral doses to be used.

Gene transfer to the CNS can be improved through viral capsid modifications [268,269] or modifications to the BBB/BSCB using hyperosmolar agents [270,271], receptor modifications [272], or fatty acids [273]. However, none of these methods allow for focal targeting, which may be vital for the treatment of disease such as spinal cord injury (SCI), traumatic brain injury, CNS cancers, or Parkinson's disease. A potential solution allowing for transient focal disruption of the BBB/BSCB is the application of focused ultrasound (FUS) in combination with intravenous microbubble (MB). Following IV injection of MBs, sonication causes MBs to cavitate which generates microstreaming or jetting, causing shear stress on adjacent tissues. These shear stresses result in a widening of tight junctions of the BBB/BSCB allowing otherwise imperviable molecules to enter the parenchyma [274,275]. FUS+MB has been shown to successfully and transiently permeabilize the BBB/BSCB allowing for focal delivery of therapeutics in preclinical

studies [276-278], and there are currently two active clinical trials assessing safety and feasibility for clinical use (NCT04804709 & NCT05615623).

Smith et al. successfully used FUS+MB to deliver tratuzumab (a monoclonal antibody) to the thoracic spinal cord of rats and Weber-Adrian et al. used a similar approach to attempt to deliver AAV9 to the cervical spinal cord of rats, but the histology of this study appears inconclusive [277,279]. To date, no studies have optimized FUS+MB to transiently permeabilize the BSCB in the lumbar spinal cord for AAV delivery. The primary goals of the current study are to; 1) optimize FUS+MB for focal targeting of the spinal cord in a preclinical animal model and 2) once optimized, evaluate gene transfer utilizing IV low-dose AAV coupled with FUS+MB. We chose to target the lumbar spinal cord as it houses the hindlimb locomotor central pattern generators (CPGs) [69,280-282] and following SCI neuromodulation of the lumbar enlargement improves locomotor function [283], bladder function [284], and regulates blood pressure [285]. Furthermore, since Kathe et al recently identified a subset of neurons in the lumbar enlargement that are likely responsible for the improved locomotor function seen with neuromodulation, we aimed to made gene transfer cell specific [286].

Methods

Bone attenuation testing

Prior to *in vivo* experiments, the amount of attenuation from bone was evaluated. A 0.2-mm needle hydrophone (Precision Acoustics, Dorset, UK) was attached to a micromanipulator and suspended in a water-filled tank, along with a clinical ultrasound transducer (P4-1, ATL, Seattle, WA). The transducer was used with an ultrasound imaging

system (Vantage 64 LE, Verasonics, Kirkland, WA) to transmit B-mode ultrasound pulses (2.5 MHz center frequency, 2 MPa peak rarefactional output pressure). For control measures, the transducer was positioned 3 cm away from the hydrophone and aimed at the tip of the hydrophone. The hydrophone was moved via the micromanipulator and measurements were taken at 0.05-inch intervals. Measurements were repeated 3 times at each location and averaged. For vertebral column measures, a rat vertebral column was suspended in the tank and the hydrophone guided into the vertebral foramen. The transducer was aimed at the vertebral bodies of interest and measurements were taken in the same manner as control measures. Following thoracolumbar testing, a laminectomy was performed to remove the posterior aspect of the vertebrae, and measurements were repeated.

In vivo ultrasound and microbubble procedures

All animal procedures were reviewed and approved by the University of Louisville Institutional Animal Care and Use Committee and Institutional Biosafety Committee. A total of N=24 female Sprague Dawley rats (180–220 g: Inotiv Maryland Heights, MO) were used. Groups were as follows; N=15 for *in vivo* optimization of MB dose (3 per group), N=6 for (3 per group) for 24 hour versus 7 days, and N=3 for viral delivery. Prior to procedures, animals were housed two per cage with *ad libitum* food and water light/dark cycle and were handled by researchers daily prior to any procedures or behavioral testing.

Two weeks prior to ultrasound procedures, T12 laminectomies were performed to remove bone overlying lumbar spinal cord levels 2/3 (L2/3). Animals were anesthetized with 1–2.5% isoflurane in 98% oxygen at a rate of 1 L/min. Prior to surgical openings,

animals were given 5 mL of saline (s.c.), buprenorphine (10 mg/kg, s.c.), and meloxicam (1.5 mg/kg, s.c.). Following laminectomies, muscle was sutured together, and wounds closed with surgical staples. Post-surgery, animals were single housed for 7 days, administered saline 2x/day for 3-5 days, buprenorphine 3x/day for 3 days, and meloxicam 1x/day for 3 days at previously mentioned dosages.

Neutral lipid-coated microbubbles in sterile PBS, composed of 1.9 mg DSPC, 0.02 mg DSPG, and 0.08 mg polyoxyethylene-40 stearate with a perfluorobutane gas core, were synthesized via amalgamation as previously described [287], diluted (volume/volume) in sterile phosphate buffered solution (PBS) and gently mixed. For ultrasound procedures, animals were anesthetized with 1–2.5% isoflurane in 98% oxygen at a rate of 1 L/min, given 5 mL of saline (s.c.), and given atropine (0.2mg/kg, i.m.). Animals' backs were shaved, and ultrasound gel (Aquasonic 100, Bio-medical Instruments Inc., Clinton Township, MI) liberally applied to skin overlying the thoracolumbar spine. Prior to microbubble administration and ultrasound treatment, ultrasound imaging was used to confirm correct placement of the transducer over the T12 laminectomy. For intravenous delivery of microbubbles, Evans Blue dye (E2129-10G, Sigma, St Louis, MO), and virus, a 5G winged catheter (SC 25BLK, Terumo, Somerset, NJ) was inserted into the tail vein. Successful tail vein insertion was confirmed by injecting 0.1-0.3 mL of saline prior to administration of microbubbles, Evans Blue dye, or virus.

For microbubble delivery, 0.15 mL of microbubbles were injected (i.v.). Ultrasound transmission was started immediately following microbubble injection and transmission lasted for two minutes, the following parameters were used: 2.5 MHz

center frequency, 4 MPa peak rarefactional output pressure, 10 ms pulse duration, 1 Hz pulse repetition frequency. For microbubble dose optimization experiments, 0.4mL of sterile 3% Evans Blue was injected (i.v.) immediately following ultrasound transmission. For viral delivery, scAAV9-Syn1-NLS-EGFP(AAV) (produced by Vector Builder, Chicago, IL: titer = $1.9x10^{13}$ gc/mL) was diluted with sterile PBS and $3.5x10^{9}$ gc/gram of body weight was injected I.V. at the end of ultrasound transmission. Following ultrasound procedures animals were monitored until awake and alert. One animal did not recover from anesthesia following AAV delivery, leaving an N of 2 in the viral delivery group. Autopsy revealed no gross tissue pathology and irregular breathing was noted throughout the anesthesia period, even prior to FUS+MB delivery.

Behavioral assessments

Prior to laminectomies and ultrasound procedures, animals receiving AAV injections underwent baseline motor and sensory testing. Overground gait analyses and interlimb phase calculations were performed as previously described [94,95,288]. Phase values from overground recordings were converted to a linear scale to eliminate any lead limb preferences and allow for linear plotting. Thermal nociceptive thresholds of the hind paws were tested using the Hargreaves test, where animals were placed a warmed glass surface (32°C) and allowed to acclimate to the environment for 10-15 minutes. Infrared light was shone onto the plantar surface of the foot and latency recorded. At least 2 minutes elapsed between trials. Mechanical sensory recognition of each hind paw was tested using Semmes-Weinstein filaments [289]. Animals were placed in testing chambers to acclimate for 10-15 minutes prior to testing. The dorsum of the foot

was contacted with the starting filament (5.18 g) for up to 1 second and was considered a “hit” if the animal oriented toward the contacted paw, withdrew the paw reflexively, slowly withdrew the paw, or stepped away from the stimulus. If the stimulus was recognized, the next lowest force filament was used, and if the stimulus was not recognized, the next highest force filament was used. This was repeated for 11 trials, and at least 2 minutes elapsed between trials.

Tissue processing and microscopy

For tissue harvesting, animals were anesthetized using a cocktail of ketamine, xylazine, and acepromazine, (40, 2.5, and 1 mg/kg, i.p.), transcardially perfused with 4°C PBS (pH 7.4) followed by 4°C 4% paraformaldehyde, and spinal cords were harvested. Additionally, in animals that received AAV, livers, kidneys, and the soleus muscle were harvested. All tissues were post-fixed in 4°C 4% paraformaldehyde for 1-2 hours and transferred to 30% sucrose for 3-4 days at 4°C. The spinal lumbar enlargement, one kidney, and the median lobe of the liver were isolated, individually embedded in tissue freezing medium, cryosectioned at 30 µm, slide mounted in sets, and stored at −20°C until histologically processed.

To evaluate astrocyte reactivity (via glial fibrillary acidic protein, GFAP) red blood cell extravasation (via heme), green fluorescent protein (GFP) from AAV expression, and/or the presences of neurons (via NeuN), immunohistochemistry was used. Sections were heated at 37°C for 30 min, rehydrated in room temperature PBS for 10 min, incubated in a blocking solution made of nine parts milk solution (bovine serum albumin [BSA]), 0.75 g of powdered skim milk, and 14.25 ml 0.1% of PBS with Tween 20 (PBST)

and one part 10% normal donkey serum (NDS) and/or 10% normal goat serum (NGS) for 60 minutes. Blocking was followed by a 10 min wash in PBS and an overnight incubation at 4°C with mouse anti-GFAP at 1:250 (MAB3402, Millipore, Burlington, MA), rabbit anti-heme at 1:100 (LS-C409143, LSBio, Seattle, WA), chicken anti-GFP at 1:500 (GFP-1020, Aves, Davis, CA), and/or mouse anti-NeuN at 1:250 (MAB377, Millipore). Tissue was then washed 3 times alternating between PBS and PBST for 10 minutes each, followed by incubation with the appropriate secondary antibodies (donkey anti-rabbit Plus 488, Thermofisher, A32790, Waltham, MA; donkey anti-mouse 594, A21203, Invitrogen, Waltham, MA; donkey anti-mouse Plus 647, A32787 and goat anti-chicken 488, A32931, Invitrogen) at 1:200 at room temperature for 1 hour. For nuclear staining, sections were washed in PBS with Hoechst (ThermoFisher, Waltham, MA, 1:1000) for 10 minutes followed by more alternating washes between PBS and PBST for 10 minutes each and coverslipped with Fluoromount-G (Southern Biotech, 0100-01, Birmingham, AL).

Following the manufacture's protocol, a hematoxylin and eosin (H&E) staining kit (ab245880, Abcam, Waltham, MA) was used to qualitatively assess morphology and structure of spinal cord tissue. Slides were coverslipped with Permount (SP15-100, Fisher Scientific, Houston, TX).

Widefield fluorescent images of tissue sections were acquired using a Nikon (Melville, NY) Ti2E inverted microscope with SOLA SE LED white light engine, Hamamatsu Orca Fusion Gen III camera, and DAPI, GFP, TRITC and Cy3 filters. One slide from each set was imaged, and stitched images were acquired using a CFI60 Plan Apo λ 10X NA lens, with the appropriate filter(s). Kidney, liver, and skeletal muscle tissue were

imaged with the same equipment using a CFI Plan Fluor 4X NA lens. Widefield images of H&E stained tissue were acquired with Nikon Eclipse Ti inverted microscope.

Microscopy quantification

For percent positive area, measures of Evans Blue and GFAP and heme immunofluorescence, all images were analyzed in NIS-Elements AR (Nikon, version 5.30.05). First, thresholds were set for each marker, a rectangular region of interest (ROI) was selected at the target area (all ROIs were the same size for each image) and the % of positive area was calculated. For rostrocaudal distance measures of Evans Blue and AAV spread, thresholds were applied to determine positive areas and the greatest distance between positive points was measured.

To determine what percent of AAV expressing cells were neurons, a custom analysis program was built in Nikon elements. The program first applied thresholds to each channel, filtered and separated positive objects for each channel, and quantified the number for viral positive cells and the number for viral positive neurons so that percent positive cells could be calculated.

Statistical analyses

To evaluate bone attenuation at different levels of the vertebral column, pressure measurements were averaged at each measurement interval location and sets of locations were grouped based on the corresponding vertebral level. Two-way ANOVAs were performed in SPSS (Version 22, IBM, New York, NY) for each condition and when appropriate pairwise comparisons were performed with Tukey's HSD *post hoc* test.

For comparison of BSCB permeability (Evans Blue extravasation), the length of BSCB permeability, astrocyte reactivity, and hemoglobin extravasation, one-way ANOVAs followed by Tukey's HSD *post hoc* where appropriate were performed in Prism 9 (GraphPad Software, Version 9.5.1). Binomial Proportion Tests were used to evaluate differences in the proportion of abnormal phase values from overground kinematics and were defined as greater than 2 standard deviations from baseline measures. Hargreave's and Semmes-Weinstein test outcomes were compared using Freidman test and Dunn's multiple comparisons test *post hoc* when appropriate in Prism 9. *P* values for all analysis were considered statistically significant when $p<0.05$, and two-tailed *p* values are reported for post hoc t-tests.

Results

Laminectomy is required for FUS delivery to the lumbar spinal cord

Bone can attenuate an ultrasound signal and impair successful delivery to target tissue [290]. To verify successful delivery of ultrasound pressures to the spinal cord via the vertebral foramen, pressures were measured at multiple levels of the spinal column. Control pressure measurements (with no spinal column) were similar to pressures within the cervical spinal column at all cervical levels (Figure 12A). This indicates that at the pressures tested, rat cervical vertebrae provide little to no attenuation of ultrasound signal, which is not surprising as cervical vertebrae are less dense and the vertebral lamina and spinus process are thin compared to thoracolumbar vertebrae [291]. Contrary to cervical vertebrae, pressures in spinal foramen at all thoracolumbar levels were significantly lower (Figure 12B) compared to control measures, demonstrating that

ultrasound signal is attenuated at these levels. In an effort to increase pressures delivered to the thoracolumbar spinal foramen, a laminectomy was performed at T13, which overlies spinal levels L1-3, depending on the age of the rat. Rostral to the laminectomy at T11 and T12 the pressures were lower compared to control levels but at/near the laminectomy site pressures were similar to control measures (Figure 12C). These results indicate that a laminectomy allows successful delivery of ultrasound pressures to rat thoracolumbar spinal foramen.

Permeabilization of the BSCB requires optimized MB dosing

The relationship between microbubble concentration/dose is nonlinear related to the effects of ultrasound on the tissue and can impact the mechanical index which may result excess cavitation and tissue damage [292-294]. To achieve high levels of BSCB permeability and minimize potential side effects, various doses of MBs were evaluated. Following FUS+MB targeting of the lumbar spinal cord, Evans Blue was injected IV to evaluate BSCB permeability (Figure 13A). Percent positive area measures (Figure 13B) show that a 1% MB dose produced greater permeabilization than 0% and 0.1% MB doses and 2.5% and 5% MB doses resulted in similar levels of permeabilization, both of which were greater than all lower doses. Furthermore, the rostrocaudal spread of Evans Blue (Figure 12D) was greatest at 2.5% and 5% microbubble doses. The amount of Evans Blue spread due to BSCB permeabilization suggests that both 2.5% and 5% MB doses allow for targeting of 2-3 lumbar segments in rats [295]. However, overt tissue disruption and histopathology are seen using with 5% MB dose (Figure 13C).

As BSCB/BBB disruption can induce glial reactivity [296-298] and cause extravasation

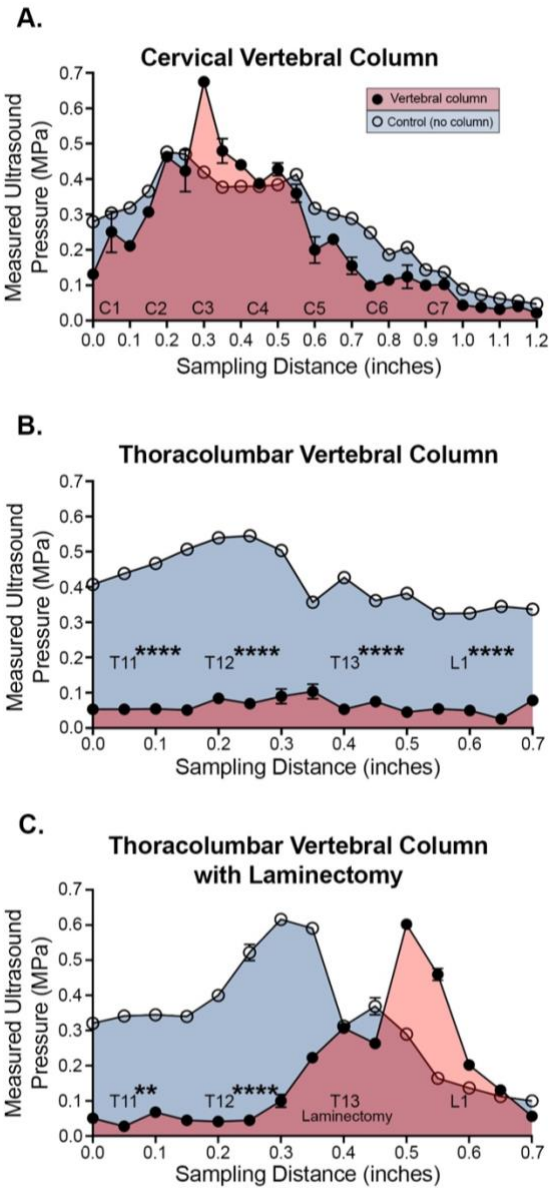

Figure 12. Laminectomy is required for ultrasound delivery to thoracolumbar spinal foramen. **A.** Graph showing ultrasound pressure measurements in at various levels of the intact cervical spinal column (filled circles and red area under the curve), overlayed with control measures (open circles, blue area under the curve). (Two-way ANOVA; between groups $p < .0001$, within groups $p = .07$, interaction $p = .07$) (Pairwise comparisons between groups, $p < .0001$ for all comparisons) **B.** Graph

showing ultrasound pressure measurements at various levels of the intact thoracolumbar spinal column (filled circles, and red area under the curve), overlayed with control measures (open circles, blue area under the curve) (Two-way ANOVA; between groups p <.0001, within groups p <.0001, interaction p <.0001) (Pairwise comparisons between groups, p <.0001 for all comparisons)**C.** Graph showing ultrasound pressures measurements at various levels of the of the thoracolumbar spinal column following laminectomy (filled circles and red area under the curve), overlayed with control measures (open circles and blue area under the curve). All circles represent means of 3 measurements and, if present, error bars represent standard deviations of those measures. (Two-way ANOVA; between groups p = .01, within groups p =.001, interaction p = .001) (Pairwise comparisons between groups, T11, p = .006; T12, p < .0001, T13, p = .61; L1 p = .31). **p<.01, ***p<.001 ****p<.0001, significance on graphs represents between group comparisons at each spinal level.

of red blood cells (RBCs) [275,299] into the parenchyma, we immunohistochemically evaluated astrocyte reactivity via GFAP expression (Figure 14A) and RBC presence via hemoglobin (Figure 14B). Percent positive areas for GFAP expression were low at 0%, 0.1%, and 1% MB doses and increased at 2.5% and 5% MB doses. Similarly, hemoglobin extravasation was minimal at low MB doses and significantly increased at 2.5% and 5% MB doses. While increased glial reactivity and hemoglobin presence were seen at 2.5% MB dose, this dose also allowed for successful permeabilization of 2-3 spinal segments and produced no visible histopathology. Therefore, the 2.5% MB dose was used for subsequent experiments.

BSCB disruption, glial reactivity, and hemoglobin extravasation are transient with 2.5% MBs

To confirm integrity of the BSCB at 7 days following FUS+MB, Evans Blue was delivered IV at 7 days. Percent positive area of Evans Blue was lower at 7 days post-FUS+MB compared to 0 days post-FUS+MB (Figure 15A), indicating that by at least 7 days after FUS+MB BSCB integrity is restored. Additionally, glial reactivity (Figure 15B) and the presence of hemoglobin (Figure 15C) were significantly lower by 7 days post-FUS+MB. These findings suggest that glial reactivity and leakage of other potentially harmful molecules into the parenchyma following FUS+MB are resolved by 7 days post-FUS+MB.

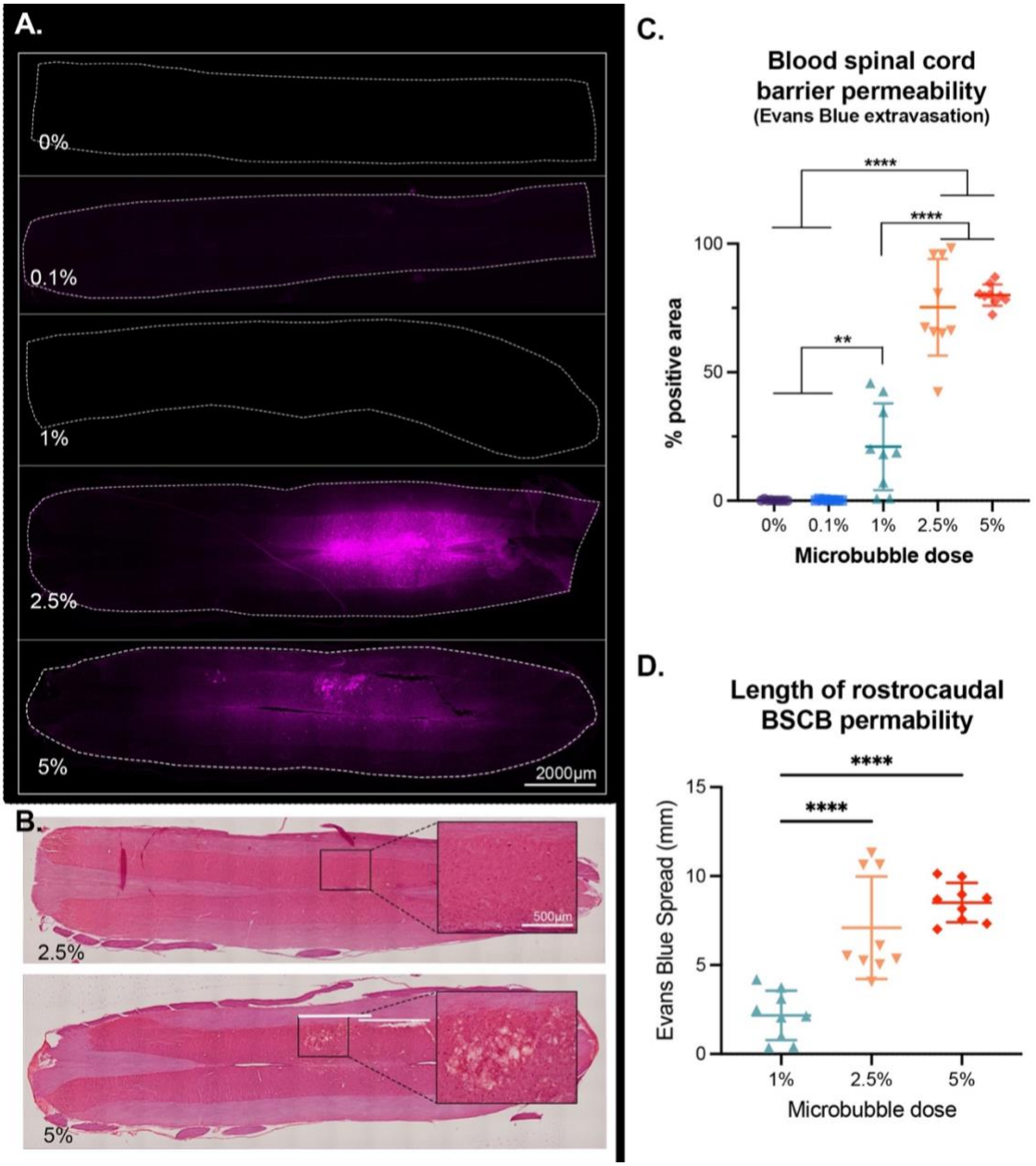

Figure 13. 2.5% microbubble dose allows for maximal rostrocaudal targeting of the spinal cord without disruptions in tissue morphology. **A.** Representative longitudinal sections of the lumbar enlargement showing Evans Blue extravasation (magenta) into the parenchyma at various microbubble doses. **B.** Representative H&E-stained longitudinal sections of the lumbar enlargement following 2.5% and 5% microbubble

doses. Sections shown are adjacent sections to those shown in 2A. **C.** Evans Blue Percent positive area comparisons between groups show that 1, 2, and 5% (One-way ANOVA, $p<.0001$) microbubble doses allow for Evans blue extravasation compared to 0 and 0.1%, and 2.5 and 5% allows for maximal Evans Blue extravasation. (Tukey's multiple comparisons test; 0% vs 1%, p= .004; 0% vs. 2.5% or 5%, p <.0001; 0.1% vs. 1%, p=.004; 0.1% vs.2.5% or 5%, p <.0001; 1% vs 2.5% or 5%, p<.0001) **D.** Rostrocaudal length of Evans Blue extravasation is greater (One-way ANOVA, $p<.0001$) at 2.5 and 5% microbubble dose compared to 1%.(Tukey's multiple comparisons test; 1% vs 2.5% or 5%, p<.0001) **C&D** Large center lines show group means and error bars are standard deviations. **$p<.01$, **** $p<.0001$.

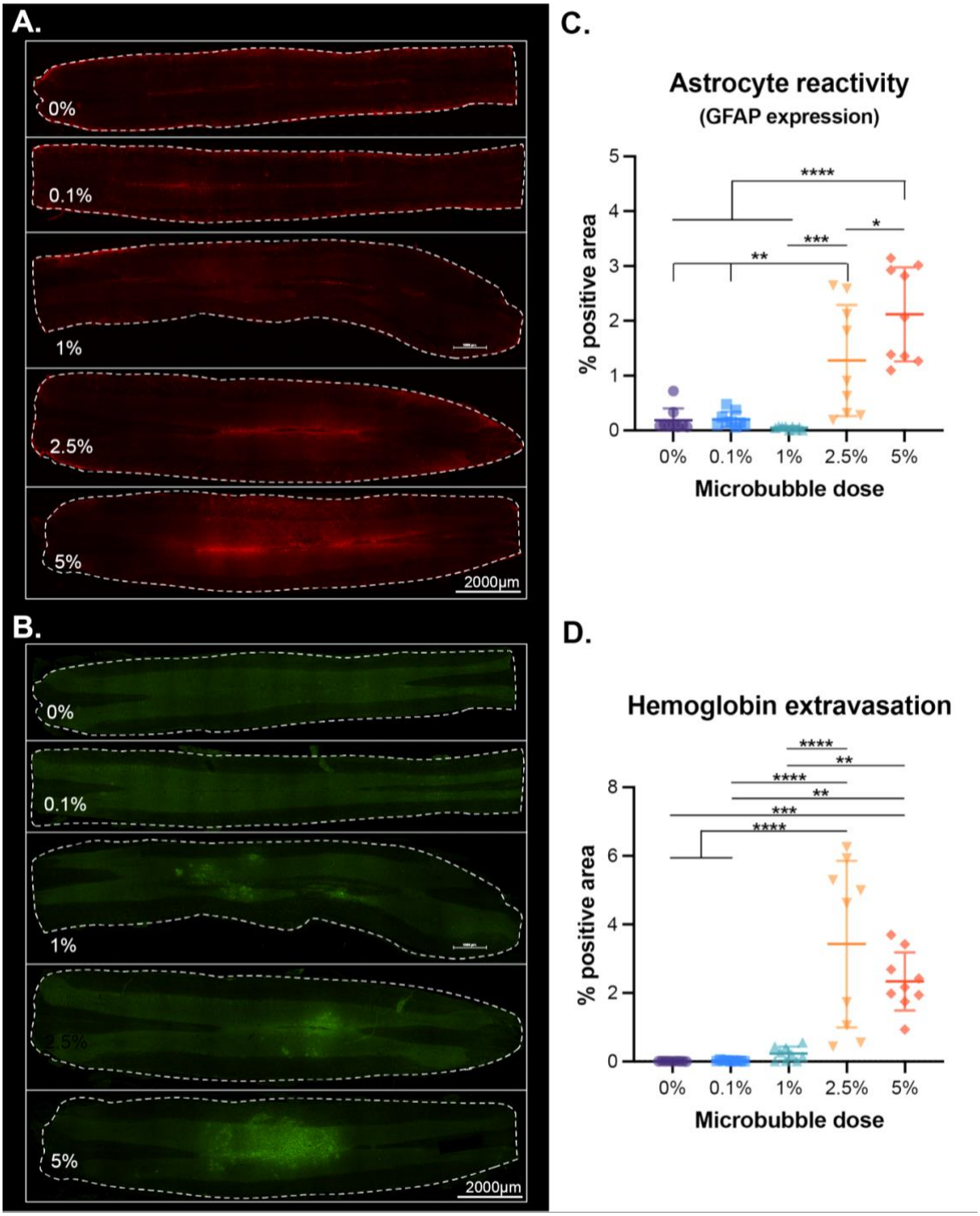

Figure 14. 2.5% and 5% microbubble doses cause astrocyte reactivity and hemoglobin extravasation into the lumbar spinal cord parenchyma. **A.** Representative longitudinal sections of the lumbar enlargement showing GFAP (red) at various microbubble doses**.**

B. Representative longitudinal sections of the lumbar enlargement showing the presence of hemoglobin (green) in the parenchyma at various microbubble doses. **C.** Percent GFAP positive area is greater One-way ANOVA, $p<.0001$) with 2.5 and 5% microbubble doses. (Tukey's multiple comparisons test; 0% vs 2.5%, p= .004; 0% vs.5%, p <.0001; 0.1% vs. 2.5%, p=.005; 0.1% vs. 5%, p <.0001; 1% vs 2.5%, p=.001, 1% vs. 5%, p<.0001; 2.5% vs. 5%, p=.04) **D.** Percent positive area of hemoglobin is greater (One-way ANOVA, p<.0001) with 2.5 and 5% microbubble doses. (Tukey's multiple comparisons test; 0% vs 2.5%, p<.0001; 0% vs.5%, p=.001; 0.1% vs. 2.5%, p<.0001; 0.1% vs. 5%, p <.0001; 1% vs. 5%, p=.004) **C&D** Large center lines show group means and error bars are standard deviations. $**p<.01$, $***p<.001$, **** $p<.0001$.

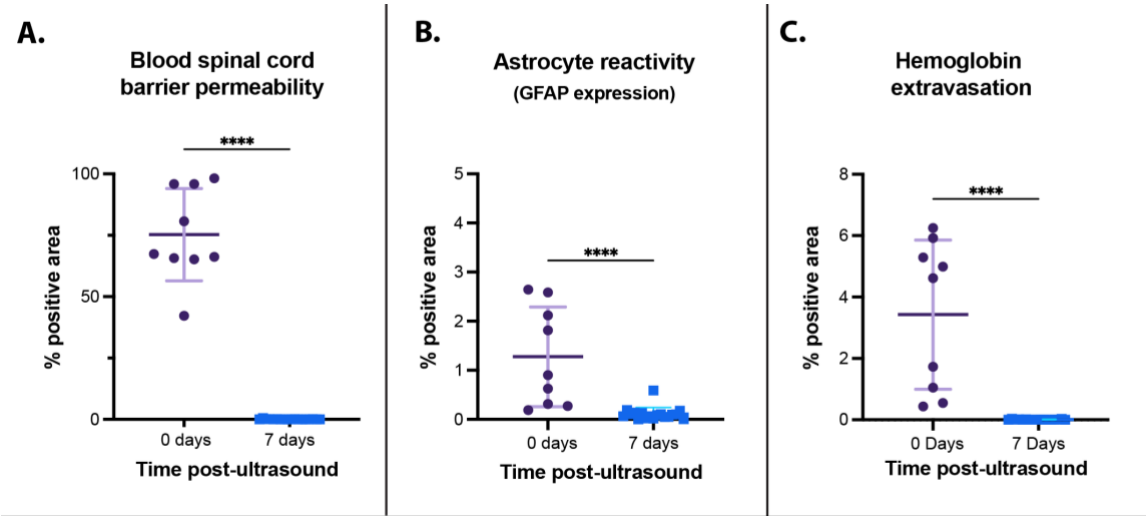

Figure 15. 7 days following FUS + 2.5% MB potential side effects in the lumbar enlargement are resolved. **A.** Evans blue extravasation is not seen 7 days after pFUS+MB. (unpaired *t* test, $p<.0001$) **B.** Hemoglobin presences is lower 7 days after FUS + MB compared to 24 hours**.** (unpaired *t* test, $p<.0001$) **C.** Astrocyte reactivity (GFAP presence) is decreased 7 days following FUS + MB compared to 24 hours. (unpaired *t* test, $p<.0001$) **A-C.** Large center lines show group means and error bars are standard deviations. **** $p<.0001$.

Low dose AAV and FUS +MB confers spatially regulated and cell-specific gene transfer in the lumbar spinal cord

To evaluate gene transfer to the lumbar enlargement, immediately following FUS+MB, scAAV9-Syn1-NLS-EGFP was injected IV at $3.5x10^9$ gc/gram of body weight. Gene transfer was successful in both animals (Figure 16A-D). In animal 1, 1406 vector expressing cells out of 1516 were neurons, and in animal two 3292 of 3491 vector expressing cells were colocalized with the neuronal marker (Figure 16E). This indicates that a high level of neuron-specific gene transfer was achieved. In both animals, the rostrocaudal spread of viral expressing cells was enough for expression of 1-2 levels in the rat lumbar spinal cord (Figure 16F) (distance in µm $\pm$ SD; animal 1: 4053 $\pm$ 321.2, animal 2: 5416 $\pm$ 178.6). IV delivery of virus may inadvertently target peripheral tissues [180,300]. However, no expression was seen in skeletal kidney, liver, or skeletal muscle tissue (Figure 16G).

FUS + MB and low dose AAV causes minimal functional deficits

While no histopathology was seen, potential deleterious effects at the target area are ameliorated by 1-week post-FUS+MB, and neuron-specific gene transfer was achieved, it is vital to evaluate potential functional deficits should clinical translation be the goal. In both animals that received FUS+MB and IV AAV, hindpaw thermal sensitivity was evaluated using the Hargreaves' test (Figures 17A,B,E,F). The only difference in thermal sensitivity was an increase in response latency for animal 2's right hindpaw where latency increased from 1 week to 4 weeks post-FUS (mean withdraw time in seconds $\pm$ SD; baseline: 5.2 $\pm$ 0.7 ,1 week: 6.0 $\pm$ 1.5, 4 weeks: 8.9 $\pm$ 4.8). Mechanical

hindpaw thresholds were also tested for each animal using Semmes-Weinstein filaments and no differences were seen (Figures 17C,D,G,H).

Sensitive and in-depth analysis of locomotor function was performed using overground gait kinematics. Coupling patterns of each limb pair were determined by dividing the initial contact time of one limb by the stride time of the other limb. Resulting phase values of 0 or 1 indicate synchrony and values of 0.5 alternation of the limb pair. To eliminate discrepancies in of the lead limb selection and for ease of visualization, phase values were converted to a linear scale of 0.0 - 0.5 or 0.5 – 1.0. Mean phase values of the limb pairs were calculated at baseline and any value >2 standard deviations from these means were considered 'irregular', as indicated by the blue boxes (Figure 17I-P). Animal 1 had a small but statistically significant increase in the number of irregular steps for the hindlimbs at 1 and 4 weeks post-FUS+MB (Figure 17I) (irregular/total phases; baseline: 1/36, 1 week: 8 / 34, 4 weeks: 6 /37), and an increase in irregular steps of the contralateral limb pairs at 4 weeks post-FUS+MB (Figure 17K) (irregular/total phases; baseline: 2/65 ,1 week: 4/61, 4 weeks: 11/58). Animal 2 showed a decrease in the number of irregular hindlimb steps at week 4 (Figure 17M) (irregular/total phases; baseline: 2/31, 1 week: 4/32, 4 weeks: 0/34), but an increase for the contralateral (Figure 17O) (irregular/total phases; baseline: 3/52, 1 week: 1/55, 4 weeks: 11 /53), and ipsilateral limb pairs (Figure 17P) (irregular/total phases; baseline: 2/54, 1 week: 4/56, 4 weeks: 15/58). For the 'irregular' phase values seen, interlimb coordination is not shifted enough to represent a transition from limb synchrony to alteration or vice versa, and no gross deficits were apparent during overground

locomotion testing. Both sensory and locomotor testing show that pFUS+MB with low dose IV AAV delivery produce minimal functional deficits.

Discussion

Focal targeting and routes of administration

Targeting the spinal cord for therapeutic delivery is made difficult by the BSCB which prevents >99% of large and small molecule drugs from entering the parenchyma following systemic administration [301]. The BSCB can be bypassed via other routes of administration such as intrathecal, intracerebroventricular, or via direct intraparenchymal injection. Direct injection allows for focal targeting but carries the inherent risk of complications [302]. FUS+MB provides a means to disrupt the BSCB noninvasively, transiently, and focally which allows the passage of large molecules and therapeutics into the parenchyma [303,304]. Here, we optimized FUS+MB parameters systemic delivery of a scAAV9 with a neuron-specific promoter for focal gene transfer in the lumbar spinal cord. While permeabilization of BSCB/BBB from FUS+MB is transient and function returns to normal within hours [305], FUS+MB may have undesired effects on the neurovascular units or allow potentially harmful molecules or cells into the parenchyma [306,307]. FUS+MB targeting the hippocampus and cerebral cortex in rats show that astrocyte reactivity begins as early as 3 hours after and may persists for up to 7 weeks [298,308,309]. In the spinal cord, we report that astrocyte reactivity, or lack thereof, returns to baseline levels at least by 7 days. Furthermore, BSCB permeability can allow the passage of RBCs into the parenchyma [275,299]. The presence of RBCs brings about the potential for ferroptosis, a non-necrotic form a cell death [310].

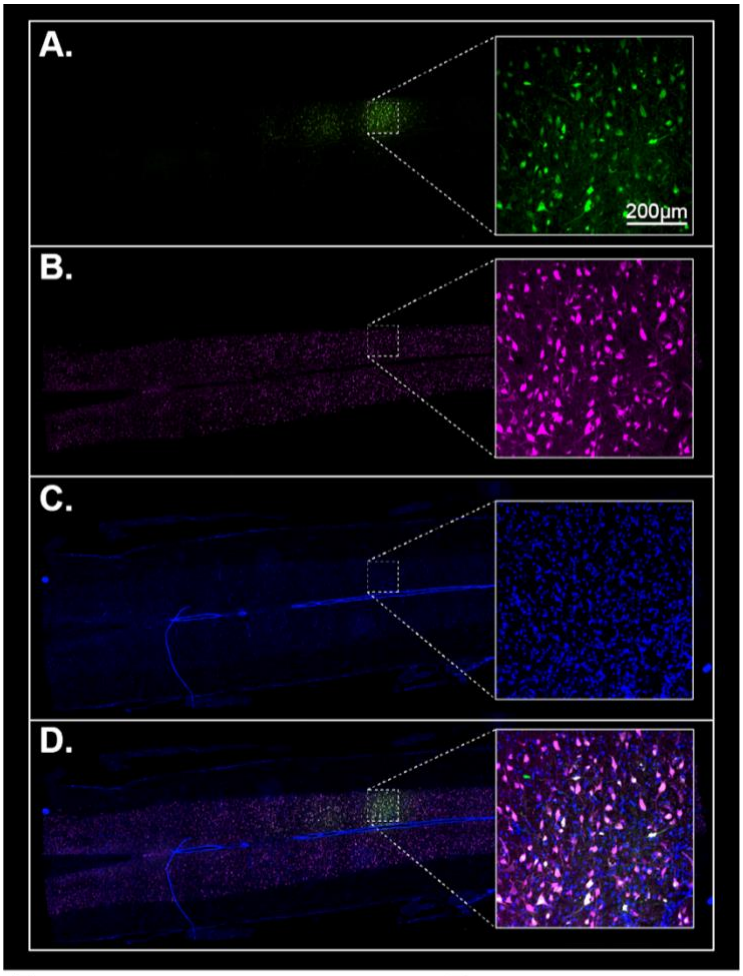
A.
200µm
B.
C.
D.

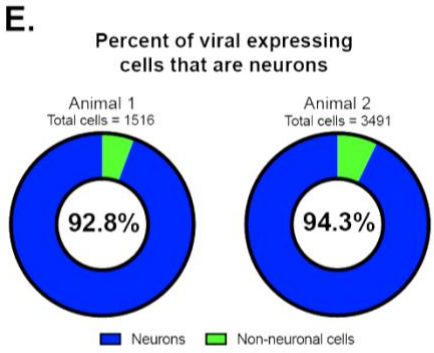
E.
Percent of viral expressing cells that are neurons
Animal 1
Total cells = 1516
92.8%
Animal 2
Total cells = 3491
94.3%
Neurons
Non-neuronal cells

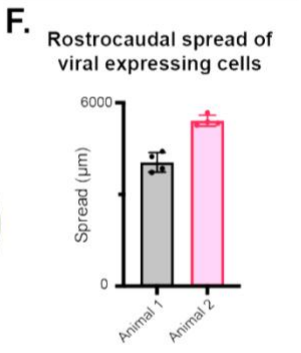
F.
Rostrocaudal spread of viral expressing cells
6000
Spread (µm)
0
Animal 1
Animal 2

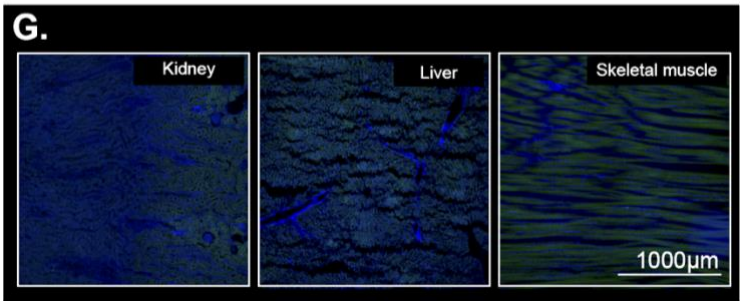
G.
Kidney
Liver
Skeletal muscle
1000µm

Figure 16. Intravenous AAV delivery following FUS+MB successfully targets neurons in the lumbar spinal cord with >90% accuracy. A-D. Longitudinal section of lumbar enlargement 4 weeks after FUS + MB and intravenous AAV delivery. Viral expression (green) is seen the target site (**A),** and immunohistochemistry for neurons (magenta) (**B**) and nuclear staining (blue) (**C**) are shown. **D.** Merged channels show colocalization of viral expression and neuronal marker (white). **E.** Donut graphs for each animal show the portion of viral expressing cells that are neurons is greater than 90%. **F.** Bar graph showing he rostrocaudal spread of virally expressing cells in the spinal cord. Error bars represent standard deviations. G. Microscopy showing that there is no off target viral expression in peripheral tissues following intravenous AAV delivery. Blue is nuclear staining with Hoechst and images are over exposed to show tissue structure.

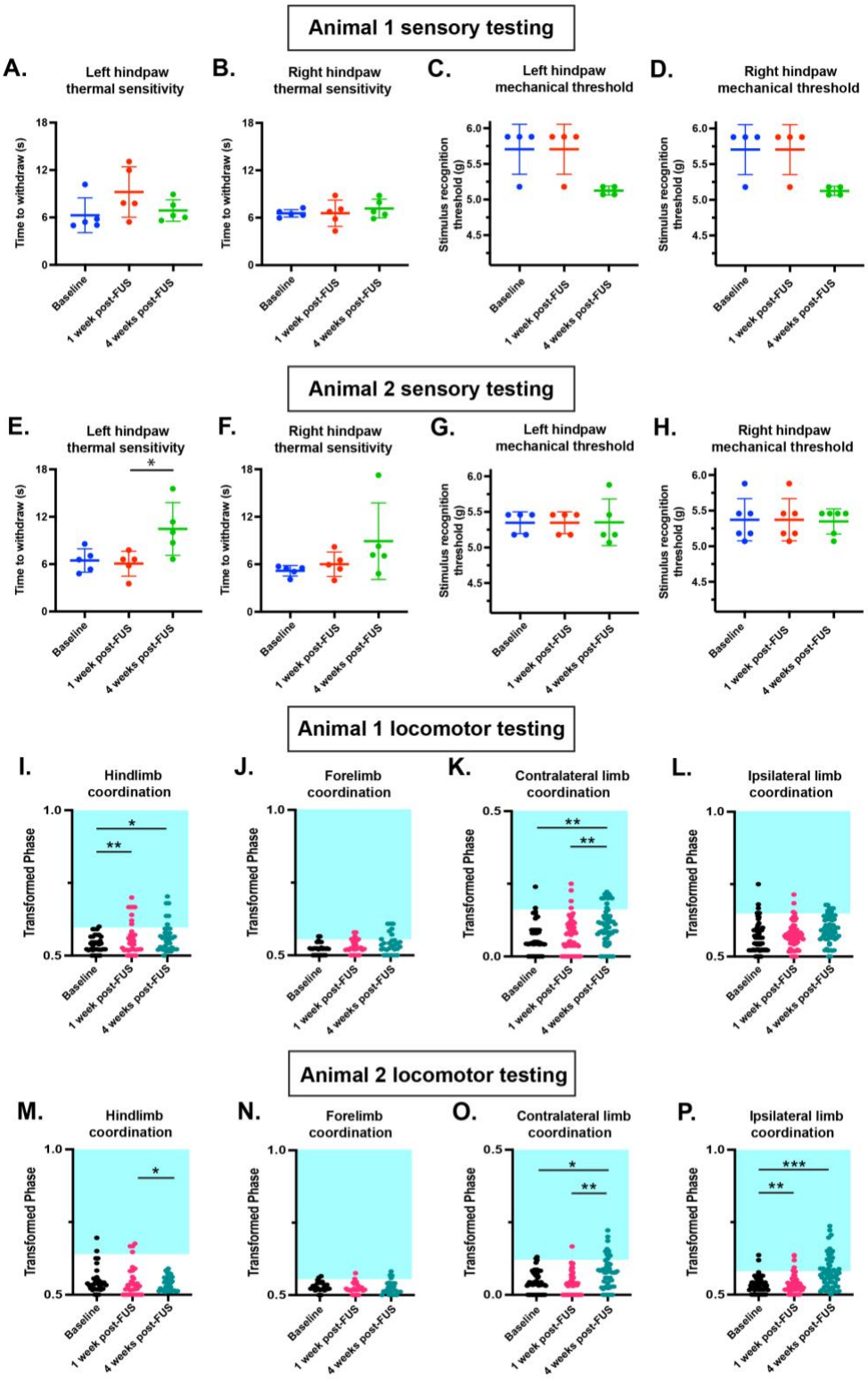
Animal 1 sensory testing
A.
Left hindpaw thermal sensitivity
B.
Right hindpaw thermal sensitivity
C.
Left hindpaw mechanical threshold
D.
Right hindpaw mechanical threshold
Time to withdraw (s)
Stimulus recognition threshold (g)
Baseline
1 week post-FUS
4 weeks post-FUS
Animal 2 sensory testing
E.
Left hindpaw thermal sensitivity
F.
Right hindpaw thermal sensitivity
G.
Left hindpaw mechanical threshold
H.
Right hindpaw mechanical threshold
Animal 1 locomotor testing
I.
Hindlimb coordination
J.
Forelimb coordination
K.
Contralateral limb coordination
L.
Ipsilateral limb coordination
Transformed Phase
Animal 2 locomotor testing
M.
Hindlimb coordination
N.
Forelimb coordination
O.
Contralateral limb coordination
P.
Ipsilateral limb coordination

Figure 17. Functional deficits following FUS+MB and intravenous AAV are minimal **A&B**. No differences in left or right hindpaw thermal sensitivity were seen for animal 1. (Friedman test, left $p = 0.18$, right $p = .52$) **C&D.** No differences in left or right mechanical stimulation detection were seen for either hindpaw of animal 1 (Friedman test, left $p = 0.11$, right $p = .66$) **E.** An increase in response latency in the left hindpaw thermal sensitivity in animal 2 at 4 weeks post-FUS+MB and IV AAV delivery compared to 1 week (Friedman test, $p = .02$; Dunn's multiple comparisons tests; baseline vs. 1 week, $p > .99$; baseline vs. 4 weeks, $p = .08$; 1 week vs. 4 weeks, $p = .03$) **F.** No differences were detected in right hindpaw thermal sensitive in animal 2 (Friedman test, $p = 0.18$) **G&H.** FUS+ MB and IV AAV delivery caused no differences in left or right hindpaw mechanical sensitivity in animal 2. **I-L.** Interlimb coordination in animal 1 showed an increase in the abnormal number of phase values of the hindlimbs (**I**) (binomial proportions test, baseline vs. 1 week, $p < .01$; baseline vs. 4 weeks $p < .05$) and of the contralateral limb pairs (**K**) (binomial proportions test, baseline vs. 4 weeks, $p < .005$; 1 week vs. 4 weeks $p < .05$). **M-P.** Interlimb coordination in animal 2 showed differences in the number of abnormal phase values for the hindlimbs (**M**) (binomial proportions test, 1 week vs. 4 weeks $p < .05$), the contralateral limb pairs (**O**) (binomial proportions test, baseline vs. 4 weeks, $p < .05$; 1 week vs. 4 weeks $p < .005$), and the ipsilateral limb pairs (**P**) (binomial proportions test, baseline vs. 4 weeks, $p < .001$; 1 week vs. 4 weeks $p = .005$). **A-H.** Large center lines show group means and error bars are standard deviations. **I-P.** blue background indicate phase values that are >2SDs from baseline measures. *$p<.05$, **$p<.01$, ***p<.001

Here, we found an increase in RBCs in the lumbar spinal cord following FUS+MB, but these cells were cleared from the parenchyma at least by 7 days post-FUS+MB. As ferroptotic cell death is not fully understood [311,312], future studies should examine whether the amount and duration of RBCs/hemoglobin present in the parenchyma following FUS+MB induces ferroptosis and which cells might be impacted

AAV delivery

Here FUS+MB allowed for successful focal gene transfer to the lumbar spinal cord using low dose intravenous AAV. Gene transfer in the CNS allows for long term transgene expression which subverts the need for repeated dosing of drug dosing and/or implantation of intracerebroventricular or intrathecal pumps (cite). The AAV serotype used here, AAV9, successfully targets the CNS in multiple species following IV administration [313-316], is currently approved for clinical use [262], but the relatively high doses (1.1×10^{14} vg/kg) needed for successful gene transfer and therapeutic effects can cause ataxia, DRG pathology, and death [266,267]. Here the AAV0 dose used is 2-fold lower, likely providing a safe and effect means of targeting the lumbar enlargement without risk of pathology. Other capsids have been developed allowing for CNS gene transfer at lower doses, however gene transfer does not appear to be ubiquitous among species or even strains of the same species [317,318]. Thus, we have shown that using a well characterized AAV serotype at low doses can be used to successful focal targeting of the lumbar enlargement.

Moreover, expression was restricted to neurons with >90% of virally expressing cells colocalizing with a neuronal marker. Previous studies show that in neonates IV

AAV9 confers highly specific neuronal transgene expression, but neuronal expression decreases in adult where AAV9 primarily infects glia [319,320]. Without BBB/BSCB disruption AAV9 is able to cross into the parenchyma and infect CNS cells via receptor-mediated transcytosis by endothelial cells [321], which might be the reason for decreased neuronal transgene expression in adults. It is plausible that during transcytosis virions undergo modification leading to an increase in non-neuronal tropism, or it may be proximity related as glial are part of the neurovascular unit and therefore adjacent to endothelial cells. Regardless of the rationale for the increase in non-neuronal tropism in adulthood, here we were able to successfully limit transgene expression to neurons in the target area of the adult CNS.

Conclusions

Optimization of microbubble dose allowed for successful permeabilization of the blood spinal cord barrier in the lumbar enlargement and adverse cellular responses at the target cite were ameliorated by 7 days post-FUS+MB. This allowed for focal and neuronal specific gene transfer to the lumbar spinal cord using low dose intravenous AAV9 ($3.5x10^{12}$ vg/kg), which resulted in minimal functional deficits at acute and chronic timepoints. More work is needed to determine if gene transfer will be similar in the pathologic spinal cord, but these results show feasibility for the use of FUS+MB and low-dose intravenous AAV to deliver focal and cell specific gene therapies to the spinal cord.

CHAPTER V

DISCUSSION

We know what we don't know, yet it goes unstudied: Cruxes of spinal cord injury research

Albert Einstein is credited with saying, **"**If I were given an hour in which to do a problem upon which my life depended, I would spend 40 minutes studying it, 15 minutes reviewing it and 5 minutes solving it." Unfortunately, is seems that the field of SCI research has taken the opposite approach, with the majority of efforts put forth being attempts to "cure" or "treat" the pathologic spinal cord, and a minority of efforts put towards understanding the spinal cord in a non-pathologic or pathologic state. This is evident as querying NIH reporter for funded projects in 2023 related to spinal cord and locomotion returns 58 results, 32 of which are related to studying the pathologic spinal cord and treatments. While some spinal cord circuitry is well elucidated, and we have principles by which we understand some spinal circuity and its function(s), our understanding of spinal cord connectomics is lacking [381]. Compared to the fidelity withwhich the brain connectome has been mapped, our knowledge of the spinal cord connectome is meagre. This discrepancy is surprising, but also somewhat expected. Surprising because the brain contains 400 times more neurons than the spinal cord, making it much easier to map the spinal cord. Yet, this is also expected as the spinal cord is often thought of as simply a conduit to relay top-down commands and unfortunately

this thought is prorogated in in medical textbooks and coursework [2,3]. However, the spinal cord is capable of complex processing of varied inputs, memory formation, and contains the required circuity to produce locomotion [8,382,383].

A common approach to understanding the structure and function of systems (whether they be mechanical, technological, or biological) is reverse engineering. This involves parsing out individual components/structures of a system so that something similar can be produced [384]. In an effort to reverse engineer the spinal cord and add to the spinal connectome, techniques were developed and optimized for mesoscale connectomics analyses of anatomically defined subsets of propriospinal neurons, the long ascending propriospinal neurons (LAPNs). The use of highly specific dual-viral tracing and large volume imaging allowed for precise and detailed characterization of LAPNs. Prior to this, our knowledge of LAPN anatomy was relegated to spinal laminar location and cell counts showing that approximately half of LAPNs project ipsilaterally and the other half contralaterally [91]. Poctrasky et al showed that LAPNs are involved in coupling primarily of the contralateral and hindlimb pairs, and LAPNs' influence on locomotion is only seen during non-exploratory overground locomotion on a high friction surface [94]. These findings coincide with the anatomical characterization of LAPNs here as dorsoventral neurite orientations were seen in two of three LAPN subsets suggesting that LAPNs receive incoming sensory input that is required for LAPNs to have influence/oversight on the locomotor circuitry. Furthermore, the fact that LAPN axons/collaterals densities were greatest in lamina IX in the cervical spinal cord suggests that LAPNs do no do not form a of "closed loop" circuit with the reciprocal long descending propriospinal neuron pathway

(LDPNs), as suggested by Shepard et al. but are more likely pre-motoneurons that have direct influence on output to forelimb muscles [95].

More specifically, based on how we have anatomically defined LAPNs, one would suggest that their primary role would be interlimb coordination of the hindlimb-forelimb pairs. However, LAPNs' most prominent role in locomotor function seems to be related to hindlimb-hindlimb coordination, as evident by the large disruptions in hindlimb-hindlimb coordination when LAPNs are silenced [94,95]. While not discussed in previous chapters, large volume confocal images showed extensive branching of neurites (some presumably axons) at the level of cell bodies and more caudally, descending axons were found in the ventral gray matter, providing an anatomical substrate for the role LAPNs play in hindlimb coordination. Overall, the anatomy and previously characterized function LAPN suggest that LAPNs are not "master coordinators" of the hindlimbs and forelimbs but rather their effects on hindlimb-forelimb coordination are an underlying consequence of their role in hindlimb-hindlimb (or potentially forelimb-forelimb) coordination. Thus, it seems that the pathways and circuitry that secure interlimb coordination of the hindlimb-forelimb pairs remains at least partially unknown.

The three subsets of LAPNs found here differed in size, neurite orientation, and complexity, which undoubtedly impacts their electrochemical properties and as hypothesized in Chapter 3 these subsets may be active at different locomotor speeds or be involved in different aspects of locomotor function. Literature defining spinal interneurons based on embryonic lineage, shows that V2a neurons have differential effects on motor outputs related to location in the spinal cord [385]. Ablation of V2a neurons

throughout the spinal cord disrupts hindlimb-hindlimb coordination [386], but targeted ablation in the cervical spinal cord has no impact on forelimb-forelimb coordination but impacts reaching and grasping [387]. These data indicate that despite being transcriptionally and structurally the same, subsets of spinal interneurons can have differing functional roles, which suggests that LAPN subsets may play differential roles related to behaviors that we have yet to elucidate.

Future studies are needed to determine if ipsilateral or contralateral LAPNs differ in structure or function and to evaluate if subsets of LAPNs are active/recruited at different locomotor speeds. To evaluate the latter, dual-viral tracing of LAPNs can be used and animals split into two groups. Groups would be allowed to express their full range of overground gaits, but speed (and therefore locomotor pattern) could be modulated by the length of runway/tank animals are allowed placed in. A with a short runway (1.5 meters) typically allows for only lower locomotor speeds to be expressed, while a longer runway (>3 meters) allows for maximal speeds to be reached and a full range of gait patterns to be expressed [388-390]. Immediately following locomotion on either of the runways, tissue would be harvested, subsequently sectioned, and immuno-stained for a marker of neuronal activity (cFOS). If differences in cFOS labeling is seen between LAPN subsets it is likely that they are recruited at different locomotor speeds and their context specificity is even more complex than what was shown by Pocratsky et al and Shepard et al [94,95].

Unfortunately, other major gaps in knowledge remain related to the synaptic inputs and outputs of LAPNs both pre- and post-SCI. Based on known soma locations, laminar targets of descending motor centers and electrophysiology studies, we can

speculate on LAPN inputs. In cats, stimulation of the mesencephalic locomotor region (MLR) produces monosynaptic field potentials from L4 to S1 in lamina 3-10, lamina where LAPN somata in cats likely reside [391]. It is likely these monosynaptic field potentials (MFPs) result from MLR→ reticular formation → lumbar enlargement, which may include LAPNs as targets. In *ex vivo* preparations, afferent input from muscle and joint receptors causes locomotor-like behavior, indicating that proprioceptive afferents can provide inputs to spinal locomotor circuits in the lumbar cord [392], and preliminary data for my NRSA fellowship (NIH/NINDS 5F31NS116935) showed that LAPNs receive putative Vglut1 synapses, which in the lumbar spinal cord are likely to be from sensory afferents [393]. The phenotype seen by Pocratsky et al. only occurred on high friction surfaces which likely provides more sensory input from the skin and muscles of the hindlimbs and only seen on high friction surfaces, and dorsoventral neurite orientation seen here all suggest that LAPNs likely receive inputs from sensory afferents [94].

In an effort to determine LAPN inputs, three years of testing and troubleshooting were undergone to unbiasedly label LAPN monosynaptic inputs throughout the neuroaxis in rats. To do so, first cre-recombinase dependent expression in an anatomically defined subset of neurons of two vectors is needed: 1) a TVA receptor and 2) the G protein from the rabies virus genome. Second, modified rabies virus is needed which has restricted transsynaptic spread (G-gene deletion) and restricted tropism via pseudotyping (envelope A pseudotyping). These modifications then allow for the modified rabies to initially infect the target cell population and jump retrogradely 1 synapse labeling monosynaptic inputs of the starter cells (LAPNs). Conceptually this is possible, but technically, these

experiments are challenging as they involve expression of 4 different viral vectors at the appropriate ratios and injections occur at multiple timepoints to target same subset of neurons [394]. We built cell lines to test each of the viral vectors and all conferred appropriate gene transfer *in vitro*. We also achieved successful expression of the first 3 vectors together *in vivo* but the fourth vector (modified rabies) has remained elusive. This is either due scar tissue at injection site making stereotaxic injections to target the location difficult and/or degradation of rabies virions prior to expression in the starter cell population. This is plausible as one of the viral vectors delivered during the initial set of injections (HiRet-Lenti) has been modified to contain portions of the rabies viral envelope, and given the CNS is capable of some level of immune memory, the subsequent injection of rabies virions could be recognized and targeted for degradation before gene transfer can be achieved [395]. However, there is a potential way to (biasedly) evaluate inputs of LAPNs. This would involve target-defined labeling of LAPNs, anterograde tracing of potential input pathways such as the reticular formation or afferent sensory nerves, followed by immunohistochemistry for pre- and post-synaptic markers, and high magnification confocal imaging for putative synapses onto LAPNs. These experiments were however beyond the scope of my defined research projects.

Injury-induced neuroplasticity. What matters? What doesn't?

In multiple species, injury-induced plasticity is seen throughout the nervous system. Sensory afferents sprout caudal to the injury [348,349], the cortex reorganizes [396], propriospinal neurons sprout [103], reticulospinal neurons sprout to contact cervical propriospinal neurons [102], motoneuron dendrite orientations shift and thalamic relay

circuits are altered [397,398]. Some of this injury-induced plasticity is adaptive and assists in recovery of function, while some leads to aberrant circuity that has deleterious functional effects. Given that we know little about the spinal connectome pre- and post-SCI, it is difficult to parse out which circuity plasticity is adaptive and maladaptive. This is made increasingly difficult as circuitry that governs function pre-injury may not be the same circuitry that is responsible for some level of recovery post-SCI. This is evident from a non-human primate study that showed post-SCI cervical propriospinal neurons are capable of restoring hand dexterity that is governed by cortical projections pre-injury [399]. Additionally, following staggered hemisection injuries, propriospinal neurons relay commands caudally and improve hindlimb function, circuitry which plays little role in locomotion pre-SCI [103]. This propriospinal plasticity has been credited with improved function, however the staggered hemisection model does not recapitulate human SCI. In the more clinically relevant contusion model used by Shepard et al. [83,95], silencing LAPNs or LDPNs improved locomotor functions after SCI. Thus, while the field has pushed the narrative that propriospinal relays contribute to improved function, this is not true for all injuries. Additionally, as LAPNs are located caudal to the lesion, they are subject to different inputs that may influence their plasticity and the circuits they form post-SCI. Due to this location, LAPNs are less impacted by top-down locomotor influences which may be partially required to "guide" adaptive propriospinal plasticity post-SCI. Perhaps the redundancy in top-down circuits is sufficient to correctly "guide" propriospinal plasticity rostral to the injury, while plasticity below the injury has insufficient guidance, resulting in maladaptive plasticity.

Interestingly, spontaneous recovery post-SCI is partially reliant on proprioceptive afferents that help to "guide" circuit reorganization caudal to the lesion [382,400]. Specifically, proprioceptive afferents sprout below the injury and increasingly contact spinal pre-motoneurons and interneurons. This increase in contacts is selective for propriospinal and interneuron populations that received little to no proprioceptive input prior to injury, which likely includes the subsets of LAPNs that have a more dorsoventral orientation post-SCI. This brings about a dichotomy as proprioceptive afferents are needed for spontaneous recovery of function (likely involving new contacts with LAPNs) but removing LAPNs from the circuitry improves function. If LAPNs are targets of these sprouting afferents, perhaps these sprouts are needed to achieve some level of homeostatic plasticity that accounts for the level of recovered function seen, but the resultant circuitry could further benefit refinement. Activity-based rehabilitation has been shown to increase adaptive plasticity post-SCI [401]. This at least partially results from precise and functionally relevant somatosensory input from muscle, skin, and fascia, which is known to play a key role in retraining locomotor systems [103,400,402,403]. Determining the modality of sensory input(s) and what peripheral tissue(s) exert the greatest influence on activity-based rehab plasticity caudal to the lesion would aid in refining activity-based rehab and likely result in further refinement of the locomotor circuitry.

Lastly, circuit/pathway modification throughout the CNS has only led to marginal improvements in locomotor function in rodent studies (see table 1 below for examples), making it difficult to determine for which pathway plasticity matters most in recovered

TABLE 1 – Functional improvements from circuit modifications	
Circuit/pathway modification	**Functional change**
Long ascending propriospinal silencing (rats)	BBB increase 11 → 13
Long descending propriospinal silencing (rats)	BBB increase 11 → 13
Epidural spinal cord stimulation (rats)	BBB increase 9 → 13
KCC2 upregulation (mice)	BMS increase 1 → 3
Increased corticospinal sprouting via growth factor delivery (rats)	BBB increase 16 → 18
Mesencephalic locomotor region stimulation (rats)	BBB increase 6 → 9
Functional electrical stimulation (rats)	BBB increase 3 → 9

95 83 404 186 405 406 407

function post-SCI. Because of this, the next section will explore if specific pathways or neuronal subpopulations need to be targeted to improve function post-SCI.

Locomotor function post-SCI; The circuitry doesn't need to be perfect, just good enough

Does post-SCI circuitry need to resemble pre-SCI circuitry to improve function? This is something that I have pondered throughout my graduate work and asked guest speakers Dr Shawn Hochman (Emory University), Dr Mark Tuszynski (University of California San Diego), and Dr Dale Sengelaub (Indiana University). Current consensus is that the circuitry doesn't need recapitulate pre-SCI circuitry, it just needs to allow for functionally relevant output. Insights into this can be gleaned from the success of neuromodulation via epidural spinal cord stimulation, deep brain stimulation, and/or peripheral nerve stimulation to treat various CNS pathologies. As noted in the previous section, injury-induced pathology occurs throughout the CNS, some of which is aberrant. However, epidural stimulation of the lumbar enlargement is able to modulate the circuitry leading to improved locomotor function. Kathe et al recently provided some mechanistic insight and showed that epidural stimulation (which is believed to activate large diameter sensory afferents) decreases overall activity in the lumbar cord, allowing relevant signal/circuitry (sensory input and descending input/intention) to have a greater influence on spinal locomotor circuits resulting in improved function in humans and rodents [286]. Broadly, this can be thought of as a signal-to-noise problem, where aberrant circuitry and detrimental changes in neurotransmitter function produce excess "noise" making it difficult for the locomotor system to produce relevant "signal" for

desired behavior output. As the findings of Kathe et al indicate, epidural stimulation seems to turn the down "noise" allowing the ratio of "signal" to be greater [286]

Our understanding of the mechanism(s) that allow epidural stimulation to improve function are in their infancy. However, the mechanism(s) by which deep brain stimulation (DBS) corrects bradykinesia, rigidity, and resting tremor in Parkinson's Disease (PD) are better understood. In PD patients, maladaptive circuits form as a result of a loss of dopaminergic neurons in the substantia nigra pars compacta, which is followed by a cascade of changes in basal ganglia circuits [408]. High-frequency DBS of the subthalamic nucleus (STN) causes orthodromic and antidromic action potentials, which can partially cancel out the firing pattern of STN neurons. Constant antidromic potentials override the refractory period disrupting the previously seen firing pattern of neurons in STN leading to inhibition of action potentials and reducing firing rates long term. Ultimately, this results in an uncoupling of STN neurons and axons and produces a functional deafferentation from upstream and downstream structures [409,410]. This firing pattern does not resemble non-pathologic firing of these circuits, but it does interfere with and replace the output of aberrant circuits [411]. The clinical outcomes of DBS are surprisingly similar to the effects with destructive lesions of thalamic and subthalamic nuclei that physically disrupt the circuitry [412-414]. Additionally, similar mechanisms underly peripheral nerve stimulation for pain modulation which through activation of larger diameter afferents (Aα/β) interferes with the interaction of nociceptive fibers and their spinal cord targets [415-417]. This leads to activation of polysynaptic spinal circuits

resulting in reduced firing of superficial and deep dorsal horn neurons which disrupts the transmission of nociceptive signals in the spinal cord.

The commonality among all of these successful neuromodulatory approaches is a disruption of aberrant circuits, tilting the "signal-to-noise" ratio in favor of meaningful output. Surprisingly, just this disruption allows the remaining circuitry to achieve output that is behaviorally relevant and improves patient function. This idea provides a promising approach for therapeutic development which is discussed in the next section.

A potential path forward for treating spinal cord injury. Is there a *silver bullet*?

As outlined at the end of Chapter 1, the development of small and large molecule drugs for SCI has yet to yield results in the clinic, as there is currently only one drug currently approved for use in SCI patients, pregabalin. Therefore, it seems critical to develop new strategies to target and treat SCI. Gene therapies provide relatively unexplored option and advances delivery methods, targeting, and gene expression can be modified at various steps points of transcription and translation.

Here, focused ultrasound and intravenous microbubbles were used in an effort to achieve focal and cell-specific gene transfer in the lumbar spinal cord. This was successful, as targeting was >90% specific to neurons in the lumbar enlargement, but there are many hurdles to overcome if clinical translation is the goal. The largest of these hurdles are listed below:

1. Post-SCI, standard of care involves surgical decompression via laminectomy [112,113] which would allow FUS+MB targeting of the injury epicenter without bone attenuation. However, areas away from the epicenter provide promising targets

as neuromodulation of the lumbar spinal cord chronically improves various functions post-SCI [283-286]. An additional laminectomy to target the lumbar enlargement would involve a major surgery and destabilize the spinal column [418,419]. O'Reilly et al have developed a potential solution, involving focused multiarray delivery of ultrasound to the spinal cord and/or paravertebral delivery [420,421]. This approach has shown feasibility in *ex vivo* testing with human vertebrae and success in a large animal model and will be imperative to translation [422].

2. Targeting of the lumbar enlargement here was fairly crude as magnetic resonance guided imaging (MRI-guided) was not used. Clinically, MRI-guided targeting and real-time monitoring of BSCB permeability will be needed for precise targeting and real time monitoring for safe and effective BSCB permeabilization [423,424].
3. While targeting here was not as precise MRI-guided FUS, gene transfer spanned roughly 5 mm rostrocaudally. Rostral lumbar segments in humans span 11-13mm, indicating that for successful targeting of humans spinal segments, ultrasound delivery would likely involve multiple focal targets bilaterally [425].
4. Post-SCI changes in receptor expression are seen throughout the CNS [426,427]. Furthermore, in pathologic states intracellular trafficking of AAV virions may be impacted as endosome trafficking and nuclear pore complexes are impaired [428-430]. Because of this, AAV9 tropism and transgene expression may differ post-SCI.

Future studies will need to determine whether AAV9 (or other serotypes) will provide successful gene transfer using FUS+MB in the injury spinal cord.

5. Thousands of genes are differentially expressed post-SCI. Determining which gene(s) and cellular processes should be targeted will likely prove difficult. Potential targets include regenerative pathways, circuit modifying pathways, or degradation of the glial scar to promote regeneration and/or circuit plasticity [186,431-433]. The targets will have to be carefully chosen as unregulated axon sprouting and/or formation of aberrant circuits may cause further functional deficits [325,434,435].

Given the overwhelming number of genes that are differentially expressed post-SCI, the numerous cell types that are impacted, and the heterogeneity of injuries, determining a single gene that may act as a "silver bullet" is likely impossible. However, insights and ideas from the previous section and prior therapeutic development at least provide candidate genes and/or cellular modifications using gene therapy approaches that may hold some promise. The previous section discussed the effects of neuromodulation and showed that the common theme among successful neuromodulation is the perturbing of pathological circuits which favorably alters the "signal-to-noise" ratio. One potential for doing this is to upregulate the chloride potassium symporter, KCC2, which is down regulated post-SCI, allowing GABA to act as an excitatory neurotransmitter. Chen et al has done this by delivering an AAV.PHP.B-KCC2 intravenously acutely post-SCI and found improved locomotor function. However, the doses used (approximately $5.2x10^{14}$ vg/kg) were higher than doses that cause liver

toxicity, DRG pathology, and death in larger animal models and clinical trials [186,265,436] . A potential solution to this packaging limit problem is to develop a shortened functional isoform of KCC2 that can be successfully packaged into AAVs for lower doses to be used for IV injection and paired with FUS+MB targeting the lumbar spinal cord. Alternatively, direct circuit modification might be achieved through chemogenetic manipulation. It is conceivable that designer receptors exclusively activated by designer drugs (DREADDs) could be used to activate or inhibit neurons at a target site. Using FUS+MB and intravenous AAV to express an inhibitory or excitatory DREADD receptor would allow for systemic delivery of DREADD actuators (drugs) to modulate firing rates of infected cells. Furthermore, actuator doses could be adjusted for an optimal inhibition or activation the designer receptors. This approach would benefit from the development of neuron subtype-specific capsids and/or promoters that would allow for precise targeting of neuron subtypes and allow for activity and/or inhibition of these subtypes. The most attractive subtype for this type of manipulation is a subset of V2a neurons that Kathe et al showed are likely the neurons in the lumbar spinal cord that "restore walking" post-SCI [286].

Lastly, of therapeutics that have advanced clinical trials, Cethrin, a Rho inhibitor that allowed for increased axon growth/regeneration, has seemed most promising. I will not suggest Rho as a target here but will suggest BDNF as it has similar effects and is known to promote axonal sprouting [437], stimulate dendrite growth and remodeling [438], and promote synaptic plasticity via long term potentiation [439]. BDNF overexpression is also an attractive target would exert it effects on cells that gene transfer was not successful in as it is released from somata, dendrites, and axons [440]. This makes BDNF expression increasingly

attractive as pathways such as LAPNs that have long range projections and collaterals throughout the spinal cord and brainstem could have widespread effects on the locomotor circuitry. BDNF overexpression may contribute to aberrant circuit formation [441]. However, this may be overcome using an elegant system called 'X_{on}' that was developed by Monteys et al [442]. The X_{on} platform allows for a precise temporal control of transgene expression, in this case BDNF, through the use of a small molecule (LMI070) that is orally administered. The robustness of expression can be modulated by the dose of LMI070 that is given, which may prevent the potential deleterious effects of continuous BDNF expression. Using this approach in combination with specific activity-based training (i.e., locomotor or respiratory training) would allow for an increase in circuit plasticity via BDNF overexpression in a temporally controlled manner in tandem with providing functionally relevant sensory and motor inputs from activity-based training that would then refine that circuitry.

To conclude, future studies will need to further elucidate the spinal connectome both before and after SCI and make concerted efforts to decipher the pathways involved in adaptive and maladaptive plasticity following SCI. Doing so will likely provide for pathway- and/or connectome-specific therapeutics to be developed. Gene therapy based approached will need to be tightly regulated to prevent potential negative effects and avoid contributing to maladaptive plasticity. Additionally, therapeutics that promote plasticity will need to be combined with task-specific therapies to provide the system with functionally relevant motor and sensory inputs to guide adaptive plasticity and improve patient outcomes.

Epilogue: contributions to the field and personal development

As chapter 1 began with quote from Santiago Ramon y Cajal, it seems fitting to end with one as well. Chapter 8 of Cajal's book *Advice for a Young Investigator* finishes with, "Because the judgement of scientific authorities abroad is critical in determining the future of the young investigator, he will reflect thoughtfully before submitting his work to them. He will assure himself of the truth and originality of the data by way of painstaking bibliographic research, and better yet, through consultation with some famous specialist. And he must not forget that the right to make mistakes is tolerated only in the famous." The original work done here has further elucidated the spinal cord connectome by detailed characterization of LAPNs and showing that even following a mild SCI, neurons caudal to the epicenter are subject to intense injury induced plasticity. Prior to this, nothing was known about the injury response of propriospinal neurons caudal to the injury, which is surprising as epidural stimulation directly targets this area for neuromodulation. Furthermore, gene therapy for treating SCI has been increasingly coming up in prospective(s) papers and at seminars but delivery of gene therapies for SCI, until this work has not been explored. The proof-of-concept experiments in Chapter 4 provide a promising means for non-invasive and focal targeting of the spinal cord which overcomes major hurdles if clinical translation is the ultimate goal.

Lastly, as any scientist knows, there are multiple failed experiments for every successful one. Both the successful experiments presented here, and the failed experiments that have not been presented have provided invaluable insight into troubleshooting, experimental design, and perseverance throughout the scientific

processes. Most notably, the time spent understanding viral vector design, production, and delivery will undoubtably pay dividends as my next scientific endeavors will be focused on gene therapies for CNS diseases.

REFERENCES

1. Andersen BB, Korbo L, Pakkenberg B. A quantitative study of the human cerebellum with unbiased stereological techniques. *J Comp Neurol.* 1992;326(4):549-560.
2. Pelvig DP, Pakkenberg H, Stark AK, Pakkenberg B. Neocortical glial cell numbers in human brains. *Neurobiol Aging.* 2008;29(11):1754-1762.
3. Bahney J, von Bartheld CS. The Cellular Composition and Glia-Neuron Ratio in the Spinal Cord of a Human and a Nonhuman Primate: Comparison With Other Species and Brain Regions. *Anat Rec (Hoboken).* 2018;301(4):697-710.
4. Drachman DA. Do we have brain to spare? *Neurology.* 2005;64(12):2004-2005.
5. Pakkenberg B, Pelvig D, Marner L, et al. Aging and the human neocortex. *Exp Gerontol.* 2003;38(1-2):95-99.
6. Van Essen DC, Ugurbil K, Auerbach E, et al. The Human Connectome Project: a data acquisition perspective. *Neuroimage.* 2012;62(4):2222-2231.
7. Oh SW, Harris JA, Ng L, et al. A mesoscale connectome of the mouse brain. *Nature.* 2014;508(7495):207-214.
8. Kiehn O. Decoding the organization of spinal circuits that control locomotion. *Nat Rev Neurosci.* 2016;17(4):224-238.
9. Sidman RL, Angevine JB, Pierce ET. Atlas of the mouse brain and spinal cord. *(No Title).* 1971.

10. Rexed B. A cytoarchitectonic atlas of the spinal cord in the cat. *J Comp Neurol.* 1954;100(2):297-379.

11. Molander C, Xu Q, Grant G. The cytoarchitectonic organization of the spinal cord in the rat. I. The lower thoracic and lumbosacral cord. *J Comp Neurol.* 1984;230(1):133-141.

12. Maxwell DJ, Fyffe RE, Rethelyi M. Morphological properties of physiologically characterized lamina III neurones in the cat spinal cord. *Neuroscience.* 1983;10(1):1-22.

13. Light AR, Willcockson HH. Spinal laminae I-II neurons in rat recorded in vivo in whole cell, tight seal configuration: properties and opioid responses. *Journal of Neurophysiology.* 1999;82(6):3316-3326.

14. Cervero F, Lumb BM. Bilateral inputs and supraspinal control of viscerosomatic neurones in the lower thoracic spinal cord of the cat. *J Physiol.* 1988;403:221-237.

15. Brown AG. The dorsal horn of the spinal cord. *Q J Exp Physiol.* 1982;67(2):193-212.

16. Nissen UV, Mochida H, Glover JC. Development of projection-specific interneurons and projection neurons in the embryonic mouse and rat spinal cord. *J Comp Neurol.* 2005;483(1):30-47.

17. Skinner RD, Remmel RS. Monosynaptic inputs to lumbar interneurons from the lateral vestibulospinal tract and the medial longitudinal fasciculus. *Neurosci Lett.* 1978;10(3):259-264.

18. Matthews MA, Willis WD, Williams V. Dendrite bundles in lamina IX of cat spinal cord: a possible source for electrical interaction between motoneurons? *Anat Rec.* 1971;171(2):313-327.

19. Casale EJ, Light AR, Rustioni A. Direct projection of the corticospinal tract to the superficial laminae of the spinal cord in the rat. *J Comp Neurol.* 1988;278(2):275-286.

20. Ralston DD, Ralston HJ, 3rd. The terminations of corticospinal tract axons in the macaque monkey. *J Comp Neurol.* 1985;242(3):325-337.

21. Heffner R, Masterton B. Variation in form of the pyramidal tract and its relationship to digital dexterity. *Brain Behav Evol.* 1975;12(3):161-200.

22. Heffner RS, Masterton RB. The role of the corticospinal tract in the evolution of human digital dexterity. *Brain Behav Evol.* 1983;23(3-4):165-183.

23. Kuypers HG. The Descending Pathways to the Spinal Cord, Their Anatomy and Function. *Prog Brain Res.* 1964;11:178-202.

24. Palmer E, Ashby P. Corticospinal projections to upper limb motoneurones in humans. *J Physiol.* 1992;448:397-412.

25. Lemon RN, Kirkwood PA, Maier MA, Nakajima K, Nathan P. Direct and indirect pathways for corticospinal control of upper limb motoneurons in the primate. *Prog Brain Res.* 2004;143:263-279.

26. Lawrence DG, Kuypers HG. The functional organization of the motor system in the monkey. II. The effects of lesions of the descending brain-stem pathways. *Brain.* 1968;91(1):15-36.

27. Muir GD, Whishaw IQ. Complete locomotor recovery following corticospinal tract lesions: measurement of ground reaction forces during overground locomotion in rats. *Behav Brain Res.* 1999;103(1):45-53.

28. Eidelberg E, Yu J. Effects of corticospinal lesions upon treadmill locomotion by cats. *Exp Brain Res.* 1981;43(1):101-103.

29. Schubert M, Curt A, Jensen L, Dietz V. Corticospinal input in human gait: modulation of magnetically evoked motor responses. *Exp Brain Res.* 1997;115(2):234-246.

30. Beloozerova IN, Sirota MG. The role of the motor cortex in the control of vigour of locomotor movements in the cat. *J Physiol.* 1993;461:27-46.

31. Friel KM, Martin JH. Bilateral activity-dependent interactions in the developing corticospinal system. *J Neurosci.* 2007;27(41):11083-11090.

32. Karadimas SK, Satkunendrarajah K, Laliberte AM, et al. Sensory cortical control of movement. *Nat Neurosci.* 2020;23(1):75-84.

33. Brownstone RM, Chopek JW. Reticulospinal Systems for Tuning Motor Commands. *Front Neural Circuits.* 2018;12:30.

34. Liang H, Watson C, Paxinos G. Terminations of reticulospinal fibers originating from the gigantocellular reticular formation in the mouse spinal cord. *Brain Struct Funct.* 2016;221(3):1623-1633.

35. Mitani A, Ito K, Mitani Y, McCarley RW. Descending projections from the gigantocellular tegmental field in the cat: cells of origin and their brainstem and spinal cord trajectories. *J Comp Neurol.* 1988;268(4):546-566.

36. Noga BR, Kriellaars DJ, Brownstone RM, Jordan LM. Mechanism for activation of locomotor centers in the spinal cord by stimulation of the mesencephalic locomotor region. *J Neurophysiol.* 2003;90(3):1464-1478.

37. Lemieux M, Bretzner F. Glutamatergic neurons of the gigantocellular reticular nucleus shape locomotor pattern and rhythm in the freely behaving mouse. *PLoS Biol.* 2019;17(4):e2003880.

38. Bouvier J, Caggiano V, Leiras R, et al. Descending command neurons in the brainstem that halt locomotion. *Cell.* 2015;163(5):1191-1203.

39. Liang H, Schofield E, Paxinos G. Imaging Serotonergic Fibers in the Mouse Spinal Cord Using the CLARITY/CUBIC Technique. *J Vis Exp.* 2016(108):53673.

40. Capelli P, Pivetta C, Soledad Esposito M, Arber S. Locomotor speed control circuits in the caudal brainstem. *Nature.* 2017;551(7680):373-377.

41. Matsuyama K, Mori F, Kuze B, Mori S. Morphology of single pontine reticulospinal axons in the lumbar enlargement of the cat: a study using the anterograde tracer PHA-L. *Journal of Comparative Neurology.* 1999;410(3):413-430.

42. Gautier A, Geny D, Bourgoin S, Bernard JF, Hamon M. Differential innervation of superficial versus deep laminae of the dorsal horn by bulbo-spinal serotonergic pathways in the rat. *IBRO Rep.* 2017;2:72-80.

43. Cazalets J, Sqalli-Houssaini Y, Clarac F. Activation of the central pattern generators for locomotion by serotonin and excitatory amino acids in neonatal rat. *The Journal of physiology.* 1992;455(1):187-204.

44. Branchereau P, Rodriguez JJ, Delvolve I, Abrous DN, Le Moal M, Cabelguen JM. Serotonergic systems in the spinal cord of the amphibian urodele Pleurodeles waltl. *J Comp Neurol.* 2000;419(1):49-60.

45. Barbeau H, Rossignol S. The effects of serotonergic drugs on the locomotor pattern and on cutaneous reflexes of the adult chronic spinal cat. *Brain Res.* 1990;514(1):55-67.

46. Flaive A, Fougère M, Van der Zouwen CI, Ryczko D. Serotonergic modulation of locomotor activity from basal vertebrates to mammals. *Frontiers in Neural Circuits.* 2020;14:590299.

47. Bengel D, Murphy DL, Andrews AM, et al. Altered brain serotonin homeostasis and locomotor insensitivity to 3, 4-methylenedioxymethamphetamine ("Ecstasy") in serotonin transporter-deficient mice. *Molecular pharmacology.* 1998;53(4):649-655.

48. Kalueff AV, Jensen CL, Murphy DL. Locomotory patterns, spatiotemporal organization of exploration and spatial memory in serotonin transporter knockout mice. *Brain Res.* 2007;1169:87-97.

49. Hendricks TJ, Fyodorov DV, Wegman LJ, et al. Pet-1 ETS gene plays a critical role in 5-HT neuron development and is required for normal anxiety-like and aggressive behavior. *Neuron.* 2003;37(2):233-247.

50. Muir GD, Whishaw IQ. Red nucleus lesions impair overground locomotion in rats: a kinetic analysis. *Eur J Neurosci.* 2000;12(3):1113-1122.

51. Rho MJ, Lavoie S, Drew T. Effects of red nucleus microstimulation on the locomotor pattern and timing in the intact cat: a comparison with the motor cortex. *J Neurophysiol.* 1999;81(5):2297-2315.

52. Grillner S, Hongo T, Lund S. Convergent effects on alpha motoneurones from the vestibulospinal tract and a pathway descending in the medial longitudinal fasciculus. *Exp Brain Res.* 1971;12:457-479.

53. Grillner S. Supraspinal and segmental control of static and dynamic-motoneurones in the cat. 1969.

54. Orlovsky G. Activity of vestibulospinal neurons during locomotion. *Brain research.* 1972;46:85-98.

55. Shamboul KM. Lumbosacral predominance of vestibulospinal fibre projection in the rat. *J Comp Neurol.* 1980;192(3):519-530.

56. Liang H, Bacskai T, Watson C, Paxinos G. Projections from the lateral vestibular nucleus to the spinal cord in the mouse. *Brain Struct Funct.* 2014;219(3):805-815.

57. Shinoda Y, Ohgaki T, Futami T, Sugiuchi Y. Vestibular projections to the spinal cord: the morphology of single vestibulospinal axons. *Prog Brain Res.* 1988;76:17-27.

58. Sathyamurthy A, Barik A, Dobrott CI, et al. Cerebellospinal neurons regulate motor performance and motor learning. *Cell reports.* 2020;31(6).

59. Arends JJ, Allan RW, Zeigler HP. Organization of the cerebellum in the pigeon (Columba livia): III. Corticovestibular connections with eye and neck premotor areas. *J Comp Neurol.* 1991;306(2):273-289.

60. Shefchyk SJ, Stein RB, Jordan LM. Synaptic transmission from muscle afferents during fictive locomotion in the mesencephalic cat. *J Neurophysiol.* 1984;51(5):986-997.

61. Roseberry TK, Lee AM, Lalive AL, Wilbrecht L, Bonci A, Kreitzer AC. Cell-Type-Specific Control of Brainstem Locomotor Circuits by Basal Ganglia. *Cell.* 2016;164(3):526-537.

62. Beresovskii VK, Bayev KV. New locomotor regions of the brainstem revealed by means of electrical stimulation. *Neuroscience.* 1988;26(3):863-869.

63. Orlovskii GN. [Electrical activity in the brain stem and descending pathways in guided locomotion]. *Fiziol Zh SSSR Im I M Sechenova.* 1969;55(4):437-444.

64. Ferreira-Pinto MJ, Ruder L, Capelli P, Arber S. Connecting Circuits for Supraspinal Control of Locomotion. *Neuron.* 2018;100(2):361-374.

65. Danner SM, Shevtsova NA, Frigon A, Rybak IA. Computational modeling of spinal circuits controlling limb coordination and gaits in quadrupeds. *Elife.* 2017;6.

66. Barlow SM, Estep M. Central pattern generation and the motor infrastructure for suck, respiration, and speech. *Journal of communication disorders.* 2006;39(5):366-380.

67. von Euler C. On the functional organization of the generators of rhythmic motor synergy in breathing. In: *Central Neurone Environment and the Control Systems of Breathing and Circulation.* Springer; 1983:157-163.

68. Harris-Warrick RM. General principles of rhythmogenesis in central pattern generator networks. *Prog Brain Res.* 2010;187:213-222.

69. Brown TG. The intrinsic factors in the act of progression in the mammal. *Proceedings of the Royal Society of London Series B, containing papers of a biological character.* 1911;84(572):308-319.

70. Brown TG. On the nature of the fundamental activity of the nervous centres; together with an analysis of the conditioning of rhythmic activity in progression, and a theory of the evolution of function in the nervous system. *The Journal of physiology.* 1914;48(1):18.

71. Cazalets JR, Borde M, Clarac F. Localization and organization of the central pattern generator for hindlimb locomotion in newborn rat. *J Neurosci.* 1995;15(7 Pt 1):4943-4951.

72. Whelan P, Bonnot A, O'Donovan MJ. Properties of rhythmic activity generated by the isolated spinal cord of the neonatal mouse. *J Neurophysiol.* 2000;84(6):2821-2833.

73. Cowley KC, Schmidt BJ. Regional distribution of the locomotor pattern-generating network in the neonatal rat spinal cord. *J Neurophysiol.* 1997;77(1):247-259.

74. Grillner S, Zangger P. On the central generation of locomotion in the low spinal cat. *Exp Brain Res.* 1979;34(2):241-261.

75. Sherrington CS, Laslett EE. Observations on some spinal reflexes and the interconnection of spinal segments. *J Physiol.* 1903;29(1):58-96.

76. Menetrey D, De Pommery J, Roudier F. Propriospinal fibers reaching the lumbar enlargement in the rat. *Neuroscience letters.* 1985;58(2):257-261.

77. Skinner RD, Coulter JD, Adams RJ, Remmel RS. Cells of origin of long descending propriospinal fibers connecting the spinal enlargements in cat and monkey determined by horseradish peroxidase and electrophysiological techniques. *J Comp Neurol.* 1979;188(3):443-454.

78. Nathan P, Smith M, Deacon P. Vestibulospinal, reticulospinal and descending propriospinal nerve fibres in man. *Brain.* 1996;119(6):1809-1833.

79. Skinner R, Adams R, Remmel R. Responses of long descending propriospinal neurons to natural and electrical types of stimuli in cat. *Brain research.* 1980;196(2):387-403.

80. Brink E, Suzuki I, Timerick S, Wilson V. Tonic neck reflex of the decerebrate cat: a role for propriospinal neurons. *Journal of neurophysiology.* 1985;54(4):978-987.

81. Alstermark B, Kummel H, Tantisira B. Monosynaptic raphespinal and reticulospinal projection to forelimb motoneurones in cats. *Neurosci Lett.* 1987;74(3):286-290.

82. Ruder L, Takeoka A, Arber S. Long-Distance Descending Spinal Neurons Ensure Quadrupedal Locomotor Stability. *Neuron.* 2016;92(5):1063-1078.

83. Shepard CT, Brown BL, Van Rijswijck MA, et al. Silencing long-descending inter-enlargement propriospinal neurons improves hindlimb stepping after contusive spinal cord injuries. *BioRxiv.* 2022:2022.2008. 2030.505848.

84. English AW, Tigges J, Lennard PR. Anatomical organization of long ascending propriospinal neurons in the cat spinal cord. *J Comp Neurol.* 1985;240(4):349-358.

85. Dutton RC, Carstens MI, Antognini JF, Carstens E. Long ascending propriospinal projections from lumbosacral to upper cervical spinal cord in the rat. *Brain Res.* 2006;1119(1):76-85.

86. Molenaar I. The distribution of propriospinal neurons projecting to different motoneuronal cell groups in the cat's brachial cord. *Brain Res.* 1978;158(1):203-206.

87. Giovanelli Barilari M, Kuypers HG. Propriospinal fibers interconnecting the spinal enlargements in the cat. *Brain Res.* 1969;14(2):321-330.

88. Miller S, Van Der Burg J, Van Der Meche F. Coordination of movements of the kindlimbs and forelimbs in different forms of locomotion in normal and decerebrate cats. *Brain Res.* 1975;91(2):217-237.

89. Miller S, van Berkum R, van der Burg J, van der Meche FG. Interlimb co-ordination in stepping in the cat. *J Physiol.* 1973;230(1):30P-31P.

90. Juvin L, Simmers J, Morin D. Propriospinal circuitry underlying interlimb coordination in mammalian quadrupedal locomotion. *J Neurosci.* 2005;25(25):6025-6035.

91. Reed WR, Shum-Siu A, Onifer SM, Magnuson DS. Inter-enlargement pathways in the ventrolateral funiculus of the adult rat spinal cord. *Neuroscience.* 2006;142(4):1195-1207.

92. Magnuson DS, Trinder TC, Zhang YP, Burke D, Morassutti DJ, Shields CB. Comparing deficits following excitotoxic and contusion injuries in the thoracic and lumbar spinal cord of the adult rat. *Exp Neurol.* 1999;156(1):191-204.

93. Hadi B, Zhang YP, Burke DA, Shields CB, Magnuson DS. Lasting paraplegia caused by loss of lumbar spinal cord interneurons in rats: no direct correlation with motor neuron loss. *J Neurosurg.* 2000;93(2 Suppl):266-275.

94. Pocratsky AM, Shepard CT, Morehouse JR, et al. Long ascending propriospinal neurons provide flexible, context-specific control of interlimb coordination. *Elife.* 2020;9.

95. Shepard CT, Pocratsky AM, Brown BL, et al. Silencing long ascending propriospinal neurons after spinal cord injury improves hindlimb stepping in the adult rat. *Elife.* 2021;10.

96. NSCIS C. Facts and Figures at a Glance. *Birmingham, AL: University of Alabama at Birmingham.* 2016;10.

97. Talbott JF, Whetstone WD, Readdy WJ, et al. The Brain and Spinal Injury Center score: a novel, simple, and reproducible method for assessing the severity of acute cervical spinal cord injury with axial T2-weighted MRI findings. *J Neurosurg Spine.* 2015;23(4):495-504.

98. Basso DM, Beattie MS, Bresnahan JC. Graded histological and locomotor outcomes after spinal cord contusion using the NYU weight-drop device versus transection. *Exp Neurol.* 1996;139(2):244-256.

99. Mummaneni N, Burke JF, DiGiorgio AM, et al. Injury volume extracted from MRI predicts neurologic outcome in acute spinal cord injury: A prospective TRACK-SCI pilot study. *J Clin Neurosci.* 2020;82(Pt B):231-236.

100. Bareyre FM, Kerschensteiner M, Raineteau O, Mettenleiter TC, Weinmann O, Schwab ME. The injured spinal cord spontaneously forms a new intraspinal circuit in adult rats. *Nat Neurosci.* 2004;7(3):269-277.

101. Asboth L, Friedli L, Beauparlant J, et al. Cortico-reticulo-spinal circuit reorganization enables functional recovery after severe spinal cord contusion. *Nat Neurosci.* 2018;21(4):576-588.

102. Filli L, Engmann AK, Zorner B, et al. Bridging the gap: a reticulo-propriospinal detour bypassing an incomplete spinal cord injury. *J Neurosci.* 2014;34(40):13399-13410.

103. Courtine G, Song B, Roy RR, et al. Recovery of supraspinal control of stepping via indirect propriospinal relay connections after spinal cord injury. *Nat Med.* 2008;14(1):69-74.

104. Vavrek R, Girgis J, Tetzlaff W, Hiebert GW, Fouad K. BDNF promotes connections of corticospinal neurons onto spared descending interneurons in spinal cord injured rats. *Brain.* 2006;129(Pt 6):1534-1545.

105. Venkatesh K, Ghosh SK, Mullick M, Manivasagam G, Sen D. Spinal cord injury: pathophysiology, treatment strategies, associated challenges, and future implications. *Cell Tissue Res.* 2019;377(2):125-151.

106. Fehlings MG, Tetreault LA, Wilson JR, et al. A Clinical Practice Guideline for the Management of Acute Spinal Cord Injury: Introduction, Rationale, and Scope. *Global Spine J.* 2017;7(3 Suppl):84S-94S.

107. Keane RW, Davis AR, Dietrich WD. Inflammatory and apoptotic signaling after spinal cord injury. *J Neurotrauma.* 2006;23(3-4):335-344.

108. Min YS, Chang Y, Park JW, et al. Change of Brain Functional Connectivity in Patients With Spinal Cord Injury: Graph Theory Based Approach. *Ann Rehabil Med.* 2015;39(3):374-383.

109. Bastien D, Lacroix S. Cytokine pathways regulating glial and leukocyte function after spinal cord and peripheral nerve injury. *Exp Neurol.* 2014;258:62-77.

110. Sauerbeck AD, Laws JL, Bandaru VV, Popovich PG, Haughey NJ, McTigue DM. Spinal cord injury causes chronic liver pathology in rats. *J Neurotrauma.* 2015;32(3):159-169.

111. Soden RJ, Walsh J, Middleton JW, Craven ML, Rutkowski SB, Yeo JD. Causes of death after spinal cord injury. *Spinal Cord.* 2000;38(10):604-610.

112. Fehlings MG, Perrin RG. The timing of surgical intervention in the treatment of spinal cord injury: a systematic review of recent clinical evidence. *Spine (Phila Pa 1976).* 2006;31(11 Suppl):S28-35; discussion S36.

113. Fehlings MG, Vaccaro A, Wilson JR, et al. Early versus delayed decompression for traumatic cervical spinal cord injury: results of the Surgical Timing in Acute Spinal Cord Injury Study (STASCIS). *PLoS One.* 2012;7(2):e32037.

114. Green D, Lee MY, Lim AC, et al. Prevention of thromboembolism after spinal cord injury using low-molecular-weight heparin. *Ann Intern Med.* 1990;113(8):571-574.

115. Green D, Chen D, Chmiel JS, et al. Prevention of thromboembolism in spinal cord injury: role of low molecular weight heparin. *Arch Phys Med Rehabil.* 1994;75(3):290-292.

116. Walters BC, Hadley MN, Hurlbert RJ, et al. Guidelines for the management of acute cervical spine and spinal cord injuries: 2013 update. *Neurosurgery.* 2013;60(CN_suppl_1):82-91.

117. Milligan NM, Newcombe R, Compston DA. A double-blind controlled trial of high dose methylprednisolone in patients with multiple sclerosis: 1. Clinical effects. *J Neurol Neurosurg Psychiatry.* 1987;50(5):511-516.

118. Taoka Y, Okajima K, Uchiba M, Johno M. Methylprednisolone reduces spinal cord injury in rats without affecting tumor necrosis factor-α production. *Journal of neurotrauma.* 2001;18(5):533.

119. Sharma A, Tiwari R, Badhe P, Sharma G. Comparison of methylprednisolone with dexamethasone in treatment of acute spinal injury in rats. 2004.

120. Jiang S, Khan M, Middlemiss P, et al. AIT-082 and methylprednisolone singly, but not in combination, enhance functional and histological improvement after acute spinal cord injury in rats. *International Journal of Immunopathology and Pharmacology.* 2004;17(3):353-366.

121. Chikawa T, Ikata T, Katoh S, Hamada Y, Kogure K, Fukuzawa K. Preventive effects of lecithinized superoxide dismutase and methylprednisolone on spinal cord injury in rats: transcriptional regulation of inflammatory and neurotrophic genes. *Journal of neurotrauma.* 2001;18(1):93-103.

122. Bracken MB, Shepard MJ, Holford TR, et al. Methylprednisolone or tirilazad mesylate administration after acute spinal cord injury: 1-year follow up: results of the third National Acute Spinal Cord Injury randomized controlled trial. *Journal of neurosurgery.* 1998;89(5):699-706.

123. Bracken MB, Shepard MJ, Holford TR, et al. Administration of methylprednisolone for 24 or 48 hours or tirilazad mesylate for 48 hours in the treatment of acute spinal cord injury: results of the third national acute spinal cord injury randomized controlled trial. *Jama.* 1997;277(20):1597-1604.

124. Festoff BW, Ameenuddin S, Arnold PM, Wong A, Santacruz KS, Citron BA. Minocycline neuroprotects, reduces microgliosis, and inhibits caspase protease expression early after spinal cord injury. *Journal of neurochemistry.* 2006;97(5):1314-1326.

125. Lee SM, Yune TY, Kim SJ, et al. Minocycline reduces cell death and improves functional recovery after traumatic spinal cord injury in the rat. *J Neurotrauma.* 2003;20(10):1017-1027.

126. Wells JE, Hurlbert RJ, Fehlings MG, Yong VW. Neuroprotection by minocycline facilitates significant recovery from spinal cord injury in mice. *Brain.* 2003;126(Pt 7):1628-1637.

127. Elewa HF, Hilali H, Hess DC, Machado LS, Fagan SC. Minocycline for short-term neuroprotection. *Pharmacotherapy: The Journal of Human Pharmacology and Drug Therapy.* 2006;26(4):515-521.

128. Pi R, Li W, Lee NT, et al. Minocycline prevents glutamate-induced apoptosis of cerebellar granule neurons by differential regulation of p38 and Akt pathways. *J Neurochem.* 2004;91(5):1219-1230.

129. Teng YD, Choi H, Onario RC, et al. Minocycline inhibits contusion-triggered mitochondrial cytochrome c release and mitigates functional deficits after spinal cord injury. *Proc Natl Acad Sci U S A.* 2004;101(9):3071-3076.

130. Casha S, Zygun D, McGowan MD, Bains I, Yong VW, Hurlbert RJ. Results of a phase II placebo-controlled randomized trial of minocycline in acute spinal cord injury. *Brain.* 2012;135(Pt 4):1224-1236.

131. De Sarro G, Siniscalchi A, Ferreri G, Gallelli L, De Sarro A. NMDA and AMPA/kainate receptors are involved in the anticonvulsant activity of riluzole in DBA/2 mice. *European journal of pharmacology.* 2000;408(1):25-34.

132. Romettino S, Lazdunski M, Gottesmann C. Anticonvulsant and sleep-waking influences of riluzole in a rat model of absence epilepsy. *European journal of pharmacology.* 1991;199(3):371-373.

133. Carbone M, Duty S, Rattray M. Riluzole neuroprotection in a Parkinson's disease model involves suppression of reactive astrocytosis but not GLT-1 regulation. *BMC Neurosci.* 2012;13:38.

134. Fehlings MG, Nakashima H, Nagoshi N, Chow DS, Grossman RG, Kopjar B. Rationale, design and critical end points for the Riluzole in Acute Spinal Cord Injury Study (RISCIS): a randomized, double-blinded, placebo-controlled parallel multi-center trial. *Spinal Cord.* 2016;54(1):8-15.

135. Doble A. The pharmacology and mechanism of action of riluzole. *Neurology.* 1996;47(6 Suppl 4):S233-241.

136. Gloviczki B, Torok DG, Marton G, et al. Delayed Spinal Cord-Brachial Plexus Reconnection after C7 Ventral Root Avulsion: The Effect of Reinnervating Motoneurons Rescued by Riluzole Treatment. *J Neurotrauma.* 2017;34(15):2364-2374.

137. Hosier H, Peterson D, Tsymbalyuk O, et al. A Direct Comparison of Three Clinically Relevant Treatments in a Rat Model of Cervical Spinal Cord Injury. *J Neurotrauma.* 2015;32(21):1633-1644.

138. Ates O, Cayli SR, Gurses I, et al. Comparative neuroprotective effect of sodium channel blockers after experimental spinal cord injury. *J Clin Neurosci.* 2007;14(7):658-665.

139. Vasconcelos NL, Gomes ED, Oliveira EP, et al. Combining neuroprotective agents: effect of riluzole and magnesium in a rat model of thoracic spinal cord injury. *Spine J.* 2016;16(8):1015-1024.

140. Young W, Flamm ES, Demopoulos HB, Tomasula JJ, DeCrescito V. Effect of naloxone on posttraumatic ischemia in experimental spinal contusion. *J Neurosurg.* 1981;55(2):209-219.

141. Arias MJ. Effect of naloxone on functional recovery after experimental spinal cord injury in the rat. *Surg Neurol.* 1985;23(4):440-442.

142. Bracken MB, Shepard MJ, Collins WF, et al. A randomized, controlled trial of methylprednisolone or naloxone in the treatment of acute spinal-cord injury.

Results of the Second National Acute Spinal Cord Injury Study. *N Engl J Med.* 1990;322(20):1405-1411.

143. Chua SJ, Bielecki R, Yamanaka N, Fehlings MG, Rogers IM, Casper RF. The effect of umbilical cord blood cells on outcomes after experimental traumatic spinal cord injury. *Spine (Phila Pa 1976).* 2010;35(16):1520-1526.

144. Dasari VR, Veeravalli KK, Tsung AJ, et al. Neuronal apoptosis is inhibited by cord blood stem cells after spinal cord injury. *J Neurotrauma.* 2009;26(11):2057-2069.

145. Lu Y, Wang MY. Neural stem cell grafts for complete spinal cord injury. *Neurosurgery.* 2012;71(6):N13-15.

146. Ziv Y, Avidan H, Pluchino S, Martino G, Schwartz M. Synergy between immune cells and adult neural stem/progenitor cells promotes functional recovery from spinal cord injury. *Proc Natl Acad Sci U S A.* 2006;103(35):13174-13179.

147. Cusimano M, Biziato D, Brambilla E, et al. Transplanted neural stem/precursor cells instruct phagocytes and reduce secondary tissue damage in the injured spinal cord. *Brain.* 2012;135(Pt 2):447-460.

148. Ahuja CS, Mothe A, Khazaei M, et al. The leading edge: Emerging neuroprotective and neuroregenerative cell-based therapies for spinal cord injury. *Stem Cells Transl Med.* 2020;9(12):1509-1530.

149. Silvestro S, Bramanti P, Trubiani O, Mazzon E. Stem Cells Therapy for Spinal Cord Injury: An Overview of Clinical Trials. *Int J Mol Sci.* 2020;21(2).

150. Cheng H, Liu X, Hua R, et al. Clinical observation of umbilical cord mesenchymal stem cell transplantation in treatment for sequelae of thoracolumbar spinal cord injury. *J Transl Med.* 2014;12:253.

151. Anderson AJ, Piltti KM, Hooshmand MJ, Nishi RA, Cummings BJ. Preclinical efficacy failure of human CNS-derived stem cells for use in the pathway study of cervical spinal cord injury. *Stem Cell Reports.* 2017;8(2):249-263.

152. Tator CH. Update on the pathophysiology and pathology of acute spinal cord injury. *Brain Pathol.* 1995;5(4):407-413.

153. Kakulas BA. A review of the neuropathology of human spinal cord injury with emphasis on special features. *J Spinal Cord Med.* 1999;22(2):119-124.

154. Bradbury EJ, Carter LM. Manipulating the glial scar: chondroitinase ABC as a therapy for spinal cord injury. *Brain Res Bull.* 2011;84(4-5):306-316.

155. Houle J. The structural integrity of glial scar tissue associated with a chronic spinal cord lesion can be altered by transplanted fetal spinal cord tissue. *J Neurosci Res.* 1992;31(1):120-130.

156. Nishio Y, Koda M, Kitajo K, et al. Delayed treatment with Rho-kinase inhibitor does not enhance axonal regeneration or functional recovery after spinal cord injury in rats. *Exp Neurol.* 2006;200(2):392-397.

157. McKerracher L, Anderson KD. Analysis of recruitment and outcomes in the phase I/IIa Cethrin clinical trial for acute spinal cord injury. *J Neurotrauma.* 2013;30(21):1795-1804.

158. Fang L, Shen Z, Xu S, Chen Y, Wang S. Mining novel natural reactive oxygen species (ROS) inhibitors by targeting Rho Kinase for prevention of secondary spinal cord injury: An in-silico trial using traditional Chinese medicinal compounds. *Journal of King Saud University-Science.* 2020;32(5):2540-2552.

159. Maier IC, Ichiyama RM, Courtine G, et al. Differential effects of anti-Nogo-A antibody treatment and treadmill training in rats with incomplete spinal cord injury. *Brain.* 2009;132(Pt 6):1426-1440.

160. Fournier AE, Takizawa BT, Strittmatter SM. Rho kinase inhibition enhances axonal regeneration in the injured CNS. *J Neurosci.* 2003;23(4):1416-1423.

161. Lord-Fontaine S, Yang F, Diep Q, et al. Local inhibition of Rho signaling by cell-permeable recombinant protein BA-210 prevents secondary damage and promotes functional recovery following acute spinal cord injury. *Journal of neurotrauma.* 2008;25(11):1309-1322.

162. Chan CC, Khodarahmi K, Liu J, et al. Dose-dependent beneficial and detrimental effects of ROCK inhibitor Y27632 on axonal sprouting and functional recovery after rat spinal cord injury. *Exp Neurol.* 2005;196(2):352-364.

163. Day JW, Finkel RS, Chiriboga CA, et al. Onasemnogene abeparvovec gene therapy for symptomatic infantile-onset spinal muscular atrophy in patients with two copies of SMN2 (STR1VE): an open-label, single-arm, multicentre, phase 3 trial. *Lancet Neurol.* 2021;20(4):284-293.

164. Russel S, Bennett J, Wellman J. Efficacy and safety of voretigene neparvovec (AAV2-hRPE65v2) in patients with RPE65-mediated inherited retinal dystrophy: a

randomised, controlled, open-label, phase 3 trial. *Lancet.* 2017;390(10097):849-860.

165. Zhong L, Li B, Mah CS, et al. Next generation of adeno-associated virus 2 vectors: point mutations in tyrosines lead to high-efficiency transduction at lower doses. *Proc Natl Acad Sci U S A.* 2008;105(22):7827-7832.

166. Kay CN, Ryals RC, Aslanidi GV, et al. Targeting photoreceptors via intravitreal delivery using novel, capsid-mutated AAV vectors. *PLoS One.* 2013;8(4):e62097.

167. Burger C, Gorbatyuk OS, Velardo MJ, et al. Recombinant AAV viral vectors pseudotyped with viral capsids from serotypes 1, 2, and 5 display differential efficiency and cell tropism after delivery to different regions of the central nervous system. *Mol Ther.* 2004;10(2):302-317.

168. Arbetman AE, Lochrie M, Zhou S, et al. Novel caprine adeno-associated virus (AAV) capsid (AAV-Go. 1) is closely related to the primate AAV-5 and has unique tropism and neutralization properties. *Journal of virology.* 2005;79(24):15238-15245.

169. Hutson TH, Verhaagen J, Yanez-Munoz RJ, Moon LD. Corticospinal tract transduction: a comparison of seven adeno-associated viral vector serotypes and a non-integrating lentiviral vector. *Gene Ther.* 2012;19(1):49-60.

170. Klein RL, Dayton RD, Tatom JB, Diaczynsky CG, Salvatore MF. Tau expression levels from various adeno-associated virus vector serotypes produce graded neurodegenerative disease states. *Eur J Neurosci.* 2008;27(7):1615-1625.

171. Klein RL, Hamby ME, Gong Y, et al. Dose and promoter effects of adeno-associated viral vector for green fluorescent protein expression in the rat brain. *Exp Neurol.* 2002;176(1):66-74.

172. Chamberlin NL, Du B, de Lacalle S, Saper CB. Recombinant adeno-associated virus vector: use for transgene expression and anterograde tract tracing in the CNS. *Brain Res.* 1998;793(1-2):169-175.

173. Tervo DG, Hwang BY, Viswanathan S, et al. A Designer AAV Variant Permits Efficient Retrograde Access to Projection Neurons. *Neuron.* 2016;92(2):372-382.

174. Chan PKW, Geng L, Gao Y, Keung W, Li RA. AAV-mediated conversion of human pluripotent stem cell-derived pacemaker. *Biochem Biophys Res Commun.* 2017;494(1-2):346-351.

175. Wu Z, Yang H, Colosi P. Effect of genome size on AAV vector packaging. *Mol Ther.* 2010;18(1):80-86.

176. Gurda BL, De Guilhem De Lataillade A, Bell P, et al. Evaluation of AAV-mediated Gene Therapy for Central Nervous System Disease in Canine Mucopolysaccharidosis VII. *Mol Ther.* 2016;24(2):206-216.

177. Hordeaux J, Buza EL, Jeffrey B, et al. MicroRNA-mediated inhibition of transgene expression reduces dorsal root ganglion toxicity by AAV vectors in primates. *Sci Transl Med.* 2020;12(569).

178. Agarwal S. High-dose AAV gene therapy deaths. *Nat Biotechnol.* 2020;38(910):853.

179. Ling C, Li B, Ma W, Srivastava A. Development of optimized AAV serotype vectors for high-efficiency transduction at further reduced doses. *Human Gene Therapy Methods.* 2016;27(4):143-149.

180. Zincarelli C, Soltys S, Rengo G, Rabinowitz JE. Analysis of AAV serotypes 1-9 mediated gene expression and tropism in mice after systemic injection. *Mol Ther.* 2008;16(6):1073-1080.

181. Merkel SF, Andrews AM, Lutton EM, et al. Trafficking of adeno-associated virus vectors across a model of the blood-brain barrier; a comparative study of transcytosis and transduction using primary human brain endothelial cells. *J Neurochem.* 2017;140(2):216-230.

182. Samaranch L, Salegio EA, San Sebastian W, et al. Adeno-associated virus serotype 9 transduction in the central nervous system of nonhuman primates. *Hum Gene Ther.* 2012;23(4):382-389.

183. Gray SJ, Nagabhushan Kalburgi S, McCown TJ, Jude Samulski R. Global CNS gene delivery and evasion of anti-AAV-neutralizing antibodies by intrathecal AAV administration in non-human primates. *Gene Ther.* 2013;20(4):450-459.

184. Pietersz KL, Martier RM, Baatje MS, et al. Transduction patterns in the CNS following various routes of AAV-5-mediated gene delivery. *Gene Ther.* 2021;28(7-8):435-446.

185. Brommer B, He M, Zhang Z, et al. Improving hindlimb locomotor function by Non-invasive AAV-mediated manipulations of propriospinal neurons in mice with complete spinal cord injury. *Nat Commun.* 2021;12(1):781.

186. Chen B, Li Y, Yu B, et al. Reactivation of Dormant Relay Pathways in Injured Spinal Cord by KCC2 Manipulations. *Cell.* 2018;174(6):1599.

187. Schutt EG, Klein DH, Mattrey RM, Riess JG. Injectable microbubbles as contrast agents for diagnostic ultrasound imaging: the key role of perfluorochemicals. *Angew Chem Int Ed Engl.* 2003;42(28):3218-3235.

188. Quaia E. Contrast-specific ultrasound techniques. *Radiol Med.* 2007;112(4):473-490.

189. Sheikov N, McDannold N, Jolesz F, Zhang YZ, Tam K, Hynynen K. Brain arterioles show more active vesicular transport of blood-borne tracer molecules than capillaries and venules after focused ultrasound-evoked opening of the blood-brain barrier. *Ultrasound Med Biol.* 2006;32(9):1399-1409.

190. Sheikov N, McDannold N, Sharma S, Hynynen K. Effect of focused ultrasound applied with an ultrasound contrast agent on the tight junctional integrity of the brain microvascular endothelium. *Ultrasound Med Biol.* 2008;34(7):1093-1104.

191. Cho H, Lee H-Y, Han M, et al. Localized down-regulation of P-glycoprotein by focused ultrasound and microbubbles induced blood-brain barrier disruption in rat brain. *Scientific reports.* 2016;6(1):31201.

192. Karakatsani ME, Blesa J, Konofagou EE. Blood-brain barrier opening with focused ultrasound in experimental models of Parkinson's disease. *Mov Disord.* 2019;34(9):1252-1261.

193. Gasca-Salas C, Fernández-Rodríguez B, Pineda-Pardo JA, et al. Blood-brain barrier opening with focused ultrasound in Parkinson's disease dementia. *Nature communications.* 2021;12(1):779.

194. Weber-Adrian D, Thévenot E, O'Reilly MA, et al. Gene delivery to the spinal cord using MRI-guided focused ultrasound. *Gene therapy.* 2015;22(7):568-577.

195. Nassi JJ, Cepko CL, Born RT, Beier KT. Neuroanatomy goes viral! *Front Neuroanat.* 2015;9:80.

196. Lanciego JL, Wouterlood FG. Neuroanatomical tract-tracing techniques that did go viral. *Brain Struct Funct.* 2020;225(4):1193-1224.

197. Ugolini G. Viruses in connectomics: Viral transneuronal tracers and genetically modified recombinants as neuroscience research tools. *J Neurosci Methods.* 2020;346:108917.

198. Zeng H. Mesoscale connectomics. *Curr Opin Neurobiol.* 2018;50:154-162.

199. Wong JK, Middlebrooks EH, Grewal SS, Almeida L, Hess CW, Okun MS. A Comprehensive Review of Brain Connectomics and Imaging to Improve Deep Brain Stimulation Outcomes. *Mov Disord.* 2020;35(5):741-751.

200. Horn A, Fox MD. Opportunities of connectomic neuromodulation. *Neuroimage.* 2020;221:117180.

201. Hu Z, Liu G, Dong Q, Niu H. Applications of Resting-State fNIRS in the Developing Brain: A Review From the Connectome Perspective. *Front Neurosci.* 2020;14:476.

202. Cao J, Khan B, Hervey N, et al. Evaluation of cortical plasticity in children with cerebral palsy undergoing constraint-induced movement therapy based on functional near-infrared spectroscopy. *J Biomed Opt.* 2015;20(4):046009.

203. Yeh CH, Jones DK, Liang X, Descoteaux M, Connelly A. Mapping Structural Connectivity Using Diffusion MRI: Challenges and Opportunities. *J Magn Reson Imaging.* 2020.

204. Jeurissen B, Descoteaux M, Mori S, Leemans A. Diffusion MRI fiber tractography of the brain. *NMR Biomed.* 2019;32(4):e3785.

205. Fox MD, Raichle ME. Spontaneous fluctuations in brain activity observed with functional magnetic resonance imaging. *Nat Rev Neurosci.* 2007;8(9):700-711.

206. Horn A, Reich M, Vorwerk J, et al. Connectivity Predicts deep brain stimulation outcome in Parkinson disease. *Ann Neurol.* 2017;82(1):67-78.

207. Joutsa J, Horn A, Hsu J, Fox MD. Localizing parkinsonism based on focal brain lesions. *Brain.* 2018;141(8):2445-2456.

208. Okromelidze L, Tsuboi T, Eisinger RS, et al. Functional and Structural Connectivity Patterns Associated with Clinical Outcomes in Deep Brain Stimulation of the Globus Pallidus Internus for Generalized Dystonia. *AJNR Am J Neuroradiol.* 2020;41(3):508-514.

209. Lanciego JL, Wouterlood FG. A half century of experimental neuroanatomical tracing. *J Chem Neuroanat.* 2011;42(3):157-183.

210. Wouterlood FG, Bloem B, Mansvelder HD, Luchicchi A, Deisseroth K. A fourth generation of neuroanatomical tracing techniques: exploiting the offspring of genetic engineering. *J Neurosci Methods.* 2014;235:331-348.

211. Glover JC, Petursdottir G, Jansen JK. Fluorescent dextran-amines used as axonal tracers in the nervous system of the chicken embryo. *J Neurosci Methods.* 1986;18(3):243-254.

212. Naumann T, Hartig W, Frotscher M. Retrograde tracing with Fluoro-Gold: different methods of tracer detection at the ultrastructural level and neurodegenerative changes of back-filled neurons in long-term studies. *J Neurosci Methods.* 2000;103(1):11-21.

213. Chen S, Aston-Jones G. Evidence that cholera toxin B subunit (CTb) can be avidly taken up and transported by fibers of passage. *Brain Res.* 1995;674(1):107-111.

214. Dado RJ, Burstein R, Cliffer KD, Giesler GJ, Jr. Evidence that Fluoro-Gold can be transported avidly through fibers of passage. *Brain Res.* 1990;533(2):329-333.

215. Lai BQ, Qiu XC, Zhang K, et al. Cholera Toxin B Subunit Shows Transneuronal Tracing after Injection in an Injured Sciatic Nerve. *PLoS One.* 2015;10(12):e0144030.

216. Deng L, Ruan Y, Chen C, et al. Characterization of dendritic morphology and neurotransmitter phenotype of thoracic descending propriospinal neurons after complete spinal cord transection and GDNF treatment. *Exp Neurol.* 2016;277:103-114.

217. Wertz A, Trenholm S, Yonehara K, et al. PRESYNAPTIC NETWORKS. Single-cell-initiated monosynaptic tracing reveals layer-specific cortical network modules. *Science.* 2015;349(6243):70-74.

218. Zingg B, Chou XL, Zhang ZG, et al. AAV-Mediated Anterograde Transsynaptic Tagging: Mapping Corticocollicular Input-Defined Neural Pathways for Defense Behaviors. *Neuron.* 2017;93(1):33-47.

219. Atasoy D, Aponte Y, Su HH, Sternson SM. A FLEX switch targets Channelrhodopsin-2 to multiple cell types for imaging and long-range circuit mapping. *J Neurosci.* 2008;28(28):7025-7030.

220. Chan KY, Jang MJ, Yoo BB, et al. Engineered AAVs for efficient noninvasive gene delivery to the central and peripheral nervous systems. *Nat Neurosci.* 2017;20(8):1172-1179.

221. Aschauer DF, Kreuz S, Rumpel S. Analysis of transduction efficiency, tropism and axonal transport of AAV serotypes 1, 2, 5, 6, 8 and 9 in the mouse brain. *PLoS One.* 2013;8(9):e76310.

222. Liu G, Martins IH, Chiorini JA, Davidson BL. Adeno-associated virus type 4 (AAV4) targets ependyma and astrocytes in the subventricular zone and RMS. *Gene Ther.* 2005;12(20):1503-1508.

223. Klaw MC, Xu C, Tom VJ. Intraspinal AAV Injections Immediately Rostral to a Thoracic Spinal Cord Injury Site Efficiently Transduces Neurons in Spinal Cord and Brain. *Mol Ther Nucleic Acids.* 2013;2:e108.

224. Hollis Ii ER, Kadoya K, Hirsch M, Samulski RJ, Tuszynski MH. Efficient Retrograde Neuronal Transduction Utilizing Self-complementary AAV1. *Mol Ther.* 2008;16(2):296-301.

225. Klein RL, Dayton RD, Tatom JB, Henderson KM, Henning PP. AAV8, 9, Rh10, Rh43 vector gene transfer in the rat brain: effects of serotype, promoter and purification method. *Mol Ther.* 2008;16(1):89-96.

226. Rosenberg JB, Sondhi D, Rubin DG, et al. Comparative efficacy and safety of multiple routes of direct CNS administration of adeno-associated virus gene transfer vector serotype rh.10 expressing the human arylsulfatase A cDNA to nonhuman primates. *Hum Gene Ther Clin Dev.* 2014;25(3):164-177.

227. Hirano M, Kato S, Kobayashi K, Okada T, Yaginuma H, Kobayashi K. Highly efficient retrograde gene transfer into motor neurons by a lentiviral vector pseudotyped with fusion glycoprotein. *PLoS One.* 2013;8(9):e75896.

228. Tanabe S, Uezono S, Tsuge H, et al. A note on retrograde gene transfer efficiency and inflammatory response of lentiviral vectors pseudotyped with FuG-E vs. FuG-B2 glycoproteins. *Sci Rep.* 2019;9(1):3567.

229. Kato S, Kobayashi K, Inoue K, et al. A lentiviral strategy for highly efficient retrograde gene transfer by pseudotyping with fusion envelope glycoprotein. *Hum Gene Ther.* 2011;22(2):197-206.

230. Kitagawa R, Miyachi S, Hanawa H, Takada M, Shimada T. Differential characteristics of HIV-based versus SIV-based lentiviral vector systems: Gene

delivery to neurons and axonal transport of expressed gene. *Neurosci Res.* 2007;57(4):550-558.

231. Kato S, Kuramochi M, Kobayashi K, et al. Selective neural pathway targeting reveals key roles of thalamostriatal projection in the control of visual discrimination. *J Neurosci.* 2011;31(47):17169-17179.

232. Wang X, Liu Y, Li X, et al. Deconstruction of Corticospinal Circuits for Goal-Directed Motor Skills. *Cell.* 2017;171(2):440-455 e414.

233. Zhang YP, Burke DA, Shields LB, et al. Spinal cord contusion based on precise vertebral stabilization and tissue displacement measured by combined assessment to discriminate small functional differences. *J Neurotrauma.* 2008;25(10):1227-1240.

234. Reed WR, Shum-Siu A, Whelan A, Onifer SM, Magnuson DS. Anterograde labeling of ventrolateral funiculus pathways with spinal enlargement connections in the adult rat spinal cord. *Brain Res.* 2009;1302:76-84.

235. Watson C, Paxinos G, Kayalioglu G. *The spinal cord: a Christopher and Dana Reeve Foundation text and atlas.* Academic press; 2009.

236. Jiang X, Johnson RR, Burkhalter A. Visualization of dendritic morphology of cortical projection neurons by retrograde axonal tracing. *J Neurosci Methods.* 1993;50(1):45-60.

237. Srivastava A. In vivo tissue-tropism of adeno-associated viral vectors. *Curr Opin Virol.* 2016;21:75-80.

238. Bartlett JS, Samulski RJ, McCown TJ. Selective and rapid uptake of adeno-associated virus type 2 in brain. *Hum Gene Ther.* 1998;9(8):1181-1186.

239. Hollis ER, 2nd, Kadoya K, Hirsch M, Samulski RJ, Tuszynski MH. Efficient retrograde neuronal transduction utilizing self-complementary AAV1. *Mol Ther.* 2008;16(2):296-301.

240. Salegio EA, Samaranch L, Kells AP, et al. Axonal transport of adeno-associated viral vectors is serotype-dependent. *Gene Ther.* 2013;20(3):348-352.

241. Santoro SW, Schultz PG. Directed evolution of the site specificity of Cre recombinase. *Proc Natl Acad Sci U S A.* 2002;99(7):4185-4190.

242. Gibb B, Gupta K, Ghosh K, Sharp R, Chen J, Van Duyne GD. Requirements for catalysis in the Cre recombinase active site. *Nucleic Acids Res.* 2010;38(17):5817-5832.

243. Sun L, Tang Y, Yan K, et al. Differences in neurotropism and neurotoxicity among retrograde viral tracers. *Mol Neurodegener.* 2019;14(1):8.

244. Zhong L, Li B, Jayandharan G, et al. Tyrosine-phosphorylation of AAV2 vectors and its consequences on viral intracellular trafficking and transgene expression. *Virology.* 2008;381(2):194-202.

245. Buning H, Srivastava A. Capsid Modifications for Targeting and Improving the Efficacy of AAV Vectors. *Mol Ther Methods Clin Dev.* 2019;12:248-265.

246. Zhong L, Zhao W, Wu J, et al. A dual role of EGFR protein tyrosine kinase signaling in ubiquitination of AAV2 capsids and viral second-strand DNA synthesis. *Mol Ther.* 2007;15(7):1323-1330.

247. Waibl H. *Zur Topographie der Medulla spinalis der Albinoratte (rattus norvegicus)/Contributions to the Topography of the Spinal Cord of the Albino Rat (Rattus norvegicus).* Springer-Verlag; 2013.

248. Weiss AR, Liguore WA, Domire JS, Button D, McBride JL. Intra-striatal AAV2.retro administration leads to extensive retrograde transport in the rhesus macaque brain: implications for disease modeling and therapeutic development. *Sci Rep.* 2020;10(1):6970.

249. Matsushita M, Hosoya Y. Cells of origin of the spinocerebellar tract in the rat, studied with the method of retrograde transport of horseradish peroxidase. *Brain Res.* 1979;173(2):185-200.

250. Gawdi R, Shumway KR, Emmady PD. Physiology, Blood Brain Barrier. In: *StatPearls.* Treasure Island (FL) ineligible companies. Disclosure: Karlie Shumway declares no relevant financial relationships with ineligible companies. Disclosure: Prabhu Emmady declares no relevant financial relationships with ineligible companies.2023.

251. Dotiwala AK, McCausland C, Samra NS. Anatomy, Head and Neck: Blood Brain Barrier. In: *StatPearls.* Treasure Island (FL) ineligible companies. Disclosure: Cassidy McCausland declares no relevant financial relationships with ineligible companies. Disclosure: Navdeep Samra declares no relevant financial relationships with ineligible companies.2023.

252. Pardridge WM. The blood-brain barrier: bottleneck in brain drug development. *NeuroRx.* 2005;2(1):3-14.

253. Fowler MJ, Cotter JD, Knight BE, Sevick-Muraca EM, Sandberg DI, Sirianni RW. Intrathecal drug delivery in the era of nanomedicine. *Adv Drug Deliv Rev.* 2020;165-166:77-95.

254. Hardcastle N, Boulis NM, Federici T. AAV gene delivery to the spinal cord: serotypes, methods, candidate diseases, and clinical trials. *Expert Opin Biol Ther.* 2018;18(3):293-307.

255. Hinderer C, Nosratbakhsh B, Katz N, Wilson JM. A Single Injection of an Optimized Adeno-Associated Viral Vector into Cerebrospinal Fluid Corrects Neurological Disease in a Murine Model of GM1 Gangliosidosis. *Hum Gene Ther.* 2020;31(21-22):1169-1177.

256. Bailey RM, Rozenberg A, Gray SJ. Comparison of high-dose intracisterna magna and lumbar puncture intrathecal delivery of AAV9 in mice to treat neuropathies. *Brain research.* 2020;1739:146832.

257. Householder KT, Dharmaraj S, Sandberg DI, Wechsler-Reya RJ, Sirianni RW. Fate of nanoparticles in the central nervous system after intrathecal injection in healthy mice. *Sci Rep.* 2019;9(1):12587.

258. S Hersh D, S Wadajkar A, B Roberts N, et al. Evolving drug delivery strategies to overcome the blood brain barrier. *Current pharmaceutical design.* 2016;22(9):1177-1193.

259. Rapoport SI. Osmotic opening of the blood-brain barrier: principles, mechanism, and therapeutic applications. *Cell Mol Neurobiol.* 2000;20(2):217-230.

260. McCown TJ, Xiao X, Li J, Breese GR, Samulski RJ. Differential and persistent expression patterns of CNS gene transfer by an adeno-associated virus (AAV) vector. *Brain Res.* 1996;713(1-2):99-107.

261. Betz AL, Shakui P, Davidson BL. Gene transfer to rodent brain with recombinant adenoviral vectors: effects of infusion parameters, infectious titer, and virus concentration on transduction volume. *Experimental neurology.* 1998;150(1):136-142.

262. Mendell JR, Al-Zaidy S, Shell R, et al. Single-dose gene-replacement therapy for spinal muscular atrophy. *New England Journal of Medicine.* 2017;377(18):1713-1722.

263. Day JW, Finkel RS, Chiriboga CA, et al. Onasemnogene abeparvovec gene therapy for symptomatic infantile-onset spinal muscular atrophy in patients with two copies of SMN2 (STR1VE): an open-label, single-arm, multicentre, phase 3 trial. *The Lancet Neurology.* 2021;20(4):284-293.

264. Philippidis A. Novartis Confirms Deaths of Two Patients Treated with Gene Therapy Zolgensma. *Hum Gene Ther.* 2022;33(17-18):842-844.

265. High-dose AAV gene therapy deaths. *Nat Biotechnol.* 2020;38(8):910.

266. Hordeaux J, Buza EL, Dyer C, et al. Adeno-Associated Virus-Induced Dorsal Root Ganglion Pathology. *Hum Gene Ther.* 2020;31(15-16):808-818.

267. Hinderer C, Katz N, Buza EL, et al. Severe Toxicity in Nonhuman Primates and Piglets Following High-Dose Intravenous Administration of an Adeno-Associated Virus Vector Expressing Human SMN. *Hum Gene Ther.* 2018;29(3):285-298.

268. Goertsen D, Flytzanis NC, Goeden N, et al. AAV capsid variants with brain-wide transgene expression and decreased liver targeting after intravenous delivery in mouse and marmoset. *Nat Neurosci.* 2022;25(1):106-115.

269. Chan KY, Jang MJ, Yoo BB, et al. Engineered AAVs for efficient noninvasive gene delivery to the central and peripheral nervous systems. *Nature neuroscience.* 2017;20(8):1172-1179.

270. Breitkreuz-Korff O, Tscheik C, Del Vecchio G, et al. M01 as a novel drug enhancer for specifically targeting the blood-brain barrier. *Journal of Controlled Release.* 2021;338:137-148.

271. Neuwelt E, Howieson J, Frenkel E, et al. Therapeutic efficacy of multiagent chemotherapy with drug delivery enhancement by blood-brain barrier modification in glioblastoma. *Neurosurgery.* 1986;19(4):573-582.

272. Kim D-G, Bynoe MS. A2A adenosine receptor modulates drug efflux transporter P-glycoprotein at the blood-brain barrier. *The Journal of clinical investigation.* 2016;126(5):1717-1733.

273. Shen J, Yu M, Meng Q, Li J, Lv Y, Lu W. Fatty acid-based strategy for efficient brain targeted gene delivery. *Pharmaceutical research.* 2013;30:2573-2583.

274. Chen H, Kreider W, Brayman AA, Bailey MR, Matula TJ. Blood vessel deformations on microsecond time scales by ultrasonic cavitation. *Physical review letters.* 2011;106(3):034301.

275. Sheikov N, McDannold N, Vykhodtseva N, Jolesz F, Hynynen K. Cellular mechanisms of the blood-brain barrier opening induced by ultrasound in

presence of microbubbles. *Ultrasound in medicine & biology.* 2004;30(7):979-989.

276. Kofoed RH, Dibia CL, Noseworthy K, et al. Efficacy of gene delivery to the brain using AAV and ultrasound depends on serotypes and brain areas. *J Control Release.* 2022;351:667-680.

277. Smith P, Ogrodnik N, Satkunarajah J, O'Reilly MA. Characterization of ultrasound-mediated delivery of trastuzumab to normal and pathologic spinal cord tissue. *Scientific Reports.* 2021;11(1):4412.

278. Choi JJ, Wang S, Tung Y-S, Morrison III B, Konofagou EE. Molecules of various pharmacologically-relevant sizes can cross the ultrasound-induced blood-brain barrier opening in vivo. *Ultrasound in medicine & biology.* 2010;36(1):58-67.

279. Weber-Adrian D, Thevenot E, O'Reilly MA, et al. Gene delivery to the spinal cord using MRI-guided focused ultrasound. *Gene Ther.* 2015;22(7):568-577.

280. Dimitrijevic MR, Gerasimenko Y, Pinter MM. Evidence for a spinal central pattern generator in humans. *Ann N Y Acad Sci.* 1998;860:360-376.

281. Kiehn O, Kjaerulff O. Distribution of central pattern generators for rhythmic motor outputs in the spinal cord of limbed vertebrates. *Ann N Y Acad Sci.* 1998;860:110-129.

282. Grillner S. Locomotion in vertebrates: central mechanisms and reflex interaction. *Physiol Rev.* 1975;55(2):247-304.

283. Harkema S, Gerasimenko Y, Hodes J, et al. Effect of epidural stimulation of the lumbosacral spinal cord on voluntary movement, standing, and assisted stepping

after motor complete paraplegia: a case study. *Lancet.* 2011;377(9781):1938-1947.

284. Herrity AN, Williams CS, Angeli CA, Harkema SJ, Hubscher CH. Lumbosacral spinal cord epidural stimulation improves voiding function after human spinal cord injury. *Sci Rep.* 2018;8(1):8688.

285. Harkema SJ, Wang S, Angeli CA, et al. Normalization of Blood Pressure With Spinal Cord Epidural Stimulation After Severe Spinal Cord Injury. *Front Hum Neurosci.* 2018;12:83.

286. Kathe C, Skinnider MA, Hutson TH, et al. The neurons that restore walking after paralysis. *Nature.* 2022;611(7936):540-547.

287. Centner CS, Murphy EM, Priddy MC, et al. Ultrasound-induced molecular delivery to erythrocytes using a microfluidic system. *Biomicrofluidics.* 2020;14(2):024114.

288. Pocratsky AM, Burke DA, Morehouse JR, et al. Reversible silencing of lumbar spinal interneurons unmasks a task-specific network for securing hindlimb alternation. *Nat Commun.* 2017;8(1):1963.

289. Weinstein S. Fifty years of somatosensory research: from the Semmes-Weinstein monofilaments to the Weinstein Enhanced Sensory Test. *Journal of Hand therapy.* 1993;6(1):11-22.

290. Pinton G, Aubry JF, Bossy E, Muller M, Pernot M, Tanter M. Attenuation, scattering, and absorption of ultrasound in the skull bone. *Med Phys.* 2012;39(1):299-307.

291. Mahadevan V. Anatomy of the vertebral column. *Surgery (Oxford).* 2018;36(7):327-332.

292. Huang Y, Vykhodtseva NI, Hynynen K. Creating brain lesions with low-intensity focused ultrasound with microbubbles: a rat study at half a megahertz. *Ultrasound Med Biol.* 2013;39(8):1420-1428.

293. Lampaskis M, Averkiou M. Investigation of the relationship of nonlinear backscattered ultrasound intensity with microbubble concentration at low MI. *Ultrasound Med Biol.* 2010;36(2):306-312.

294. Martinez P, Bottenus N, Borden M. Correction: Martinez et al. Cavitation Characterization of Size-Isolated Microbubbles in a Vessel Phantom Using Focused Ultrasound. Pharmaceutics 2022, 14, 1925. *Pharmaceutics.* 2022;14(10).

295. Toossi A, Bergin B, Marefatallah M, et al. Comparative neuroanatomy of the lumbosacral spinal cord of the rat, cat, pig, monkey, and human. *Sci Rep.* 2021;11(1):1955.

296. Chatterjee S, Fisher AB. Mechanotransduction: forces, sensors, and redox signaling. *Antioxid Redox Signal.* 2014;20(6):868-871.

297. Kovacs ZI, Kim S, Jikaria N, et al. Disrupting the blood-brain barrier by focused ultrasound induces sterile inflammation. *Proc Natl Acad Sci U S A.* 2017;114(1):E75-E84.

298. Kovacs ZI, Tu TW, Sundby M, et al. MRI and histological evaluation of pulsed focused ultrasound and microbubbles treatment effects in the brain. *Theranostics.* 2018;8(17):4837-4855.

299. McDannold N, Zhang Y, Vykhodtseva N. Blood-brain barrier disruption and vascular damage induced by ultrasound bursts combined with microbubbles can be influenced by choice of anesthesia protocol. *Ultrasound Med Biol.* 2011;37(8):1259-1270.

300. Srivastava A, Carter BJ. AAV Infection: Protection from Cancer. *Hum Gene Ther.* 2017;28(4):323-327.

301. Pardridge WM. The blood-brain barrier and neurotherapeutics. *NeuroRx.* 2005;2(1):1-2.

302. Goodman BS, Posecion LW, Mallempati S, Bayazitoglu M. Complications and pitfalls of lumbar interlaminar and transforaminal epidural injections. *Curr Rev Musculoskelet Med.* 2008;1(3-4):212-222.

303. Wu SK, Tsai CL, Huang Y, Hynynen K. Focused Ultrasound and Microbubbles-Mediated Drug Delivery to Brain Tumor. *Pharmaceutics.* 2020;13(1).

304. Liu HL, Fan CH, Ting CY, Yeh CK. Combining microbubbles and ultrasound for drug delivery to brain tumors: current progress and overview. *Theranostics.* 2014;4(4):432-444.

305. Burgess A, Ayala-Grosso CA, Ganguly M, Jordao JF, Aubert I, Hynynen K. Targeted delivery of neural stem cells to the brain using MRI-guided focused ultrasound to disrupt the blood-brain barrier. *PLoS One.* 2011;6(11):e27877.

306. McMahon D, Hynynen K. Acute Inflammatory Response Following Increased Blood-Brain Barrier Permeability Induced by Focused Ultrasound is Dependent on Microbubble Dose. *Theranostics.* 2017;7(16):3989-4000.

307. Kovacs ZI, Burks SR, Frank JA. Focused ultrasound with microbubbles induces sterile inflammatory response proportional to the blood brain barrier opening: Attention to experimental conditions. *Theranostics.* 2018;8(8):2245-2248.

308. Pandit R, Koh WK, Sullivan RKP, Palliyaguru T, Parton RG, Gotz J. Role for caveolin-mediated transcytosis in facilitating transport of large cargoes into the brain via ultrasound. *J Control Release.* 2020;327:667-675.

309. Resnick N, Yahav H, Shay-Salit A, et al. Fluid shear stress and the vascular endothelium: for better and for worse. *Prog Biophys Mol Biol.* 2003;81(3):177-199.

310. Zhu D, Wu S, Li Y, et al. Ferroptosis-related gene SLC1A5 is a novel prognostic biomarker and correlates with immune infiltrates in stomach adenocarcinoma. *Cancer Cell Int.* 2022;22(1):124.

311. Dixon SJ, Lemberg KM, Lamprecht MR, et al. Ferroptosis: an iron-dependent form of nonapoptotic cell death. *Cell.* 2012;149(5):1060-1072.

312. Hirschhorn T, Stockwell BR. The development of the concept of ferroptosis. *Free Radical Biology and Medicine.* 2019;133:130-143.

313. Federici T, Taub JS, Baum GR, et al. Robust spinal motor neuron transduction following intrathecal delivery of AAV9 in pigs. *Gene Ther.* 2012;19(8):852-859.

314. Chuapoco MR, Flytzanis NC, Goeden N, et al. Intravenous gene transfer throughout the brain of infant Old World primates using AAV. *bioRxiv.* 2022:2022.2001. 2008.475342.

315. Jackson KL, Dayton RD, Fisher-Perkins JM, et al. Initial gene vector dosing for studying symptomatology of amyotrophic lateral sclerosis in non-human primates. *J Med Primatol.* 2015;44(2):66-75.

316. Duque S, Joussemet B, Riviere C, et al. Intravenous administration of self-complementary AAV9 enables transgene delivery to adult motor neurons. *Mol Ther.* 2009;17(7):1187-1196.

317. Mathiesen SN, Lock JL, Schoderboeck L, Abraham WC, Hughes SM. CNS Transduction Benefits of AAV-PHP.eB over AAV9 Are Dependent on Administration Route and Mouse Strain. *Mol Ther Methods Clin Dev.* 2020;19:447-458.

318. Dayton RD, Grames MS, Klein RL. More expansive gene transfer to the rat CNS: AAV PHP.EB vector dose-response and comparison to AAV PHP.B. *Gene Ther.* 2018;25(5):392-400.

319. Gray JT, Zolotukhin S. Design and construction of functional AAV vectors. *Methods Mol Biol.* 2011;807:25-46.

320. Foust KD, Nurre E, Montgomery CL, Hernandez A, Chan CM, Kaspar BK. Intravascular AAV9 preferentially targets neonatal neurons and adult astrocytes. *Nature biotechnology.* 2009;27(1):59-65.

321. Stanimirovic DB, Sandhu JK, Costain WJ. Emerging Technologies for Delivery of Biotherapeutics and Gene Therapy Across the Blood-Brain Barrier. *BioDrugs.* 2018;32(6):547-559.

322. Leibinger M, Zeitler C, Gobrecht P, Andreadaki A, Gisselmann G, Fischer D. Transneuronal delivery of hyper-interleukin-6 enables functional recovery after severe spinal cord injury in mice. *Nat Commun.* 2021;12(1):391.

323. Zholudeva LV, Lane MA. *Spinal interneurons: Plasticity after spinal cord injury.* Academic Press; 2022.

324. Brown BL, Zalla RM, Shepard CT, et al. Dual-Viral Transduction Utilizing Highly Efficient Retrograde Lentivirus Improves Labeling of Long Propriospinal Neurons. *Front Neuroanat.* 2021;15:635921.

325. Kakulas BA. Neuropathology: the foundation for new treatments in spinal cord injury. *Spinal Cord.* 2004;42(10):549-563.

326. Basso DM, Beattie MS, Bresnahan JC. Descending systems contributing to locomotor recovery after mild or moderate spinal cord injury in rats: experimental evidence and a review of literature. *Restor Neurol Neurosci.* 2002;20(5):189-218.

327. Grau JW. Influence of naloxone on shock-induced freezing and analgesia. *Behavioral Neuroscience.* 1984;98(2):278.

328. Scheff S, Roberts KN. Infinite horizon spinal cord contusion model. *Animal models of acute neurological injuries.* 2009:423-432.

329. Renier N, Wu Z, Simon DJ, Yang J, Ariel P, Tessier-Lavigne M. iDISCO: a simple, rapid method to immunolabel large tissue samples for volume imaging. *Cell.* 2014;159(4):896-910.

330. Marshak S, Nikolakopoulou AM, Dirks R, Martens GJ, Cohen-Cory S. Cell-autonomous TrkB signaling in presynaptic retinal ganglion cells mediates axon arbor growth and synapse maturation during the establishment of retinotectal synaptic connectivity. *J Neurosci.* 2007;27(10):2444-2456.

331. Carrascal L, Nieto-Gonzalez JL, Torres B, Nunez-Abades P. Diminution of voltage threshold plays a key role in determining recruitment of oculomotor nucleus motoneurons during postnatal development. *PLoS One.* 2011;6(12):e28748.

332. Harper A, Lawson S. Electrical properties of rat dorsal root ganglion neurones with different peripheral nerve conduction velocities. *The Journal of physiology.* 1985;359(1):47-63.

333. Purves D, Hume RI. The relation of postsynaptic geometry to the number of presynaptic axons that innervate autonomic ganglion cells. *Journal of Neuroscience.* 1981;1(5):441-452.

334. Holmes JR, Berkowitz A. Dendritic orientation and branching distinguish a class of multifunctional turtle spinal interneurons. *Frontiers in Neural Circuits.* 2014;8:136.

335. Kjell J, Olson L. Rat models of spinal cord injury: from pathology to potential therapies. *Disease models & mechanisms.* 2016;9(10):1125-1137.

336. Bras H, Cavallari P, Jankowska E, Kubin L. Morphology of midlumbar interneurones relaying information from group II muscle afferents in the cat spinal cord. *Journal of Comparative Neurology.* 1989;290(1):1-15.

337. Rastad J, Gad P, Jankowska E, McCrea D, Westman J. Light microscopical study of dendrites and perikarya of interneurones mediating la reciprocal inhibition of cat lumbar alpha-motoneurones. *Anat Embryol (Berl).* 1990;181(4):381-388.

338. Ritz LA, Greenspan JD. Morphological features of lamina V neurons receiving nociceptive input in cat sacrocaudal spinal cord. *Journal of Comparative Neurology.* 1985;238(4):440-452.

339. Berkowitz A, Yosten GL, Ballard RM. Somato-dendritic morphology predicts physiology for neurons that contribute to several kinds of limb movements. *Journal of neurophysiology.* 2006;95(5):2821-2831.

340. Gelfan S, Kao G, Ruchkin DS. The dendritic tree of spinal neurons. *J Comp Neurol.* 1970;139(4):385-411.

341. Sterling P, Kuypers HG. Anatomical organization of the brachial spinal cord of the cat. I. The distribution of dorsal root fibers. *Brain Res.* 1967;4(1):1-15.

342. Grillner S. Evolution of the vertebrate motor system - from forebrain to spinal cord. *Curr Opin Neurobiol.* 2021;71:11-18.

343. Chew C, Sengelaub DR. Exercise is neuroprotective on the morphology of somatic motoneurons following the death of neighboring motoneurons via androgen action at the target muscle. *Developmental Neurobiology.* 2021;81(1):22-35.

344. Gray L, Smith Z, Rubel EW. Developmental and experiential changes in dendritic symmetry in n. laminaris of the chick. *Brain research.* 1982;244(2):360-364.

345. Harris RM, Woolsey TA. Dendritic plasticity in mouse barrel cortex following postnatal vibrissa follicle damage. *Journal of Comparative Neurology.* 1981;196(3):357-376.

346. Katz LC, Shatz CJ. Synaptic activity and the construction of cortical circuits. *Science.* 1996;274(5290):1133-1138.

347. Greenough WT, Volkmar FR. Pattern of dendritic branching in occipital cortex of rats reared in complex environments. *Experimental neurology.* 1973;40(2):491-504.

348. Beauparlant J, van den Brand R, Barraud Q, et al. Undirected compensatory plasticity contributes to neuronal dysfunction after severe spinal cord injury. *Brain.* 2013;136(Pt 11):3347-3361.

349. Krenz NR, Weaver LC. Sprouting of primary afferent fibers after spinal cord transection in the rat. *Neuroscience.* 1998;85(2):443-458.

350. Yin J, Yuan Q. Structural homeostasis in the nervous system: a balancing act for wiring plasticity and stability. *Frontiers in cellular neuroscience.* 2015;8:439.

351. Talifu Z, Pan Y, Gong H, et al. The role of KCC2 and NKCC1 in spinal cord injury: From physiology to pathology. *Front Physiol.* 2022;13:1045520.

352. Dailey ME, Smith SJ. The dynamics of dendritic structure in developing hippocampal slices. *J Neurosci.* 1996;16(9):2983-2994.

353. Rajan I, Cline HT. Glutamate receptor activity is required for normal development of tectal cell dendrites in vivo. *Journal of Neuroscience.* 1998;18(19):7836-7846.

354. Wu GY, Zou DJ, Rajan I, Cline H. Dendritic dynamics in vivo change during neuronal maturation. *Journal of Neuroscience.* 1999;19(11):4472-4483.

355. Dai Y, Wang H, Ogawa A, et al. Ca2+/calmodulin-dependent protein kinase II in the spinal cord contributes to neuropathic pain in a rat model of mononeuropathy. *Eur J Neurosci.* 2005;21(9):2467-2474.

356. Frey D, Schneider C, Xu L, Borg J, Spooren W, Caroni P. Early and selective loss of neuromuscular synapse subtypes with low sprouting competence in motoneuron diseases. *Journal of Neuroscience.* 2000;20(7):2534-2542.

357. Hegedus J, Putman C, Gordon T. Time course of preferential motor unit loss in the SOD1G93A mouse model of amyotrophic lateral sclerosis. *Neurobiology of disease.* 2007;28(2):154-164.

358. Sakurai M, Hayashi T, Abe K, Sadahiro M, Tabayashi K. Delayed selective motor neuron death and fas antigen induction after spinal cord ischemia in rabbits. *Brain research.* 1998;797(1):23-28.

359. He J-w, Hirata K, Wang S, Kawabuchi M. Expression of nitric oxide synthase and 27-kD heat shock protein in motor neurons of ventral root-avulsed rats. *Archives of histology and cytology.* 2003;66(1):83-93.

360. Hu G, Huang K, Hu Y, et al. Single-cell RNA-seq reveals distinct injury responses in different types of DRG sensory neurons. *Scientific reports.* 2016;6(1):31851.

361. Murray LM, Beauvais A, Gibeault S, Courtney NL, Kothary R. Transcriptional profiling of differentially vulnerable motor neurons at pre-symptomatic stage in

the Smn 2b/-mouse model of spinal muscular atrophy. *Acta neuropathologica communications.* 2015;3(1):1-17.

362. Grumbles RM, Thomas CK. Motoneuron Death after Human Spinal Cord Injury. *J Neurotrauma.* 2017;34(3):581-590.

363. Huber E, David G, Thompson AJ, Weiskopf N, Mohammadi S, Freund P. Dorsal and ventral horn atrophy is associated with clinical outcome after spinal cord injury. *Neurology.* 2018;90(17):e1510-e1522.

364. Barber RP, Vaughn JE, Roberts E. The cytoarchitecture of GABAergic neurons in rat spinal cord. *Brain Res.* 1982;238(2):305-328.

365. Delwaide P, Figiel C, Richelle C. Effects of postural changes of the upper limb on reflex transmission in the lower limb. Cervicolumbar reflex interactions in man. *Journal of Neurology, Neurosurgery & Psychiatry.* 1977;40(6):616-621.

366. Krutki P, Grottel K, Mrowczynski W. Cervical and cerebellar projections of lamina VII and VIII neurones of the S2 segment in the cat's spinal cord. *Arch Ital Biol.* 1998;136(3):181-189.

367. Millan MJ. The induction of pain: an integrative review. *Prog Neurobiol.* 1999;57(1):1-164.

368. Miller RA, Strominger NL. Efferent connections of the red nucleus in the brainstem and spinal cord of the rhesus monkey. *Journal of Comparative Neurology.* 1973;152(4):327-345.

369. Fields HL, Anderson SD, Wagner GM. The spinoreticular tract: an alternate pathway mediating pain. *Trans Am Neurol Assoc.* 1974;99:211-213.

370. Kevetter GA, Haber LH, Yezierski RP, Chung JM, Martin RF, Willis WD. Cells of origin of the spinoreticular tract in the monkey. *Journal of Comparative Neurology.* 1982;207(1):61-74.

371. Fauth M, Tetzlaff C. Opposing Effects of Neuronal Activity on Structural Plasticity. *Front Neuroanat.* 2016;10:75.

372. Leem YJ, Joh JW, Joeng KW, Suh JH, Shin JW, Leem JG. Central Pain from Excitotoxic Spinal Cord Injury Induced by Intraspinal NMDA Injection: A Pilot Study. *Korean J Pain.* 2010;23(2):109-115.

373. Borgens RB, Bohnert DM. The responses of mammalian spinal axons to an applied DC voltage gradient. *Exp Neurol.* 1997;145(2 Pt 1):376-389.

374. Ferguson AR, Huie JR, Crown ED, et al. Maladaptive spinal plasticity opposes spinal learning and recovery in spinal cord injury. *Front Physiol.* 2012;3:399.

375. Taccola G, Gad P, Culaclii S, Wang PM, Liu W, Edgerton VR. Acute neuromodulation restores spinally-induced motor responses after severe spinal cord injury. *Exp Neurol.* 2020;327:113246.

376. Varma AK, Das A, Wallace Gt, et al. Spinal cord injury: a review of current therapy, future treatments, and basic science frontiers. *Neurochem Res.* 2013;38(5):895-905.

377. Wilson JR, Forgione N, Fehlings MG. Emerging therapies for acute traumatic spinal cord injury. *CMAJ.* 2013;185(6):485-492.

378. Rosenzweig ES, Salegio EA, Liang JJ, et al. Chondroitinase improves anatomical and functional outcomes after primate spinal cord injury. *Nature neuroscience.* 2019;22(8):1269-1275.

379. Sandhu MS, Gray E, Kocherginsky M, Jayaraman A, Mitchell GS, Rymer WZ. Prednisolone Pretreatment Enhances Intermittent Hypoxia-Induced Plasticity in Persons With Chronic Incomplete Spinal Cord Injury. *Neurorehabil Neural Repair.* 2019;33(11):911-921.

380. Torres-Espin A, Forero J, Fenrich KK, et al. Eliciting inflammation enables successful rehabilitative training in chronic spinal cord injury. *Brain.* 2018;141(7):1946-1962.

381. Grillner S, El Manira A. Current Principles of Motor Control, with Special Reference to Vertebrate Locomotion. *Physiol Rev.* 2020;100(1):271-320.

382. Tan AM, Waxman SG. Spinal cord injury, dendritic spine remodeling, and spinal memory mechanisms. *Experimental neurology.* 2012;235(1):142-151.

383. Guertin P. Can the spinal cord learn and remember? *ScientificWorldJournal.* 2008;8:757-761.

384. Chikofsky EJ, Cross JH. Reverse engineering and design recovery: A taxonomy. *IEEE software.* 1990;7(1):13-17.

385. Francius C, Harris A, Rucchin V, et al. Identification of multiple subsets of ventral interneurons and differential distribution along the rostrocaudal axis of the developing spinal cord. *PLoS One.* 2013;8(8):e70325.

386. Crone SA, Quinlan KA, Zagoraiou L, et al. Genetic ablation of V2a ipsilateral interneurons disrupts left-right locomotor coordination in mammalian spinal cord. *Neuron.* 2008;60(1):70-83.

387. Pivetta C, Esposito MS, Sigrist M, Arber S. Motor-circuit communication matrix from spinal cord to brainstem neurons revealed by developmental origin. *Cell.* 2014;156(3):537-548.

388. Cohen AH, Gans C. Muscle activity in rat locomotion: movement analysis and electromyography of the flexors and extensors of the elbow. *J Morphol.* 1975;146(2):177-196.

389. Heglund NC, Taylor CR. Speed, stride frequency and energy cost per stride: how do they change with body size and gait? *J Exp Biol.* 1988;138:301-318.

390. Clarke KA, Still J. Gait analysis in the mouse. *Physiol Behav.* 1999;66(5):723-729.

391. Noga BR, Fortier PA, Kriellaars DJ, Dai X, Detillieux GR, Jordan LM. Field potential mapping of neurons in the lumbar spinal cord activated following stimulation of the mesencephalic locomotor region. *J Neurosci.* 1995;15(3 Pt 2):2203-2217.

392. Etlin A, Blivis D, Ben-Zwi M, Lev-Tov A. Long and short multifunicular projections of sacral neurons are activated by sensory input to produce locomotor activity in the absence of supraspinal control. *J Neurosci.* 2010;30(31):10324-10336.

393. Alvarez FJ, Villalba RM, Zerda R, Schneider SP. Vesicular glutamate transporters in the spinal cord, with special reference to sensory primary afferent synapses. *J Comp Neurol.* 2004;472(3):257-280.

394. Lavin TK, Jin L, Lea NE, Wickersham IR. Monosynaptic Tracing Success Depends Critically on Helper Virus Concentrations. *Front Synaptic Neurosci.* 2020;12:6.

395. Nott A, Glass CK. Immune memory in the brain. *Nature.* 2018;556(7701):312-313.

396. Chen LM, Qi HX, Kaas JH. Dynamic reorganization of digit representations in somatosensory cortex of nonhuman primates after spinal cord injury. *J Neurosci.* 2012;32(42):14649-14663.

397. Gazula VR, Roberts M, Luzzio C, Jawad AF, Kalb RG. Effects of limb exercise after spinal cord injury on motor neuron dendrite structure. *J Comp Neurol.* 2004;476(2):130-145.

398. Hua SE, Garonzik IM, Lee JI, Lenz FA. Microelectrode studies of normal organization and plasticity of human somatosensory thalamus. *J Clin Neurophysiol.* 2000;17(6):559-574.

399. Kinoshita M, Matsui R, Kato S, et al. Genetic dissection of the circuit for hand dexterity in primates. *Nature.* 2012;487(7406):235-238.

400. Takeoka A, Arber S. Functional Local Proprioceptive Feedback Circuits Initiate and Maintain Locomotor Recovery after Spinal Cord Injury. *Cell Rep.* 2019;27(1):71-85 e73.

401. Onifer SM, Smith GM, Fouad K. Plasticity after spinal cord injury: relevance to recovery and approaches to facilitate it. *Neurotherapeutics.* 2011;8(2):283-293.

402. Ballermann M, Fouad K. Spontaneous locomotor recovery in spinal cord injured rats is accompanied by anatomical plasticity of reticulospinal fibers. *Eur J Neurosci.* 2006;23(8):1988-1996.

403. Rosenzweig ES, Courtine G, Jindrich DL, et al. Extensive spontaneous plasticity of corticospinal projections after primate spinal cord injury. *Nat Neurosci.* 2010;13(12):1505-1510.

404. Li G, Fan ZK, Gu GF, et al. Epidural Spinal Cord Stimulation Promotes Motor Functional Recovery by Enhancing Oligodendrocyte Survival and Differentiation and by Protecting Myelin after Spinal Cord Injury in Rats. *Neurosci Bull.* 2020;36(4):372-384.

405. Sasaki M, Radtke C, Tan AM, et al. BDNF-hypersecreting human mesenchymal stem cells promote functional recovery, axonal sprouting, and protection of corticospinal neurons after spinal cord injury. *J Neurosci.* 2009;29(47):14932-14941.

406. Hofer AS, Scheuber MI, Sartori AM, et al. Stimulation of the cuneiform nucleus enables training and boosts recovery after spinal cord injury. *Brain.* 2022;145(10):3681-3697.

407. Beaumont E, Guevara E, Dubeau S, Lesage F, Nagai M, Popovic M. Functional electrical stimulation post-spinal cord injury improves locomotion and increases afferent input into the central nervous system in rats. *J Spinal Cord Med.* 2014;37(1):93-100.

408. Jakobs M, Fomenko A, Lozano AM, Kiening KL. Cellular, molecular, and clinical mechanisms of action of deep brain stimulation-a systematic review on established indications and outlook on future developments. *EMBO Mol Med.* 2019;11(4).

409. Arbuthnott GW, Dejean C, Hyland B. Antidromic Cortical Activity as the Source of Therapeutic Actions of Deep Brain Stimulation. *Cortico-Subcortical Dynamics in Parkinson's Disease.* 2009:393-403.

410. Valentín A, Nguyen HQ, Skupenova AM, et al. Centromedian thalamic nuclei deep brain stimulation in refractory status epilepticus. *Brain Stimulation.* 2012;5(4):594-598.

411. Jakobs M, Fomenko A, Lozano AM, Kiening KL. Cellular, molecular, and clinical mechanisms of action of deep brain stimulation—a systematic review on established indications and outlook on future developments. *EMBO molecular medicine.* 2019;11(4):e9575.

412. Gross RE, Lozano AM. Advances in neurostimulation for movement disorders. *Neurol Res.* 2000;22(3):247-258.

413. Deep-Brain Stimulation for Parkinson's Disease Study G, Obeso JA, Olanow CW, et al. Deep-brain stimulation of the subthalamic nucleus or the pars interna of the globus pallidus in Parkinson's disease. *N Engl J Med.* 2001;345(13):956-963.

414. Grill WM, Snyder AN, Miocinovic S. Deep brain stimulation creates an informational lesion of the stimulated nucleus. *Neuroreport.* 2004;15(7):1137-1140.

415. Braz J, Solorzano C, Wang X, Basbaum AI. Transmitting pain and itch messages: a contemporary view of the spinal cord circuits that generate gate control. *Neuron.* 2014;82(3):522-536.

416. Guo D, Hu J. Spinal presynaptic inhibition in pain control. *Neuroscience.* 2014;283:95-106.

417. Mendell LM. Constructing and deconstructing the gate theory of pain. *Pain.* 2014;155(2):210-216.

418. Guigui P, Benoist M, Deburge A. Spinal deformity and instability after multilevel cervical laminectomy for spondylotic myelopathy. *Spine (Phila Pa 1976).* 1998;23(4):440-447.

419. Cardoso MJ, Dmitriev AE, Helgeson M, Lehman RA, Kuklo TR, Rosner MK. Does superior-segment facet violation or laminectomy destabilize the adjacent level in lumbar transpedicular fixation? An in vitro human cadaveric assessment. *Spine (Phila Pa 1976).* 2008;33(26):2868-2873.

420. Xu R, O'Reilly MA. A Spine-Specific Phased Array for Transvertebral Ultrasound Therapy: Design and Simulation. *IEEE Trans Biomed Eng.* 2020;67(1):256-267.

421. Fletcher SP, O'Reilly MA. Analysis of Multifrequency and Phase Keying Strategies for Focusing Ultrasound to the Human Vertebral Canal. *IEEE Trans Ultrason Ferroelectr Freq Control.* 2018;65(12):2322-2331.

422. Fletcher SP, Choi M, Ogrodnik N, O'Reilly MA. A Porcine Model of Transvertebral Ultrasound and Microbubble-Mediated Blood-Spinal Cord Barrier Opening. *Theranostics.* 2020;10(17):7758-7774.

423. O'Reilly MA, Hynynen K. Blood-brain barrier: real-time feedback-controlled focused ultrasound disruption by using an acoustic emissions-based controller. *Radiology.* 2012;263(1):96-106.

424. Sun T, Zhang Y, Power C, et al. Closed-loop control of targeted ultrasound drug delivery across the blood–brain/tumor barriers in a rat glioma model. *Proceedings of the National Academy of Sciences.* 2017;114(48):E10281-E10290.

425. Ko HY, Park JH, Shin YB, Baek SY. Gross quantitative measurements of spinal cord segments in human. *Spinal Cord.* 2004;42(1):35-40.

426. Klein WL, Sullivan J, Skorupa A, Aguilar JS. Plasticity of neuronal receptors. *FASEB J.* 1989;3(10):2132-2140.

427. Ulas J, Monaghan DT, Cotman CW. Kainate receptors in the rat hippocampus: a distribution and time course of changes in response to unilateral lesions of the entorhinal cortex. *J Neurosci.* 1990;10(7):2352-2362.

428. Salvany S, Casanovas A, Piedrafita L, et al. Microglial recruitment and mechanisms involved in the disruption of afferent synaptic terminals on spinal cord motor neurons after acute peripheral nerve injury. *Glia.* 2021;69(5):1216-1240.

429. Schwenk BM, Hartmann H, Serdaroglu A, et al. TDP-43 loss of function inhibits endosomal trafficking and alters trophic signaling in neurons. *EMBO J.* 2016;35(21):2350-2370.

430. Hachiya N, Sochocka M, Brzecka A, et al. Nuclear Envelope and Nuclear Pore Complexes in Neurodegenerative Diseases-New Perspectives for Therapeutic Interventions. *Mol Neurobiol.* 2021;58(3):983-995.

431. Danilov CA, Steward O. Conditional genetic deletion of PTEN after a spinal cord injury enhances regenerative growth of CST axons and motor function recovery in mice. *Experimental neurology.* 2015;266:147-160.

432. Bradbury EJ, Moon LD, Popat RJ, et al. Chondroitinase ABC promotes functional recovery after spinal cord injury. *Nature.* 2002;416(6881):636-640.

433. Blackmore MG, Wang Z, Lerch JK, et al. Kruppel-like Factor 7 engineered for transcriptional activation promotes axon regeneration in the adult corticospinal tract. *Proc Natl Acad Sci U S A.* 2012;109(19):7517-7522.

434. Hagg T, Oudega M. Degenerative and spontaneous regenerative processes after spinal cord injury. *Journal of neurotrauma.* 2006;23(3-4):263-280.

435. Calancie B, Molano MR, Broton JG. Epidemiology and demography of acute spinal cord injury in a large urban setting. *J Spinal Cord Med.* 2005;28(2):92-96.

436. Hinderer C, Bell P, Katz N, et al. Evaluation of Intrathecal Routes of Administration for Adeno-Associated Viral Vectors in Large Animals. *Hum Gene Ther.* 2018;29(1):15-24.

437. Mamounas LA, Altar CA, Blue ME, Kaplan DR, Tessarollo L, Lyons WE. BDNF promotes the regenerative sprouting, but not survival, of injured serotonergic axons in the adult rat brain. *J Neurosci.* 2000;20(2):771-782.

438. Hickmott PW, Ethell IM. Dendritic plasticity in the adult neocortex. *Neuroscientist.* 2006;12(1):16-28.

439. Diogenes MJ, Costenla AR, Lopes LV, et al. Enhancement of LTP in aged rats is dependent on endogenous BDNF. *Neuropsychopharmacology.* 2011;36(9):1823-1836.

440. Horch HW, Katz LC. BDNF release from single cells elicits local dendritic growth in nearby neurons. *Nature neuroscience.* 2002;5(11):1177-1184.

441. Marcol W, Kotulska K, Larysz-Brysz M, Kowalik JL. BDNF contributes to animal model neuropathic pain after peripheral nerve transection. *Neurosurg Rev.* 2007;30(3):235-243; discussion 243.

442. Monteys AM, Hundley AA, Ranum PT, et al. Regulated control of gene therapies by drug-induced splicing. *Nature.* 2021;596(7871):291-295.

CURRICULUM VITA

NAME: Brandon Brown

ADDRESS: Kentucky Spinal Cord Injury Research Center
511 S Floyd St.
University of Louisville
Louisville, KY 40202

DOB: Hobart, Indiana – March 16, 1991

EDUCATION

PhD. in Translational Neuroscience, **University of Louisville,** October 2019 - Current

Area of interest: Spinal cord injury
(Advisors: Dr Scott Whittemore and Dr David Magnuson)

M.S. in Kinesiology, **Indiana University**, August 2014 - May 2016

Major: Clinical Exercise Science
Thesis project*: The effects of passive lumbo-pelvic position on the autonomic nervous system.* (Advisor: Dr Zachary Riley)

B.S. in Kinesiology, **Indiana University**, August 2009 - August 2014

Major Area: Exercise Science

ORIGINAL PEER-REVIEWED PUBLICATIONS

B.L. Brown., Anil, N., States, G.J.R., Whittemore, S.R., Magnuson, D.S.K., Kopechek, J.A., 2023. Focused ultrasound and intravenous microbubbles confer focal cell specific gene transfer in the rodent lumbar spinal cord. *Gene Therapy*. (in preparation)

B.L. Brown., Anil, N., States, G.J.R., Whittemore, S.R., Magnuson, D.S.K., 2023. Long ascending propriospinal neurons are heterogenous and subject spinal cord injury induced anatomic plasticity. *Experimental Neurology*. (in preparation).

Shepard, C.T., **Brown, B.L.**, Can Rijswijck, M.A., Zalla, R.M., Burke, D.A., Morehouse, J.R., Riegler, A.S., Whittemore, S.R., Magnuson, D.S.K., 2023. Silencing long-descending inter-enlargement propriospinal neurons improves hindlimb stepping after contusive spinal cord injuries. *Elife*.

Saraswat Ohri, S., Myers, S.A., **Brown, B.L.,** Forston, M.D., Liu, Y., Andres, K.R., Howard, R.M., Cavener, D.R., Hetman, M., Whittemore, S.R., 2023. Deletion of the integrated stress response kinase PERK in oligodendrocytes limits functional recovery after contusive SCI. *Glia.*

Saraswat Ohri, S., Andres, K.R., Howard, R.M., **Brown, B.L**., Forston, M.D., Hetman, M., Whittemore, S.R., 2023. Acute pharmacological inhibition of protein kinase r-like endoplasmic reticulum kinase signaling after spinal cord injury spares oligodendrocytes and improves locomotor recovery. *Journal of neurotrauma.*

Saraswat Ohri, S., Myers, S.A., **Brown, B.L.,** Slomnicki, L.P., Forston, M.D., Andres, K.R., Howard, R.M., Hetman, M., Whittemore, S.R., 2022. Heme regulated inhibitor deletion attenuates inflammation and improves locomotor recovery after spinal cord injury (in preparation). *Glia.*

Shepard, C.T., Pocratsky, A.M., **Brown, B.L.**, Van Rijswijck, M.A., Zalla, R.M., Burke, D.A., Morehouse, J.M., Reigler, A.S., Whittemore, S.R., Magnuson, D.S.K., 2021. Silencing long ascending propriospinal neurons after spinal cord injury improves hindlimb stepping in the adult rat. *Elife, 10,* e70058.

Brown, B.L.*, Zalla, R.M.*, Shepard, C.T., Howard, R.M., Kopechek, J.A., Magnuson, D.S.K., Whittemore, S.R., 2021. Dual-viral transduction enhances the quantity and specificity of labeling when targeting long propriospinal neurons. *Frontiers in Neuroanatomy, 15,* 12. *co-first authors

Pocratsky, A.M., Shepard, C.T., Burke, D.A., Riegler, A.S., Morehouse, J.R., Hardin, J.T., Beare, J.E., Hainline, C., States, G.R.J., **Brown, B.L.**, Whittemore, S.R., Magnuson, D.S.K., 2020. Long ascending propriospinal neurons, provide flexible, context-specific control of interlimb coordination. *Elife, 9,* e53565.

Brown, B.L., Sandelski, M.S., Drejet, S.M., Runge, E.M., Shipchandler, T.Z., Jones, K.J., Walker, C.L., 2020. Facial Nerve Repair Utilizing Intraoperative Repair Strategies. *Laryngoscope Investigative Otolaryngology, 5*(3), 552-559.

Brown, B.L., Asante, T., Welch, H.R., Sandelski, M.M., Drejet, S.M., Shah, K., Runge, E.M., Shipchandler, T.Z., Jones, K.J. and Walker, C.L., 2018. Functional and Anatomical Outcomes of Facial Nerve Injury with Application of Polyethylene Glycol in a Rat Model. *JAMA facial plastic surgery, 21*(1), 61-68.

Setter, D.O., Runge, E.M., Schartz, N.D., Kennedy, F.M., **Brown, B.L.**, McMillan, K.P., Miller, W.M., Shah, K.M., Haulcomb, M.M., Sanders, V.M. and Jones, K.J., 2018. Impact of peripheral immune status on central molecular responses to facial nerve axotomy. *Brain, behavior, and immunity, 68*, 98-110.

GRANTS & AWARDS

Ruth L. Kirschstein Predoctoral Individual National Research Service Award Predoctoral Fellowship (Parent F31), NIH/NINDS. 12/1/20 – 11/30/23

F31 NS116935-01A1, $32,123/year, The Effects of Activity on Propriospinal Neuron Morphology and Connectivity.

Travel Award - The International Symposium on Neural Regeneration, January 2020

Trainee award for conference attendance based on the content, clarity, and perceived impact of the science presented.

Bepko Learning Center Service Scholarship, Spring 2014

Structural Kinesiology Mentor; Awarded for designing and implementing multiple education sessions weekly to enhance student learning of functional anatomy.

INVITED PRESENTATIONS (academic)

Development and implementation of viral vectors for basic science, April 2022

University of Louisville Neuroscience Day.

Understanding Spinal Cord Injury & Plasticity in a Rodent Model, September 2020

American Association for Laboratory Animal Science Technician Night, virtual presentation

CONFERENCE ABSTRACTS & POSTER PRESENTATIONS

Brown, B.L., Shepard, C.T., Zalla, R.M., Reigler, A.S., Howard, R.M., Van Rijswijck, M.A., Parsch, M.V., Whittemore, S.R., Magnuson, D.S.K. (2020) Silencing a spared ascending pathway improves locomotor outcomes and illustrates the importance of understanding plasticity after contusive SCI. International Symposium on Neural Regeneration. Pacific Grove, CA.

Shepard, C.T.*, **Brown, B.L.*,** Van Rijswijck, M.A., Zalla, R.M., Parsch, M.V., Reigler, A.S., Pocratsky, A.M., Whittemore, S.R., Magnuson, D.S.K. (2019) Silencing long ascending propriospinal neurons improves hindlimb coordination and stepping precision after incomplete SCI. Society for Neuroscience Annual Meeting, Chicago, IL. *co-first authors

Brown, B.L.*, Shepard, C.T.*, Zalla, R.M., Howard, R.M., Parsch, M.V., Magnuson, D.S.K., Whittemore, S.R. (2019) Adapting Multi-Viral Systems to Map the Spinal Cord. Kentucky Spinal Cord and Head Injury Research Trust Symposium, Louisville, KY. *co-first authors

Brown B.L., Sandelski M.M., Drejet S.M., Jones K.J., Walker C.L. *The Effects of Combinatorial Treatments on Functional and Anatomical Outcomes of Facial Nerve Injury in a Rat Model.* University of Louisville Neuroscience Day, April 2018.

Brown B.L., Sandelski M.M., Drejet S.M., Shipchandler T.Z., Jones K.J., Walker C.L. *The Effects of Combinatorial Treatments on Functional and Anatomical*

Outcomes of Facial Nerve Injury in a Rat Model. Veterans Affairs Research Week, Roudebush VA Medical Center, June 2018.

Brown B.L., Sandelski M.M., Drejet S.M., Jones K.J., Walker C.L. *The Effects of Combinatorial Treatments on Functional and Anatomical Outcomes of Facial Nerve Injury in a Rat Model*. Society for Neuroscience, Louisville Chapter, April 2017.

Brown B.L., Walker C.L., Asante T.J., Welch H.R., Drejet S.M., Shah K., Jones K.J. *The Effects of Combinatorial Treatments on Accuracy of Axonal Regrowth in a Rat Model of Facial Nerve Injury.* Kentucky Spinal Cord and Head Injury Research Trust Symposium, May 2017

TEACHING EXPERIENCE

Adjunct Faculty IUPUI, Summer 2015, Fall 2016, Summer 2016, Spring 2017

Basic Physiology of Exercise (HPER-P 409); assisted with course administration as well as designed, instructed, and oversaw exercise physiology labs.

Experiences in Physical Activity (HPER-E 100); designed and implemented total body workout class allowing students participate in various types of total body exercise.

Group Exercise (HPER-E 102); designed and implemented a class in which students participated in different forms of group exercise.

IUPUI Department of Kinesiology Teaching Assistantship, Fall 2014 – Spring 2016

Basic Physiology of Exercise (HPER-P 409); assisted with course administration as well as designed, instructed, and oversaw exercise physiology labs with 50+ students each semester.

Conditioning and Weight Training (HPER-E 121); designed and implemented a course to practically convey the basic principles of conditioning and weight training to non-kinesiology majors.

Guest Lectures

Motor Learning (HPER-P 452); lectured on motor unit structure and function, motor unit recruitment, and motor control of human movement.

COMMUNITY INVOLVEMENT & SERVICE

Whiskey for Warriors, Spring-Summer 2022

Indiana; organized multi-part fundraiser to benefit the Indiana Veterans' Home and raised $5700

Louisville Regional Science and Engineering Fair Mentor, Fall-Winter 2020, Fall-Winter 2021

Louisville, KY; mentored high school and middle school students to develop, execute, analyze, and present science fair projects.

Kentucky Science and Engineer Fair Judge, March 2020
Virtual Judging; served as a judge for state high school and middle school science fair projects

Society for Neuroscience (Louisville Chapter) Special Judge, February 2020
University of Louisville, Louisville, KY; judged and awarded the *excellence in neuroscience* award for middle and high school regional science fair

Louisville Regional Science and Engineering Fair, February 2020
University of Louisville, Louisville, KY; served as a judge for high school science fair projects related to translational medicine

Undergraduate bioengineering capstone project mentor, Fall 2019
University of Louisville, KY; aided undergraduate students in designing and implementing project evaluating the potential for ultrasound to disrupt the blood brain barrier in the lumbar spinal cord

Brain Days, March 2019
Kentucky Science Center, Louisville, KY; ran various education workshops to foster community interest in neuroscience

39th National Veteran Wheelchair Games, July 2019
Kentucky Exposition Center, Louisville, KY; helped with refereeing, scoring, and athlete assistance throughout the greater Louisville area

High School Student Mentor for AP Research Course, Spring 2019
duPont Manuel High School, Louisville, KY; facilitated student-led development, implementation, analysis, and presentation of science fair project for the Kentucky Science Fair

Louisville Student Pathways Mentor, Summer 2018
University of Louisville, Louisville, KY; promoted science education through an 8-week mentorship program aimed at introducing students to the scientific process and careers in science

OTHER RELEVANT EXPERIENCE

Plenary Session Chair, May 2019
Kentucky Spinal Cord and Head Injury Research Trust Symposium, Louisville, KY; chaired plenary session at international conference

Head of Keynote Speaker Selection Committee
Kentucky Spinal Cord and Head Injury Research Trust Symposium, Louisville, KY; led committee to select and invite plenary speaker for an international conference

Scientific Liaison, Summer 2018

Pathway to Living, Chicago, IL; attended international scientific conference on Alzheimer's and dementia to relay basic and translational research findings to healthcare administrators and providers.

RESEARCH ACTIVITIES

Graduate Student (Laboratory of Molecular Neurobiology), July 2017 - Current

Research focused on elucidating anatomical plasticity of propriospinal neurons before and after spinal cord injury and exploring novel means of inducing plasticity chronically after spinal cord injury.

Jones Laboratory Affiliate, July 2016 - 2017

Volunteered 30 hours per week assisting with research projects. Main research focus evaluated various therapeutic interventions to enhance recovery following facial nerve injury.

Master's Thesis

The effects of passive lumbo-pelvic position on the autonomic nervous system. Examined how changes in passive lumbo-pelvic position alter autonomic nervous system measures. Elucidated how posture and orthopedic testing may indicate alterations the autonomic measures.

INVITED PRESENTATIONS (non-academic)

The Life & Times of a Biomedical PhD Student, April 2020

Google/Exos interns, Virtual presentation; Shared personal experience of being a biomedical PhD candidate, current research, and facilitated discussion on career paths.

Enslavement - How the Nervous System Limits Movement, October 2016

P*hysical Preparation Summit, Indianapolis, IN;* Presented relevant neuroanatomy and structural anatomy to convey how the nervous system controls degrees of freedom during movement.

Thresholds of Motor Learning, November 2015

Physical Preparation Summit, Indianapolis, IN; Presented on dynamic systems theory of motor learning, and how this impacts motor skill development.

Developing Athletes and Building Champions, July 2015

USA Weightlifting Board of Directors, Video Conference; Presented principles of motor learning and physiology related to enhance athletic development.

Developing Athletes and Building Champions, June 2015

USA Weightlifting Junior Nationals, Minneapolis, MN; Presented principles of motor learning and physiology related to enhance athletic development.